

**Advanced modelling of vinyl chloride monomer production
via thermal cracking of ethylene dichloride**

Renato do Carmo Claro Yih Wong

Thesis to obtain the Master of Science Degree in

Chemical Engineering

Supervisors: Professor Henrique Aníbal Santos de Matos
Dr. Štěpán Špatenka

Examination Committee

Chairperson: Professor Maria Fátima Costa Farelo
Supervisor: Professor Henrique Aníbal Santos de Matos
Members of the Committee: Professor Maria Joana Assis Teixeira Neiva Correia

November 2014

“Wit beyond measure is man’s greatest treasure.”

– J.K. Rowling

“Valeu a pena? Tudo vale a pena

Se a alma não é pequena.”

– Fernando Pessoa

Acknowledgments

Firstly, I would like to thank professors Carla Pinheiro and Henrique Matos, who made available this one of a time experience to take this internship at PSE. I also want to thank professor Costas Pantelides and everybody at PSE for making this opportunity available, and welcoming me these past seven months.

I would also like to thank my supervisors, both from IST and PSE. To Stepan Spatenka, thank you for sharing your knowledge and know-how during this last seven months. To professor Henrique Matos, for his guidance and assistance whenever we met.

I would also like to thank everybody at PSE who helped me with my thesis, namely Maarten and Charles, for the training course in gPROMS, and Trung, for helping me with the Macro used in the LSKM implementation.

I would be amiss if I didn't mention the great friends I found while at London, all of whom helped me build a home away from home. To all of you, my biggest gratitude, and I can't wait to see you all again.

A special acknowledgement to the interns at PSE from FEUP, Catarina and Rubina, for your support and help throughout our internship. Thank you for listening to all my problems, and entertaining me with yours.

To my house mates, Artur and Mariana, thank you for the great times. It was great living with you, and I would do it again in a heartbeat.

I would like to thank all the friends I made during these last five years at IST. You have been amazing, and are fortunately too many to mention here, but to all of you thanks.

To Ana, Duarte, and Rita, words cannot express what I feel for you. These last five years have been amazing, and I am proud to call you my friends.

To Bernardo, Leonor, and Rúben, my biggest gratitude for your friendship and hard work. With you, being friends and work partners isn't mutually exclusive, and I have enjoyed all the time spent with you.

To Margarida, Rita, Teresa, Bernardo, and Henrique, my friendship with you has only grown throughout these last five years, and for that I am eternally grateful.

Finally, to my most wonderful family, my parents and brother, for always being there for me. Nothing I do would be possible without you.

Resumo

O cloreto de vinilo (VCM) é uma das maiores comodidades, sendo a matéria-prima principal na produção do policloreto de vinilo (PVC), e é produzido através do craqueamento térmico do dicloroetano, EDC, numa fornalha. No presente trabalho, um modelo desta fornalha foi desenvolvido em linguagem gPROMS[®]. Este é composto por um modelo da serpentina, onde é descrita a reacção de craqueamento, e um modelo da câmara de combustão, onde a transferência de calor pela combustão do combustível foi considerada. Vários mecanismos cinéticos, tanto moleculares como radicalares, foram validados com dados disponíveis na literatura. Para reduzir o tempo de computação da simulação quando são utilizados mecanismos radicalares, a matriz dos coeficientes estequiométricos foi comprimida, o que permitiu diminuir o tempo de computação em metade. Relativamente ao modelo da fornalha, foram consideradas diferentes correlações para estimar a emissividade dos gases de combustão concluindo-se que os resultados obtidos entre são muito semelhantes. Foi ainda usado um modelo onde a fornalha é dividida em zonas, tendo-se concluído que a temperatura da fornalha não varia significativamente com o aumento de zonas na câmara de combustão. Finalmente, foi realizada uma análise de sensibilidade à quantidade de combustível consumido, e verificou-se um mínimo no consumo específico de combustível (87.6 kg combustível/t VCM). O uso de iniciadores foi também testado, e verificou-se que com o mecanismo utilizado, o cloro reduz a temperatura necessária na serpentina, e o tetraclorocarbono o oposto.

Palavras-chave: Modelação, VCM, craqueamento, mecanismo radicalar, gPROMS

Abstract

Vinyl chloride (VCM) is one of the most important commodity materials, being the main raw material in the production of polyvinyl chloride (PVC), and is mainly produced through the thermal cracking of dichloroethane, EDC, in a pyrolysis furnace. In the present work, a model of this furnace was developed in gPROMS[®]. This is composed of a model of the coil, where the cracking reaction is described, and a model of the firebox, where the heat transfer by the combustion of the fuel was modelled. Several kinetic mechanisms present in the literature, both molecular and radical, were implemented and validated with available data. To reduce the computing time of the simulation when using radical mechanisms, the stoichiometric matrix was compressed, which was able to the computing time in half. Regarding the firebox model, different correlations for emissivity estimation were compared using a single zone model, and it was found that the results obtained with them were very similar. A zone model was also used, where the firebox was divided in several zones, and it was concluded that the temperature profile did not change significantly with the increase of zones in the firebox. Finally, a sensitivity analysis was performed on the fuel consumption, and a minimum in specific fuel consumption (87.6 kg fuel/t VCM) was found. The use of initiators was also tested, and it was shown that with the used mechanism chlorine greatly reduces the temperature needed in the coil, and using carbon tetrachloride the opposite was observed.

Keywords: Modelling, VCM, cracking, radical mechanism, gPROMS

Contents

Acknowledgments	v
Resumo	vii
Abstract	ix
List of Tables	xiii
List of Figures	xvii
Nomenclature	xx
Glossary	xxi
1 Introduction	1
1.1 Motivation	1
1.2 Outline	2
2 Background	3
2.1 The PVC market	3
2.2 VCM production combined process [6], [7]	4
2.2.1 Other routes for VCM production	6
2.3 The pyrolysis furnace	7
2.4 Firebox models	8
2.4.1 Well-stired furnace model	8
2.4.2 Calculation of the gas emissivity	9
2.4.3 Non-grey gas effect	10
2.4.4 Zone model	11
2.5 Cracking kinetic mechanism	12
2.5.1 Molecular mechanisms	12
2.5.2 Radical mechanisms	13
2.6 Coke formation	13
2.7 Reaction initiators	14
3 Materials and Methods	17
3.1 The gPROMS Software	17
3.2 The Multiflash Software	17
3.3 Implementation of Large Scale Kinetic Mechanisms	18

3.3.1	Sparse matrix treatment	18
3.3.2	LSKM preparation	19
3.3.3	LSKM output	20
3.4	The ReadData Foreign Object	21
4	Reactor model	23
4.1	Source and sink models	23
4.2	Connections	24
4.2.1	gML Material	24
4.2.2	Distributed Thermal Contact	24
4.3	Coil model	24
4.3.1	One-dimensional tube model	24
4.3.2	gML to LSKM converter	28
4.3.3	LSKM to gML converter	28
4.4	Heat transfer models	29
4.4.1	Advanced energy input	29
4.4.2	Firebox model	29
5	Results	31
5.1	Implementation of the molecular mechanism	31
5.2	Firebox simulation	35
5.3	Implementation of the radical mechanism	38
5.3.1	LSKM performance	38
5.3.2	Model performance	40
5.4	Sensitivity analysis	42
5.4.1	Analysis of the fluid properties	42
5.4.2	Analysis on the operating conditions	44
5.4.3	Promoters	47
6	Conclusions	51
6.1	Achievements	52
6.2	Future Work	52
	Bibliography	56
A	Kinetics	57
A.1	Molecular kinetics	57
A.2	Radical kinetics	58
B	Heat Capacity	95
C	Emissivity estimation	99

List of Tables

5.1	Geometry parameters of the coil in the studied cases	31
5.2	Simulation results using the geometry in Li et al. [16] and assigning a COT of 756 K	32
5.3	Simulation results using the geometry in Li et al. [16] and assigning a conversion of 55%	34
5.4	Inputs used for the firebox model	35
5.5	Composition of the fuel used	35
5.6	Firebox results for the well–stirred furnace model	37
5.7	Firebox results using different number of zones	38
5.8	Simulation results for the radical mechanisms using the geometry in Li et al. [16] and assigning a conversion of 55%	41
5.9	Coil outlet compositions using the radical mechanisms	42
5.10	Results for the sensitivity analysis on the thermal conductivity and viscosity	43
A.1	Kinetic parameters for the mechanism by Kaggerud [13]	57
A.2	Kinetic parameters for the mechanism by Li et al. [16]	57
A.3	Kinetic parameters for the mechanism by Dimian and Bildea [6]	57
B.1	Heat capacities for the molecular species	95
B.2	Heat capacities for the molecular species (cont.)	96
B.3	Heat capacities for the radical species	96
B.4	Heat capacities for the radical species (cont.)	97
C.1	Values for the parameter b for correlation 2.10	99
C.2	Values for the parameter n for correlation 2.10	99
C.3	Values for the parameter a_0 for correlation 2.11	99
C.4	Values for the parameter a_1 for correlation 2.11	100
C.5	Values for the parameter a_2 for correlation 2.11	100
C.6	Values for the parameter a_3 for correlation 2.11	100
C.7	Constants for the degree of emission of the pure gas phase	100

List of Figures

2.1	Utilisation of PVC production capacities in various regions, 2009	4
2.2	The vinyl chloride production process	5
2.3	Scheme of the VCM pyrolysis furnace	7
3.1	LSKM excel input sheet	19
3.2	LSKM excel species sheet	20
3.3	Format of the .txt file used on the ReadData FO	22
4.1	Schematic of the models and connections used to simulate the pyrolysis furnace	23
4.2	Schematic of the coil model	28
5.1	Temperature profile in the coil for different molecular mechanisms at a fixed COT	32
5.2	Conversion profile in the coil for different molecular mechanisms at a fixed COT	32
5.3	Heat flux profile in the coil for different molecular mechanisms at a fixed COT	33
5.4	Temperature profile in the coil for different molecular mechanisms at a fixed conversion	34
5.5	Heat flux profile in the coil for different molecular mechanisms at a fixed conversion	34
5.6	Temperature profile in the coil for different emissivity correlations	36
5.7	Heat flux in the coil for different emissivity correlations	36
5.8	Temperature profile in the coil for different emissivity correlations	37
5.9	Heat flux in the coil for different emissivity correlations	38
5.10	Comparison of the number of parameters and variables using the mechanism by Borsa with and without compressing the stoichiometric matrix	39
5.11	Comparison of the run time of the initialisation procedure with and without compressing the kinetic scheme	39
5.12	Comparison of the run time of the simulation using a saved variable set with and without compressing the kinetic scheme	39
5.13	Comparison of the run time of a simulation with a 10% variation of the assigned COT from the saved variable set with and without compressing the kinetic scheme	40
5.14	Temperature profiles using the geometry by Li and the radical mechanisms	40
5.15	Conversion profiles using the geometry by Li et al. [16] and the radical mechanisms	41
5.16	Heat flux profiles using the geometry by Li et al. [16] and the radical mechanisms	41
5.17	Estimation of the heat capacity for EDC	43

5.18 Estimation of the heat capacity for VCM	43
5.19 Estimation of the heat capacity for HCl	44
5.20 Influence of fuel flowrate on EDC conversion	44
5.21 Relation between EDC and COT	45
5.22 Variation of selectivity with conversion	45
5.23 Variation of specific fuel consumption with conversion	46
5.24 Variation of conversion with feed flowrate	46
5.25 Variation of COT with feed flowrate	46
5.26 Variation of selectivity with feed flowrate	47
5.27 Variation of specific fuel consumption with feed flowrate	47
5.28 Variation of conversion with CIT	48
5.29 Variation of selectivity with CIT	48
5.30 Variation of specific fuel consumption with CIT	48
5.31 Influence of CCL_4 and Cl_2 on COT	49
5.32 Influence of CCL_4 and Cl_2 on conversion	49
5.33 Influence of CCL_4 and Cl_2 on selectivity	50
A.1 List of species used on the mechanism by Schirmeister et al. [25]	58
A.2 List of species used on the mechanism by Schirmeister et al. [25]	58
A.3 List of reactions used on the mechanism by Borsa [2]	59
A.4 List of reactions used on the mechanism by Borsa [2] (cont.)	60
A.5 List of reactions used on the mechanism by Borsa [2] (cont.)	61
A.6 List of reactions used on the mechanism by Borsa [2] (cont.)	62
A.7 List of reactions used on the mechanism by Borsa [2] (cont.)	63
A.8 List of reactions used on the mechanism by Borsa [2] (cont.)	64
A.9 List of reactions used on the mechanism by Borsa [2] (cont.)	65
A.10 List of reactions used on the mechanism by Borsa [2] (cont.)	66
A.11 List of reactions used on the mechanism by Borsa [2] (cont.)	67
A.12 List of reactions used on the mechanism by Borsa [2] (cont.)	68
A.13 List of reactions used on the mechanism by Borsa [2] (cont.)	69
A.14 List of reactions used on the mechanism by Borsa [2] (cont.)	70
A.15 List of reactions used on the mechanism by Borsa [2] (cont.)	71
A.16 List of reactions used on the mechanism by Borsa [2] (cont.)	72
A.17 List of reactions used on the mechanism by Borsa [2] (cont.)	73
A.18 List of reactions used on the mechanism by Borsa [2] (cont.)	74
A.19 List of reactions used on the mechanism by Borsa [2] (cont.)	75
A.20 List of reactions used on the mechanism by Borsa [2] (cont.)	76
A.21 List of reactions used on the mechanism by Borsa [2] (cont.)	77
A.22 List of reactions used on the mechanism by Borsa [2] (cont.)	78

A.23 List of reactions species on the mechanism by Borsa [2]	79
A.24 List of reactions species on the mechanism by Borsa [2] (cont.)	80
A.25 List of reactions species on the mechanism by Borsa [2] (cont.)	81
A.26 List of reactions species on the mechanism by Borsa [2] (cont.)	82
A.27 List of reactions species on the mechanism by Borsa [2] (cont.)	83
A.28 List of reactions species on the mechanism by Borsa [2] (cont.)	84
A.29 List of reactions species on the mechanism by Borsa [2] (cont.)	85
A.30 List of reactions species on the mechanism by Borsa [2] (cont.)	86
A.31 List of reactions species on the mechanism by Borsa [2] (cont.)	87
A.32 List of reactions species on the mechanism by Borsa [2] (cont.)	88
A.33 List of reactions species on the mechanism by Borsa [2] (cont.)	89
A.34 List of reactions species on the mechanism by Borsa [2] (cont.)	90
A.35 List of reactions species on the mechanism by Borsa [2] (cont.)	91
A.36 List of reactions species on the mechanism by Borsa [2] (cont.)	92
A.37 List of reactions species on the mechanism by Borsa [2] (cont.)	93

Nomenclature

Greek symbols

α Absorptivity.

ΔH Variation in enthalpy.

$\Delta H_f^{298.15K,IG}$ Standard enthalpy of formation of the ideal gas.

ΔS Variation in entropy.

ϵ Emissivity.

λ Thermal conductivity.

$(\Delta\epsilon)_G$ Correction factor to a water vapour–carbon dioxide mixture.

ν Viscosity.

σ Stefan–Boltzmann constant.

Roman symbols

$(\overline{GS_1})_R$ Total exchange area between gas and sink in radiative equilibrium.

A Area.

C Fraction to the total furnace area.

c_p Heat capacity.

D Diameter.

E_a Activation energy.

F Flowrate.

H Fluid's heat flux.

h Heat transfer coefficient.

h Specific enthalpy.

k Rate constant.

K_c	Equilibrium constant.
L	Mean beam length, or coil length.
N	Mass flux.
n	Reaction order.
p	Pressure.
Q	Heat exchanged.
R	Gas constant.
r	Reaction rate, or radius.
T	Temperature.
V	Volume of the firebox.
v	Velocity.
w	Mass fraction.
z	Axial direction of the coil.

Subscripts

1	Sink.
a	Air.
C	Convection.
f	Fuel, forward.
G	Flue gas.
i	Component.
in	Inner.
j	Reaction.
l	Loss.
o	Outer.
R	Radiation.
r	Reverse.

Glossary

CFD Computational Fluid Dynamics.

CIT Coil inlet temperature.

COT Coil outlet temperature.

EDC Ethylene dichloride, or dichloroethane.

FO Foreign object.

HTC High temperature chlorination.

LSKM Large scale kinetic mechanism.

LTC Low temperature chlorination.

NC Number of components.

NR Number of reactions.

PVC Polyvinyl chloride polymer.

TMT Tube metal temperature.

VCM Vinyl chloride monomer, or chloroethene.

Chapter 1

Introduction

Vinyl chloride monomer (VCM) is currently, in addition to ethylene and NaOH, one of the most important commodity materials [7]. About 95% of VCM is used for the production of polyvinyl chloride (PVC) [7], which is currently the second most abundant plastic in the world, behind only polyethylene, with a worldwide production capacity in 2009 of 30 million tonnes a year [18].

Currently, the main production process of VCM is the chlorination of ethylene to dichloroethane (also known as ethylene dichloride, or EDC), followed by its dehydrochlorination to VCM by thermal cracking. The dehydrochlorination of EDC is currently performed by its pyrolysis in cracking furnaces at temperatures about 500-550 °C [7]. This occurs via a first-order free radical mechanism [7], with a conversion of about 50-60% per pass. This is done in order to limit by-product formation, obtaining yields of about 95-99%.

Despite the high yields, a small fraction of by-products are formed in this process which, due to the large material through-put, create severe inefficiencies. A solid carbonaceous material, coke, is deposited inside the reactor coils which requires periodic shut-downs of the entire plant for its removal. Also gas phase by-products such as chloroprene and butadiene cause downstream difficulties in distillation columns.

Thus, the need arises for a model which can accurately predict by-product formation to allow for a model based optimisation of the whole process.

1.1 Motivation

The EDC cracking process presents many difficulties in modelling, the main being the complexity of modelling a large scale radical mechanism, with currently over 800 reported equations by Borsa [2]. Although these models have been implemented in sequential modelling, EDC cracking has never been implemented in an equation oriented process modelling tool such as gPROMS, eventually allowing the whole plant optimisation.

The main objective of this work is to build a model which can rigorously describe the EDC cracking process, dealing with the challenges of implementing a large radical kinetic scheme. For this, different

kinetic mechanisms are tested, in order to analyse which one better fits the experimental data.

1.2 Outline

Firstly, a review of the literature present on this topic is shown in chapter 2. Afterwards, the main tools used in the modelling of this process are present in chapter 3.

In chapter 4 the main equations and models used to describe the EDC cracking furnace are presented.

Chapter 5 describes the main results from the simulations.

Finally, chapter 6 presents the main conclusions from this work as well as suggestions for future work.

Chapter 2

Background

In this chapter, a brief analysis on the market for polyvinyl chloride PVC, the main application for vinyl chloride, is carried out. Afterwards, a description of the processes for VCM production is presented. Finally, the pyrolysis furnace is described, as well as the main mechanisms used to simulate EDC cracking, and the main models used for simulating a firebox.

2.1 The PVC market

Polyvinyl chloride (PVC) is currently the second most abundant plastic in the world, behind only polyethylene. Although PVC was first synthesised in 1830-1834, industrial production of this polymer started only in the 1930s, through the catalytic hydrogenation of acetylene. Currently most production of PVC is through VCM, in plants use a balanced process where ethylene is chlorinated through direct chlorination and oxychlorination, the latter using the HCl produced in the thermal cracking of EDC to VCM.

As mentioned in chapter 1, currently the great majority of vinyl chloride (over 95%) is used in the production of PVC.

Currently, Asia and Europe are the leading regions in terms of PVC production capacities. However, in 2009 North America's production was higher than Europe due to its higher utilisation level, as can be seen in figure 2.1. China is clearly the largest producer of PVC, with over 7 million tonnes per year (corresponding to 26% of the market share worldwide). However, up to 81% of this production is not with VCM produced by EDC cracking, but with the hydrochlorination of acetylene.

PVC produced from the rest of Asia is mainly produced in Japan by Asahimas Chemical and Shin-Etsu, Taiwan by Formosa Plastics, and South Korea by LG Chemical Ltd.

Regarding production in Europe, production of PVC is mainly from ethylene (chlorination to EDC and cracking to VCM accounts for 98% of Europe's PVC market). PVC produced in Europe tends to integrate the full production process from chlorine to PVC, due to the difficulties of transporting chlorine.

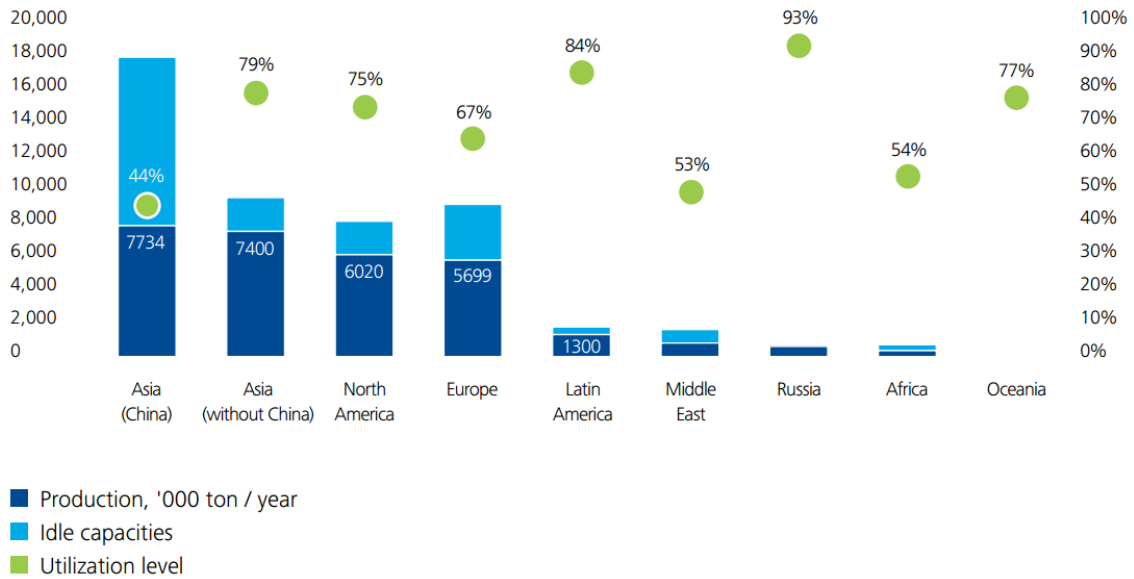
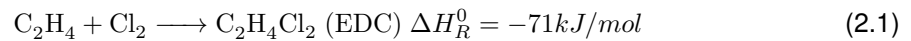


Figure 2.1: Utilisation of PVC production capacities in various regions, 2009 [18]

2.2 VCM production combined process [6], [7]

VCM production through ethylene is currently a balanced process, meaning all by-products are recycled in a way which ensure a closure of the material balance having only VCM as the final product, starting from ethylene, chlorine and oxygen. This is done through three main units:

1. Direct chlorination of ethylene to EDC:



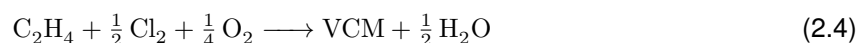
2. Oxychlorination of ethylene to EDC:



3. Cracking of EDC to produce VCM:



The balanced process can therefore be described by the overall equation:



A schematic representation of this process can be found in Figure 2.2.

The direct chlorination of ethylene to EDC is an exothermic reaction, which is most commonly performed in the liquid phase of ethylene dichloride for better temperature control. A Lewis catalyst is employed, ordinarily iron (III) chloride. The chlorination can either be at low (LTC) or high temperatures

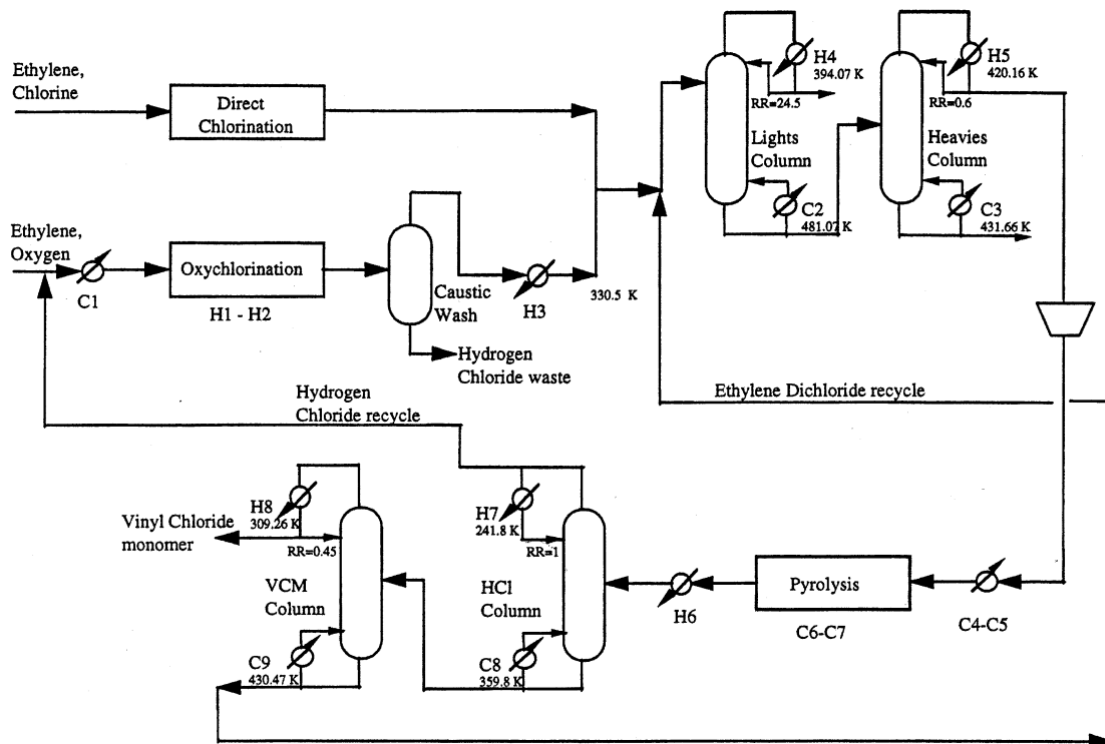


Figure 2.2: The vinyl chloride production process [14]

(HTC).

In the LTC process, ethylene and chlorine react dissolved in EDC, which acts as a solvent, at temperatures below the boiling point, around 50–70 °C. This enables a higher selectivity (over 99 %), however, steam is needed for the rectification of EDC, thus rejecting the heat of reaction.

The HTC process is carried out at around 100 °C, and thus the heat of reaction, seven times higher than the EDC's heat of vaporisation, can be used for its purification. The chemical reactor can thus be integrated as the reboiler of a distillation column, although it may be designed as an independent equipment. Also, due to the high heat of reaction mentioned before, EDC produced from the oxychlorination section can be purified in the same column. This process commonly presents a lower selectivity, however by sophisticated reactor design, yields comparable to the LTC can be obtained using a considerably lower energy consumption.

EDC is also produced, as mentioned, in the oxychlorination section. This process chlorinates the ethylene using the HCl produced in the cracking of EDC, and can be performed in a fixed bed system, or alternatively, in a fluidised bed.

In the fixed bed systems, due to the highly exothermic reaction, temperature control is a problem, which is solved by dilution of the catalyst with inactive diluents. The reactor should be constructed in nickel alloys with low carbon content.

Fluidised bed reactors are more widely used and have the advantage of improved heat transfer and almost isothermal operation. This enables using stainless steel if condensation can be avoided, except for the sparging equipment at the entrance of the reactor, which should be made of nickel alloys, as they are more resistant to chloride stress corrosion. However, backmixing cannot be avoided, which

influences conversion and selectivity.

Copper (II) salts are used as standard catalysts, with the addition of either alkali, alkaline earth or aluminium chloride to reduce its volatility. High surface alumina is used preferably as support, in the form of powder or microspheres for fluidised bed reactors, or as tablets, extrudates or spheres for fixed bed reactors.

After purification of the EDC produced on the direct chlorination and oxychlorination sections, it is thermally cracked to vinyl chloride and hydrogen in the pyrolysis furnace. This happens at about 500-550°C and 20-30 bar. Higher temperatures are undesirable, despite the conversion increase, as there is a decrease in selectivity. Therefore, the mean residence time is of about 10-20 s, which leads to about 50-60% conversion per pass. This translates in yields in vinyl chloride of up to 95-99%. The cracked gas is then quickly quenched to avoid excessive by-product formation.

The resulting stream is then distilled to recover the produced hydrogen chloride, in order to be used in the oxychlorination section. VCM is then recovered in another distillation column, where a stream of crude EDC is obtained as the bottom product, which is recycled to the reactor after purification.

The crude EDC stream is purified in two sequential distillation columns. In the first, EDC is separated from light impurities, such as butadiene, chloroprene, or dichloroethylenes. In the second distillation column, EDC is recovered on the top column, and separated from heavier components such as trichloroethane. This step is of utmost importance, as the addition of impurities in the feed leads to a decrease in both conversion and selectivity in the cracking process.

2.2.1 Other routes for VCM production

Despite worldwide VCM production being essentially through the balanced process described in section 2.2, other routes for producing vinyl chloride are possible [7].

Vinyl chloride can be obtained by the hydrochlorination of acetylene, in either the gaseous or liquid phase, despite gas phase being dominant in industrial processes. This is almost exclusively performed in fixed-bed, multitubular reactors in near isothermal operation. This process is catalysed primarily using mercury(II) chloride on activated carbon.

The production of vinyl chloride may also be performed using unpurified acetylene from high temperature cracking of naphtha or methane. This process can be advantageous, as it does not require cost-intensive separation of acetylene-ethylene mixtures. However, these processes of obtaining VCM from acetylene have the distinct drawback of using acetylene as the feed, which is more expensive than ethylene.

Catalytic dehydrochlorination of 1,2-dichloroethane is used by a minority of vinyl chloride producers. This process poses as advantages higher selectivity towards VCM and less coke formation, due to being performed at lower temperatures (200-450 °C). Conversion, however, remains nearly the same, with 60-70% conversion per pass. Moreover, with the development of improved noncatalytic gas-phase processes, the catalytic route has lost its economic attractiveness, due to the higher costs of catalytic processes and extended shut-down periods.

Direct chlorination or oxychlorination of ethylene presents a great interest by combining the exothermic reaction of ethylene chlorination or oxychlorination with the endothermic cracking reaction. In direct chlorination, the process ethylene is used in excess to limit by-product formation, and the formed hydrogen chloride can be consumed in a separate oxychlorination unit, while in the oxychlorination of ethylene, polyvalent metals are used as catalyst. Both of these routes face the problem of difficult process control and operation, characterised by low selectivity. However, in France, Atochem carries an industrial process (150 kt/a) where by-products are integrated, and thus they are intentionally produced [7].

Direct conversion from ethane to vinyl chloride could save the processing costs of ethylene, and thus considerably decrease the raw material costs and reduce dependence on cracker capacity. However, due to the lack of molecular functionality, the ethane must first undergo substitution reactions, which give rise to a variety of side-reactions. Thus, yields are quite low, at only 20–50% per pass.

2.3 The pyrolysis furnace

The vinyl chloride pyrolysis process can be classified as high pressure (20 bar outlet) or low pressure (11 bar outlet) [19].

The high pressure process is a once-through or liquid-feed design. The liquid is fed to the top of the convection zone and vaporised in the lower convection zone in a specifically designed process tube configuration before being cracked in the radiant zone.

Figure 2.3 has a schematic representation of the low pressure process. In it, the convection section is used to preheat the feed. EDC with a purity over 99% enters the convection section and is heated up to its boiling point. It is then vaporised in an external heat exchanger, where the hot fluid can be steam or, alternatively, the pyrolysis' effluent. The feed then re-enters the furnace in the shock section.

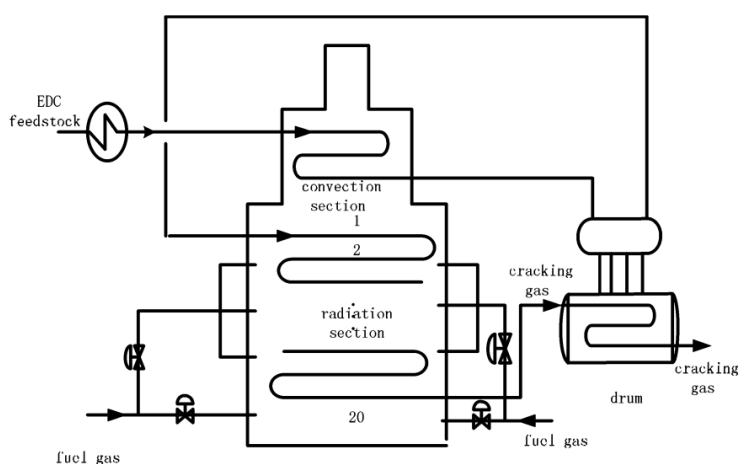


Figure 2.3: Scheme of the VCM pyrolysis furnace [17]

In the shock section the feed is superheated up to cracking reaction temperature, around 400–420°C. In this zone heat transfer is by both radiation from the firebox and convection from the flue gas.

In the radiant section, the EDC in the coil is cracked to VCM and HCl through a first-order free radical chain mechanism. Two coils are positioned horizontally in the firebox according to a symmetry plane, and average 200-300 m in length, with a residence time of 10–30 seconds. The temperature is kept, as previously mentioned, around 500-550°C, to minimise by-product formation. Due to the high temperatures in the cracking zone, chromium–nickel alloys are often used [7], such as Incoloy ([13], [25]).

The heat required for the endothermic set of reactions is commonly given by a set of burners installed in the side wall of the furnace. These are in most cases fed natural gas; however, some plants use hydrogen-driven furnaces, using hydrogen from on-site chlor-alkali plants (which produce the chlorine used in the direct chlorination step) [7].

2.4 Firebox models

2.4.1 Well-stired furnace model

Heat transfer in the firebox, or radiant section, of the furnace presents a heat transfer problem with direct radiation from the flame to both the heat sink (in this case, the coil) and the furnace walls and re-radiation from the walls to the heat sink, as well as convection and external heat losses. Various solutions for describing this model are available in the literature ([20], [22], [23], [28]), with different degrees of simplification, ranging from simple radiation modelling to CFD models, describing with great rigour the flow and temperature of the flue gas in the firebox.

The simplest model would be to consider a simple well-stirred furnace model. In this, the following simplifying assumptions are made [22]:

1. Combustion gas mass and flame are considered to be at a single temperature.
2. Combustion gas is considered grey.
3. Surface of the heat sink is grey.
4. External heat losses and convective heat transfer to the walls (internal and external) are negligible.
5. The sink and refractory wall surfaces are intimately mixed, such that the view factors to sink surfaces are the same from all points (speckled wall assumption).

Considering these assumptions, the net heat exchange from the hot gases to the sink, Q , can be given by the sum of the heat transferred by convection and radiation:

$$Q = Q_C + Q_R \quad (2.5)$$

Where the heat by convection is given through the heat transfer coefficient, h , the total coil area, A_C , and the temperatures from the flue gas and sink, T_G and T_1 respectively:

$$Q_C = hA_C(T_G - T_1) \quad (2.6)$$

The heat transferred by radiation is calculated in the following manner:

$$Q_r = (\overline{GS_1})_R \sigma (T_g^4 - T_1^4) \quad (2.7)$$

Where $(\overline{GS_1})_R$ is the total exchange area between gas and sink in radiative equilibrium, and σ is the Stefan–Boltzmann constant. According to Perry et al. [23], the total exchange area between gas and sink can be approximated by:

$$(\overline{GS_1})_R = \frac{A_1}{C_1 \left(\frac{1}{\epsilon_G} - 1 \right) + \frac{1}{\epsilon_1}} \quad (2.8)$$

In equation 2.8, A_1 is the sink's area, ϵ_G and ϵ_1 are respectively the combustion gases and the sink's emissivities. C_1 is the fraction of sink area to the total area, which encompasses the coil and furnace walls' area.

2.4.2 Calculation of the gas emissivity

Gases, as liquids and solids, also emit and absorb thermal radiation. Elementary and noble gases are practically diathermous (transparent to thermal radiation), while other gases and vapours are selective radiators, only emitting and absorbing within narrow wavelength bands. Thus, for simplified calculations of radiation exchanges in a furnace, it is usually assumed only contributions to thermal radiation by water and carbon dioxide.

The emissivity of a mixture consisting of carbon dioxide, water vapour and non–radiant components can be given by:

$$\epsilon_G = \epsilon_{H_2O} + \epsilon_{CO_2} - (\Delta\epsilon)_g \quad (2.9)$$

Where ϵ_{H_2O} and ϵ_{CO_2} represent the emissivity from water vapour and carbon dioxide respectively, and $(\Delta\epsilon)_g$ is a correction to the total emissivity needed due to the overlap of the individual emission bands of the gases involved. This correction can be read from diagrams, which can be found in [28], and the emissivities can be calculated using appropriated correlations ([23], [28]).

Alternatively, flue gas emissivities can be estimated from correlations. [23] presents two different correlations for calculating the emissivity of $H_2O:CO_2$ mixtures:

$$\epsilon_g T_G = b(pL - 0.015)^n \quad (2.10)$$

$$\log(\epsilon_G T_G) = a_0 + a_1 \log(pL) + a_2 \log(pL)^2 + a_3 \log(pL)^3 \quad (2.11)$$

For both the equations, p is the sum of the partial pressure of both components, and L is the mean

beam length, which for most geometries can be approximated to:

$$L = 0.9 \frac{4V}{A} \quad (2.12)$$

Which, in the case of the furnace, V stands for the total furnace volume and A for the total area (the coil and the walls of the firebox).

VDI-Gesellschaft [28] calculates the emissivity of the flue gases using the 'grey-and-clear gas approximation', or 'weighted sum of grey gases model'. In this model, the emissivity of a gas can be expressed as the weighted mean of a suitable number of grey gases emissivity, corresponding to the energy fractions a_i of the black body spectrum. The emissivity can thus be calculated as the following:

$$\epsilon_g = \sum_0^n a_i \epsilon_{G,i} = \sum_0^n a_i (1 - \exp(-kpL)) \quad (2.13)$$

In this equation, k is the volumetric absorption coefficient, and a_i are the weighting factors for each of the energy fractions, calculated by:

$$a_i = b_{0i} + b_{1i} T_G \quad (2.14)$$

Where b_{0i} and b_{1i} are coefficients which are adjusted for different gases.

The parameters used for estimating the flue gas emissivities can be found in appendix C

2.4.3 Non-grey gas effect

A radiating gas cannot be considered as grey if its transmittance at increasing L, instead of being constant, keeps increasing due to surface reflection, or alternatively, if the gas emissivity and absorptivity are not the same unless the gas temperature equals the sink's temperature. This should be accounted for in the calculation of the emissivity of the gas, as well as in the total radiative exchange area.

Correction on the emissivity

To correct the calculation of the emissivity, an effective emissivity, $\epsilon_{G,e}$, is defined:

$$\sigma(\epsilon_G T_G^4 - \alpha_{G1} T_1^4) \equiv \sigma \epsilon_{G,e} (T_G^4 - T_1^4) \quad (2.15a)$$

$$\epsilon_{G,e} = \frac{\epsilon_G - \alpha_{G1} (T_1^4 / T_G^4)}{1 - (T_1^4 / T_G^4)} \quad (2.15b)$$

Where α_{G1} is the absorptivity of the gas at temperature T_1 . According to Perry et al. [23], it can be calculated using the correlations used for the emissivity, evaluated at T_1 instead of T_G and pLT_1/T_G instead of pL , and multiplied by $(T_G/T_1)^{0.5}$:

$$\alpha_{G1} T_1 = \epsilon_G T_1 \left(\frac{pLT_1}{T_G} \right) \left(\frac{T_G}{T_1} \right)^{0.5} \quad (2.16)$$

VDI-Gesellschaft [28] approximates the absorptivity in a similar way to the emissivity, by considering a sum of exponential functions:

$$\alpha_G = \sum_0^n a_{1i}(1 - \exp(-kpL)) \quad (2.17)$$

Where a_{1i} are the weighting factors for the absorptivity which can be approximated to the weighting factors for the emissivity evaluated at the sink's wall temperature:

$$a_{1i}(T_1) \approx a_i(T_1) \quad (2.18)$$

Correction on the total heat exchange area

In case the gas cannot be considered grey, the total exchange area between gas and sink in radiative equilibrium must also take that into account. In this case, that area can be calculated by:

$$(\overline{GS}_1)_R = \frac{A_1}{C_1 \left(\frac{1}{\epsilon_G} - \frac{1}{a} \right) + \frac{1}{\epsilon_1} + \frac{1/a-1}{\epsilon_1 + \epsilon_r(C_r/C_1)}} \quad (2.19)$$

In this equation, C_r is the fraction of the furnace walls' area to the total area, ϵ_r the emissivity of the furnace walls, and a is the weighting factor for the grey gas in the grey-and-clear gas approximation, which is given by:

$$a = \frac{\epsilon_G(pL)^2}{2\epsilon_G(pL) - \epsilon_G(2pL)} \quad (2.20)$$

2.4.4 Zone model

In the zone method, as outlined by Hottel and Sarofim [9], the space in which radiative heat transfer has to be calculated is divided into a number of surface and volume elements which are isothermal and have uniform properties (well-mixed zones). This model was then applied in various modifications by other authors.

The tendency in rigorous firebox modelling these days is to couple a coil-side model with a CFD model of a firebox ([16], [13]). However, the rigorous modelling of the firebox is computational expensive and it is suitable mainly for firebox designs.

Since the approach to modelling in the firebox has a very small effect on yield predictions, as also confirmed by this work, simplified zone models were also applied in the literature. Li et al. [16] cites as an example of zone method, the one-dimensional Lobo-Evans model. In this model, the firebox is divided in zones along its height, and the heat balance for each zone is:

$$Q_{f1} = +\sigma A_0 (T_{G2}^4 - T_{G1}^4) - Q_1 - \Delta H_1 - Q_{l1} = 0 \quad (2.21a)$$

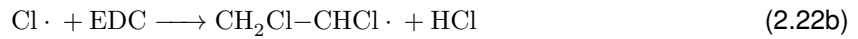
$$Q_{fn} = +\sigma A_0 (T_{G(n-1)}^4 - T_{Gn}^4) + \sigma A_0 (T_{G(n+1)}^4 - T_{Gn}^4) - Q_n - \Delta H_n - Q_{ln} = 0 \quad (2.21b)$$

$$Q_{fN} = +\sigma A_0 \left(T_{G(N-1)}^4 - T_{GN}^4 \right) - Q_N - \Delta H_N - Q_{lN} = 0 \quad (2.21c)$$

Where equation 4.17a is the heat balance for the first zone and equation 4.17c is the heat balance for the last zone, N. In this set of equations, Q_{fn} is the heat released by the fuel gas, Q_n the heat absorbed by the reactor tubes, ΔH_n the flue gas enthalpy traded in zone n, and Q_{ln} the wall heat dissipation in zone n. A_0 is the transfer area between different firebox zones. Since the zones are divided according to the furnace's height, A_0 is the product of the width with the length of the coil.

2.5 Cracking kinetic mechanism

As mentioned, EDC pyrolysis is a radical-based mechanism. Thus, thermal cracking does not occur by equation 2.3, but by a series of reactions where radical intermediates are formed, such as:



Consequently, the mechanism through which EDC is cracked is extremely complex, and many mechanisms have been proposed to describe this process.

2.5.1 Molecular mechanisms

Due to the complexity of the implementation of a radical scheme, and due to the high selectivity of the process, some simple molecular schemes have been implemented by some authors. These mechanisms fail to predict the by-products composition, and are thus inadequate if necessary to model the downstream separations. However, their simplicity assure a reduced computing time, which may be convenient if rigorous modelling of the process side is not the main objective.

Kaggerud [13] implemented a CFD simulation of the firebox side. In the process side, only the main reaction of EDC cracking was considered, and the kinetic constants were obtained by combining data from Choi et al. [5] and Howlett [10]. The process side was simulated using a polynomial fitting to the heat flux obtained from the commercial software EDC Crack[®]. It predicts for the reported conditions a conversion of approximately 50% with an outlet temperature of 504 °C.

Li et al. [16] implemented a mechanism with the main reaction as well as an added side reaction of VCM cracking, producing ethylene and hydrogen chloride. Comparison with the industrial data shows a slight overestimation of the conversion, with the selectivity equal to industrial data.

Dimian and Bildea [6] also assume a purely molecular mechanism for the simulation of the entire vinyl chloride monomer production process. In this mechanism three reactions are considered, the cracking of EDC to VCM, and the production of acetylene from VCM (producing HCl) and ethylene from EDC

(with chlorine as a by-product).

2.5.2 Radical mechanisms

The radical mechanism for EDC cracking is well-known in principle, with several experimental studies found in the literature ([10], [11]). There can also be found different rigorous mathematical models, which attempt, with more or less complexity, to predict VCM and by-product formation.

The most detailed chemical kinetic model was developed by Borsa [2]. This mechanism comprises of 818 elementary reactions, and 135 species, of which 71 are molecular and 64 radical. It consists of a large body of elementary reactions that describe all the possible species and reactions that might occur in the system up to C_4 compounds. In the development of this mechanism, available literature data was first used, and estimation techniques were used when the data was absent. After comparison with experimental results, it was found the model predicts the main by-products such as acetylene, chloroprene, butadiene, ethylene, ethane as well as other major products. However, the model fails to predict the formation of chloromethane and 1,1,2-trichloroethane. It should also be noted the model over-predicts EDC conversion when validating the model against laboratory data.

A model was developed by Lee [15] which comprises of 44 gas-phase species and 260 elementary reactions, of which only the most relevant are presented. This mechanism was validated against lab data, showing a good agreement, despite slightly over-estimating EDC conversion for higher residence times.

The model reported by Choi et al. [5] is composed of 108 reversible reactions with 47 molecular and radical species, in order to analyse the influence of adding carbon tetrachloride in the feed. It can be seen with this model, the conversion is slightly overestimated, as the concentration of the analysed by-product, acetylene.

Schirmeister et al. [25] developed a simplified model, consisting of 24 species, of which 16 are molecular and the rest radical, and 31 elementary reactions. These include the most relevant products, intermediates, and by-products, using a key component representing the high boiling products. This model was then used by Li et al. [17], where it slightly over-predicts conversion and selectivity versus plant data.

2.6 Coke formation

The thermal cracking of ethylene dichloride always accompanies the deposition of coke in the coil's walls. The formation of this carbonaceous deposit causes three main process inefficiencies. Firstly, considering the coke's low thermal conductivity, coke formation leads to a decrease in the furnace's thermal efficiency, requiring a higher temperature in the firebox to maintain EDC conversion at the desired level. Second, the increase in the coke layer decreases the cross sectional area, increasing pressure drop. Finally, coke particles entrained in the gas need to be removed from the liquid stream after the quenching to avoid plugging and other problems in downstream units.

These problems eventually force the furnace to shut down in order to proceed to the decoking. This is carried out using a mixture of air and steam to burn the coke in the reactor walls, which shortens the coil's lifetime. Thus, predicting the run length of the furnace is essential, both to maximise it avoiding unnecessary strain to the coil and to enable a reliable planning schedule, to avoid expensive storage of intermediate products. Decoking is usually performed every two years ([17], [25]), or when coil wall temperatures rise over 650 °C [25], or 900 K [17]. The decoking lasts for 3 days [1].

Regarding the mechanism of coke formation, [3] states that catalytic coke formed from reactive hydrocarbons on metal surfaces does not occur, due to the lack of filamentous coke on samples withdrawn from an industrial plant. Instead, coke is formed due to the formation of tar droplets formed from coke precursors at high temperatures, which impinge on the tube wall surfaces. These results are supported by Mochida et al. [21], who reports the formation of anisotropic pyrolytic carbon produced in the cracker reactor.

Concerning the coke precursors, Borsa et al. [3] refers an earlier study where using ¹⁴C-labelled compounds, it was found chloroprene was an effective coke precursor. The same conclusion was made by Borsa et al. [4], where it was found that the chloroprene mole fraction at the exit of a lab scale reactor correlates linearly with the mass of coke deposited. This correlation was not found when comparing the mass of coke deposited in the reactor with other by-products one would expect to be coke precursors, such as ethylene, acetylene, butadiene or benzene.

Regarding the modelling of coke formation in an EDC cracker Li et al. [17] developed a coking mechanism using the radical scheme from Schirmeister et al. [25], where coke is produced as a side reaction from acetylene.

Regarding inhibiting coke formation, there are a few patents which suggest coating the coil walls to reduce coke deposition. Jo et al. [12] suggests adding a boron compound, while Tong [27] recommends exposing the heat surface of the pyrolysis furnace to a phosphine compound. It has also been reported Dreher et al. [7] that adding 1,1,2-trichloroethane inhibits coke formation.

2.7 Reaction initiators

It is well known that ppm level of impurities in the EDC feed can act either as promoters or inhibitors on the cracking reactions. This enables a lower temperature on the pyrolysis furnace, allowing less severe conditions in the furnace. However, it should also be taken into account the effect these impurities have in the formation of by-products. If the added initiator increases coke formation, for example, any increase in VCM production could be offset by the increased maintenance costs. Also, if there is an increased formation of by-products, for example, this could increase the load on downstream separations.

Since radical species are important in the chain propagation step, several species have been used as initiators, for example chlorine, chlorine delivering compounds such as tetrachloromethane or hexachloroethane, oxygen, nitrous oxide, and other halogens, such as bromine and iodine [7].

Choi et al. [5] have investigated the effects of carbon tetrachloride on EDC pyrolysis and concluded that, for the studied conditions, adding 1200 ppm of CCl_4 leads to a 13% increase in conversion. This

was done assuming a temperature profile in the coil, and thus, due to the endothermic character of EDC cracking, a greater heat input is needed, which translates in a higher fuel consumption. Li et al. [17] also studied the effects of adding carbon tetrachloride, finding that adding 200 ppm of it to the feed increases the overall conversion by 2%. Nevertheless, the addition of CCl_4 also caused a decrease on the coil's run length from 70 weeks to around 52 weeks.

Borsa et al. [4] performed laboratory scale experiments to analyse the effect of different compounds on EDC conversion and selectivity, as well as coke formation. In this article it was found that coke deposition varied linearly with EDC conversion. However, using chlorine as an initiator, the dependence is shifted towards much percentages of EDC conversion. This was explained as chlorine acting as a strong promoter of the pyrolysis reactions due to its relatively weak Cl–Cl bond, which allow the formation of chlorine radicals at much lower temperatures. However, it should be noted larger amounts of by-product formation occur with chlorine addition, reducing VCM selectivity and possibly causing problems in downstream separation.

Chapter 3

Materials and Methods

3.1 The gPROMS Software

gPROMS[®] was the software used in the development and simulation of the models. It is developed by Process Systems Enterprise and is a platform for high-fidelity predictive modelling for the process industries, and is the foundation on which all of PSE's gPROMS family modelling and optimisation products are built.

The gPROMS ModelBuilder is used to build steady-state and dynamic process models of any complexity. It is an equation based modelling system on a numerical solution of all equations in a model or a flowsheet at the same time. This has several advantages, such as increasing the robustness and speed in comparison with traditional sequential simulations.

gPROMS also allows the usage of external software components, which provide certain computational services to gPROMS models. These are defined as parameters named Foreign Object (FO), and include physical properties packages, external unit operation modules, or even complete computational fluid dynamics (CFD) software packages.

3.2 The Multiflash Software

Multiflash[™] is a physical property package developed by Infochem Computer Services Ltd. A gPROMS interface for Multiflash is available and can be licensed together with gPROMS. This is done through a Multiflash input file (.mfl) which define all the components, physical property models, etc. that are to be used in the problem. The .mfl file is created using the graphical interface of Multiflash for Windows and then exporting this information to create the input file automatically, which can then be imported into ModelBuilder.

3.3 Implementation of Large Scale Kinetic Mechanisms

The stoichiometric matrix has a total of $NC \times NR$ elements, which means, for the mechanism reported by Borsa [2], over 100,000 elements. The computing time for a problem of this size would be quite extensive. However, the fact that the stoichiometric coefficient matrix is sparse (most of the elements in it are zero) can be exploited to compress the matrix to its significant values (all non-zero values).

The LSKM (large scale kinetic mechanism) foreign object is used to compress a kinetic mechanism, by eliminating the non-zero elements. The scheme used in the FO was reported by Tewarson [26], and is explained in section 3.3.1.

A packed form of storing a sparse matrix is one where only the non-zero elements are stored, alongside a necessary indexing information. There are four reasons for utilising this packed form of storage [26]:

- Larger matrices can be stored and handled in the internal storage of the computer, which could be otherwise impossible.
- Generally, getting the data from the compressed form is quicker than would be otherwise, which is beneficial when using external storage devices.
- Only the non-trivial operations are performed, which saves a substantial amount of computation time.
- The usage of this packed form can be particularly advantageous in multiplying several row and column vectors, useful in linear programming, for example.

Of these items, the third is for the this case the most important, as reducing computing time in the calculation of the reaction rates may pose a considerable reduction in computing time.

3.3.1 Sparse matrix treatment

In this scheme, the matrix is stored in three arrays, VE (value of elements), RI (row indices), and CIP (column index pointer). VE contains all the non-zero values of the matrix, while RI and CIP are used to extract the positions these values occupy in the matrix.

In the LSKM foreign object, the second compression scheme reported by Tewarson [26] is employed. This stores the matrix in three arrays, VE (value of elements), RI (row indices), and CIP (column index pointer). VE contains all the non-zero values of the matrix, while RI and CIP are used to extract the positions these values occupy in the matrix.

RI has the same number of elements as VE and stores the rows indexes. This means for a given $VE(\alpha)$, $RI(\alpha)$ stores the row where the value from VE used to be located.

CIP is the column index pointer. If the first non-zero element of the β^{th} column is in position t_β , then that value is stored in the β^{th} element of CIP, that is, $CIP(\beta) = t_\beta$. Considering this, the example matrix M is stored as:

$$M = \begin{bmatrix} 0 & 0 & a_{13} & 0 & 0 \\ a_{21} & 0 & 0 & a_{24} & 0 \\ 0 & 0 & 0 & 0 & 0 \\ 0 & 0 & a_{33} & 0 & 0 \\ a_{41} & 0 & 0 & 0 & a_{45} \\ 0 & a_{52} & 0 & 0 & 0 \end{bmatrix} \quad (3.1)$$

$$VE = [a_{21} \quad a_{41} \quad a_{52} \quad a_{13} \quad a_{33} \quad a_{24} \quad a_{45}] \quad (3.2a)$$

$$RI = [2 \quad 4 \quad 5 \quad 1 \quad 3 \quad 2 \quad 4] \quad (3.2b)$$

$$CIP = [1 \quad 3 \quad 4 \quad 6 \quad 7] \quad (3.2c)$$

Thus, for example, to extract a_{33} , it should first be noted $CIP(3) = 4$, and $CIP(4) = 6$, which means the VE(4) and VE(5) contain values in the third column. Since $RI(5) = 3$, it means that the value for the element in column 3 and row 3 is VE(5).

3.3.2 LSKM preparation

The input to the LSKM.FO are two .txt files, one containing the species which take part in the reaction mechanism, and another which contains the data regarding the reactions: enthalpy of reaction, forward and backwards pre-exponential factors and activation energy, the species involved in the reaction, and their respective stoichiometric coefficients and reaction orders. These text files are prepared in a separate excel file, with the following sheets:

- Control – Main sheet which generates the .txt files.
- Species – List of species in the reaction scheme.
- LSKM input – Where the control sheet gets the information regarding the reaction mechanism for the .txt file. The foreign object is able to supply data for the reaction enthalpy, as well as the forward and backwards pre-exponential factor and activation energy.

	A	B	C	D	E	F	G	H	I	J	K	L	M	N	O	P	Q	R	S	T	U	
1			Forward		Backwards (**)																	
2	Reactions	Reaction enthalpy [kcal/mol]	Pre-exponential factors	Activation energy	Pre-exponential factors	Activation energy	no. species involved	IDs of species involved			Stoichiometric coefficients of species involved			Orders for species involved								
3	1	0	-28.72	5.80E+04	-0.1	0	0	14	17	3			-1	1	1			1	1	1		
4	2	0	-28.98	5.80E+04	0.0	0	0	9	17	3			-1	1	1			1	1	1		
5	3	0	-36.91	6.90E+04	0.0	0	0	17	24	3			-1	1	1			1	1	1		
6	4	0	-23.66	4.70E+04	0.0	0	0	64	67	3			-1	1	1			1	1	1		
7	5	0	-23.66	4.70E+04	0.0	0	0	61	66	3			-1	1	1			1	1	1		

Figure 3.1: LSKM excel input sheet

	A	B
1	Species_ID	Species_Name
2	1	H2
3	2	CL2
4	3	HCL
5	4	CH4
6	5	CCL4
7	6	CHCL3
8	7	CH2CL2
9	8	CH3CL
10	9	EDC
11	10	C2H6
12	11	CH2CLCHCL2
13	12	CH2CLCH3
14	13	CHCL2CHCL2
15	14	CH3CHCL2
16	15	CH3CCL3
17	16	CHCL2CCL3
18	17	VCM

Figure 3.2: LSKM excel species sheet

3.3.3 LSKM output

The LSKM.FO foreign object, as mentioned, compresses the stoichiometric matrix as explained above. Considering the stoichiometric matrix of j rows of reactions and i columns of species, the following arrays are produced:

- ReactionSC(k) – Values of the non-zero stoichiometric coefficients stored in the matrix;
- ReactionID(k) – Returns the reaction, j , for the stoichiometric coefficient in ReactionSC(k);
- SpecStartAddress(i) – Stores the value where the stoichiometric coefficients for the component i start in the ReactionSC array.

The LSKM FO also compresses the matrix regarding the reaction orders in a similar way, producing the following arrays:

- ForwardReactionOrder(k) – Values of the non-zero reaction order of each species i in the left hand side of a reaction j ;
- ReactionID_reactant(k) – Returns the reaction, j , for the reaction order in ForwardReactionOrder(k);
- ReactantStartAddress(i) – Stores the value where the reaction orders for the component i start in the ForwardReactionOrder array.
- BackwardsReactionOrder(k) – Values of the non-zero reaction order of each species i in the right hand side of a reaction j ;
- ReactionID_product(k) – Returns the reaction, j , for the reaction order in BackwardsReactionOrder(k);
- ProductStartAddress(i) – Stores the value where the reaction orders for the component i start in the BackwardsReactionOrder array.

The foreign object also creates the following scalar outputs, which represent the problem size, and will be used to define the length of the arrays:

- NoSpecies – Returns a scalar of type INTEGER with the total number of species;

- NoReactions – Returns a scalar of type INTEGER with the total number of reactions;
- NoStoichCoeffs – Returns a scalar of type INTEGER with the total number of non-zero stoichiometric coefficients;
- NoReactants – Returns a scalar of type INTEGER with the total number of species present on the left hand side of the entire reaction scheme;
- NoProducts – Returns a scalar of type INTEGER with the total number of species present on the right hand side of the entire reaction scheme.

Finally, the foreign object also creates the following vectors, regarding the kinetic parameters of the reactions:

- ForwardPreExponentialFactor – Returns an ARRAY(NoReactions) of type REAL containing the forward pre-exponential factors;
- ForwardActivationEnergy – Returns an ARRAY(NoReactions) of type REAL containing the forward activation energies;
- BackwardPreExponentialFactor – Returns an ARRAY(NoReactions) of type REAL containing the backward pre-exponential factors;
- BackwardActivationEnergy – Returns an ARRAY(NoReactions) of type REAL containing the backward activation energies.

This transformation is then used in the tube mass balances, as will be seen in section 4.3.1.

3.4 The ReadData Foreign Object

The ReadData FO allows to add information which is not added in the LSKM FO. It reads a .txt file and converts it to arrays, where a line containing a string will become the array's name, and any lines following that string becomes data for that method. This allows to add information regarding the components, such as molecular weight, enthalpy and entropy of formation, as well as parameters necessary for calculating the fluid's heat capacity, as will be explained in chapter 4.3.1.

```
NumberOfComponents
...
NumberOfMolecularSpecies
...
NumberOfRadicalSpecies
...
ReferenceTempForCpInK
...
Molecularweight
99
62.5
36.5
...
EnthalpyOfFormation
-32.33
4.67
-22.06
...
Entropy
72.46
63
44.65
...
a0
1.18196E-08
7.75403E-09
-1.07662E-09
...
a1
-4.50849E-05
-2.98755E-05
3.27416E-06
...
a2
0.064793861
0.044462209
-0.001913248
...
```

Figure 3.3: Format of the .txt file used on the ReadData FO

Chapter 4

Reactor model

In this chapter, the models used in this work are described, as well as the connections made between the different models. A scheme of the flowsheet can be seen in figure 4.1.

The flowsheet used is composed by the coil model and the firebox model, as well as the source and sink models, used to connect the inlet and outlet streams. In this, the coil model describes the reaction side, while the firebox model calculates the heat transfer by the combustion of the flue gases.

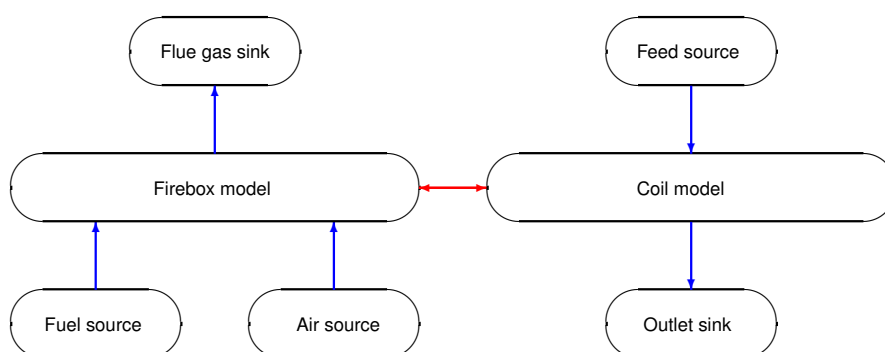


Figure 4.1: Schematic of the models and connections used to simulate the pyrolysis furnace. In this schematic the gML material connections are represented in blue and the distributed thermal contact in red.

4.1 Source and sink models

The source and sink models are part of the gML (gPROMS Modelling Library), developed by PSE. These allow to link the connections between the models, and in case of the source define the inlet conditions.

The Source model is used for defining a material stream entering the flowsheet. This model describes an infinite-volume source boundary with a single outlet port. The material may be liquid, vapour or two phase. In this model, the flow, temperature, and pressure of the stream can be assigned.

Fluid properties are taken from a physical property package complying with the gPROMS physical property interface, such as Multiflash.

The Sink model is used for defining a material stream leaving a flowsheet. The fluid state (tempera-

ture, pressure, mass fraction) specified for the Sink is necessary but is only used in the event of a flow reversal situation, which is not the case for this model.

4.2 Connections

In a flowsheet model, connection between different units are done with a Connection Type, which defines the information conveyed by the connection. This information can be parameters or variables, which may be distributed or not.

4.2.1 gML Material

The gML material connection, which is part of the gML libraries, is used to describe the material streams entering and exiting the units. This connection declares two parameters, the number of components and the physical properties foreign object used. It then contains information on the flow variables, namely the total mass flow, concentrations, temperature, and pressure.

4.2.2 Distributed Thermal Contact

The distributed thermal contact carries the information which connect the firebox model to the coil model. Thus, it connects the length and diameter of the coil, to calculate the total area of the coil. For calculating the heat transfer in the coil, its outer temperature and heat flux profile.

4.3 Coil model

The coil model is comprised by the following models:

1. Tube model;
2. gML to LSKM converter;
3. LSKM to gML converter.

The gML to LSKM and LSKM to gML converters, as will be seen, are used to change between using the physical properties from Multiflash or from the ReadData FO, and thus they are only used when the LSKM FO is used.

4.3.1 One-dimensional tube model

For the reactor model, due to the turbulent flow, as well as the low viscosity for the reaction side stream, a one-dimensional plug flow reactor model was used. The tube model also calls for different sub-models:

1. Fluid properties model;

2. Kinetic model;
3. Heat transfer coefficient model;
4. Friction factor coefficient model.

Tube model

The mass balance for the species is defined as:

$$\frac{\partial N_i A}{\partial z} = A \sum_{j=1}^{NR} (\nu_{ij} r_j) \quad (4.1)$$

Where N_i is the mass flux for component i , A the cross-sectional area, r_j the reaction rate for reaction j , and NR the number of reactions. However, when the stoichiometric matrix is compressed, the mass balance must be rewritten as:

$$\frac{\partial N_i A}{\partial z} = \sum_{k=SpecStartAddress(i)}^{SpecStartAddress(i+1)-1} (ReactionSC_k r_{ReactionID(k)}) A \quad (4.2)$$

The `SpecStartAddress` vector, as mentioned in chapter 3, identifies the starting position for component i on the `ReactionID` and `ReactionSC` vectors, which respectively contain the reactions in which component i participates in and its stoichiometric coefficient for the given reaction. Thus, this equation is in every form equal to 4.1, except it only sums the reaction rates to which the stoichiometric coefficient for component i is different than zero.

The energy balance is given by:

$$\frac{\partial H A}{\partial z} = 2\pi r_o Q \quad (4.3)$$

In this equation, r_o is the external radius, Q is the external heat flux, and H is the energy flux of the fluid, which is defined by:

$$H = N h \quad (4.4)$$

Where N is the total mass flux, which is calculated as the sum of the individual species mass flux, and h is the specific enthalpy of the stream, calculated in the fluid properties' model. As will be seen in section 4.3.1, the reference state of the components is in their elemental state and thus the enthalpy of reaction is considered in the calculation of the fluid's enthalpy and is not accounted in the energy balance.

The temperature profiles in the coil walls and in the fluid are given by:

$$Q r_o = h r_{in} (T_{gas/coke\ interface} - T_{bulk}) \quad (4.5a)$$

$$Q r_o = \frac{\lambda_{coke} (T_{inner\ wall} - T_{gas/coke\ interface})}{\log(r_{internal}/r)} \quad (4.5b)$$

$$Q_{r_o} = \frac{\lambda_{coil}(T_{outer\ wall} - T_{inner\ wall})}{\log(r_{external}/r_{internal})} \quad (4.5c)$$

Where equation 4.5a pertains to the heat transfer in the fluid bulk, 4.5b to the coke layer which is formed, and 4.5c to the heat transfer in the coil walls. In this set of equations, Q is the heat flux, h is the fluid's heat transfer coefficient, r_o and r_{in} are respectively the outer and inner radius of the coil, and λ_{coke} and λ_{coil} are respectively the thermal conductivity of the coke layer and the coil.

Regarding the pressure drop along the coil, it is calculated by:

$$0 = -NA \frac{\partial v}{\partial z} - \frac{\partial pA}{\partial z} - A\rho v^2 \left(\frac{2}{r_{in}} f_{tube} + \frac{NB}{L} f_{bends} \right) \quad (4.6)$$

Where v is the fluid's velocity, f_{tube} and f_{bends} are respectively the friction factor coefficient for the coil and for the bends, NB is the number of bends in the coil, and L is the coil length.

Fluid properties model

In this model, the properties of the fluid needed in the one-dimensional tube model are calculated. When using a molecular based mechanism, the Multiflash foreign object is used. This enables the calculation of the mixture's viscosity, thermal conductivity and the average molecular weight. The heat capacity and enthalpy are also calculated here, with the following reference state:

- Reference temperature of 298.15 K;
- Reference pressure of 1 atm;
- Components in their elemental state.

When a radical scheme is used, since Multiflash has a limited range of compounds and has no radical components in its database, another procedure for calculating the properties of the fluid was required. Regarding the specific enthalpy, it was calculated using the following equation:

$$h = \sum_{i=1}^{NC} \Delta H_{f,i}^{298.15K,IG} w_i + \sum_{i=1}^{NC} \bar{c}_p (T - T_{ref}) \quad (4.7)$$

Where \bar{c}_p is the average specific heat capacity of the fluid, which is given by the weighted average of the heat capacities of the different components. These are calculated using a 3rd order polynomial fitting using the heat capacities from [2]. Thus, the average heat capacity for a given component is:

$$\bar{c}_{p,i} = \int_{T_{ref}}^T a_0 T^3 + a_1 T^2 + a_2 T + b dT = \frac{a_0}{4} (T^4 - T_{ref}^4) + \frac{a_1}{3} (T^3 - T_{ref}^3) + \frac{a_2}{2} (T^2 - T_{ref}^2) + b(T - T_{ref}) \quad (4.8)$$

The fitting parameters, a_0 , a_1 , a_2 , and b , are included in Appendix B. These values, as well as the molecular weight and the enthalpies of formation, were imported using the ReadData foreign object when a radical mechanism was employed.

Due to the lack of data, and acknowledging the low concentration of radicals and by-products, the calculation of the viscosity and thermal conductivity was performed using Multiflash for the main components (EDC, VCM and HCl, defined in the Multiflash file in the feed source).

Kinetic model

The objective of this model is calculating the reaction rate, r , for a given reaction j , which is given by:

$$r_j = k_{f,j} \prod_{i=1}^{NC} C_i^{n_{f,ij}} \quad (4.9a)$$

$$r_j = k_{f,j} \prod_{i=1}^{NC} C_i^{n_{f,ij}} - k_{r,j} \prod_{i=1}^{NC} C_i^{n_{r,ij}} \quad (4.9b)$$

Where equation 4.9a is used if the reaction is considered irreversible, and 4.9b if the reactions are reversible. In these equations, C_i is the molar concentration, $n_{f,ij}$ and $n_{r,ij}$ are respectively the forward and reverse reaction orders for component i and reaction j , and $k_{f,j}$ and $k_{r,j}$ the forward and reverse rate constant for reaction j , respectively.

The forward rate constant is given by the following expression:

$$k_{f,j} = k_{0,j} T^{n_j} \exp\left(\frac{-E_{a,j} R}{T}\right) \quad (4.10)$$

Where T is the fluid's temperature, in K, $k_{0,j}$ is the forward pre-exponential factor, $E_{a,j}$ is the activation energy, R the perfect gas constant, and n_j is the the temperature exponent, used to correct deviations from the Arrhenius equation. The reverse rate constant is calculated using the equilibrium constant, $K_{c,j}$:

$$K_{c,j} = \frac{k_{f,j}}{k_{r,j}} \quad (4.11)$$

Which is calculated by the following expression:

$$K_{c,j} = \exp\left(\frac{\Delta S_j^\circ}{R} - \frac{\Delta H_j^\circ}{RT}\right) \left(\frac{p}{RT}\right)^{\sum_{i=1}^{NC} (n_{r,ij} - n_{f,ij})} \quad (4.12)$$

Where ΔS_j° and ΔH_j° are respectively the change of standard entropy and enthalpy during the reaction and P is the system's pressure.

Friction factor coefficient model

For calculating the friction factor coefficient for the coil, the Churchill equation [23] was employed, valid for Reynolds numbers over 4000:

$$\frac{1}{\sqrt{f_{tube}}} = \log_{10} \left(\frac{\epsilon}{3.7D} + \frac{7.0}{Re^{0.9}} \right) \quad (4.13)$$

The friction factor for the coil's bends was calculated by the Nekrasov equation, as cited by [8], p. 353:

$$f_{bend} = \left(0.7 + 0.35 \frac{\theta_{bend}}{90} \right) \left(0.051 + 0.19 \frac{2r}{r_{bend}} \right) \quad (4.14)$$

Where θ_{bend} is the angle of the bend.

Heat transfer coefficient model

For the heat transfer from the fluid to the walls the Dittus-Boelter for turbulent flow and heating equation was employed:

$$Nu = 2.43 \times 10^{-2} Re^{0.8} Pr^{0.4} \quad (4.15)$$

This equation is valid for Reynolds over 10^3 and Prandtl number between 0.7 and 170.

4.3.2 gML to LSKM converter

When the LSKM foreign object is employed, since the components defined in the LSKM foreign object are different from the defined in Multiflash, the component list must be redefined. Also, as mentioned in section 4.3.1, the calculation of the fluid's enthalpy when the LSKM FO is used is not using Multiflash, but through data from the ReadData FO. This model thus changes the component list in the gML material, as well as the physical properties FO.

4.3.3 LSKM to gML converter

The LSKM to gML converter, opposite to the gML to LSKM converter, converts gML connection back to the Multiflash components and physical properties. While this is not relevant for the modelling of the coil, it is needed in case the cracker model is integrated with other models downstream.

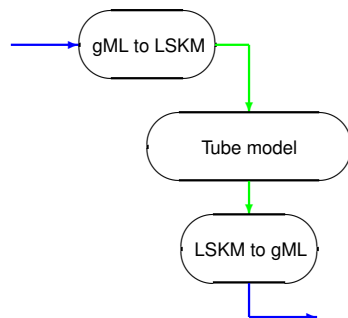


Figure 4.2: Schematic of the coil model. In this schematic the gML material which use Multiflash for property estimation are represented in blue and ones which use the ReadData.FO are in green.

4.4 Heat transfer models

4.4.1 Advanced energy input

The energy input model is used when the firebox model is not employed. In this case, this model is used to define the heat flux profile. This can be done by assuming a constant heat flux, constant temperature profile, prediction of the heat flux by estimation of the effective flame temperature. There is also an option to supply the model with a heat flux profile. For this work, only the constant heat flux option was considered.

4.4.2 Firebox model

The heat balance to the firebox is given by:

$$F_G h_G - F_f h_f - F_a h_a + Q_C + Q_R = 0 \quad (4.16)$$

Where F_G , F_f , and F_a are respectively the flowrates of the flue gas, fuel, and air fed to the furnace, and h_G , h_f , and h_a are respectively the specific enthalpies of the flue gases, fuel and air, which are calculated using Multiflash. The heat of convection, Q_C , was considered in this balance using an assigned heat transfer coefficient, using equation 2.6.

Considering the reference state as in the heat balance to the coil, the heat of combustion is not presented as it is included in the enthalpy of formation.

The heat of radiation is given by equation 2.7, considering the flue gas as non-grey gas. Thus, the total exchange area between gas and sink in radiative equilibrium, $(\overline{GS}_1)_R$, is calculated by equation 2.19, where the emissivity used is the effective emissivity, calculated using equation 2.15.

The furnace was also assumed to be able to be divided as explained in section 2.4.4. However, the heat balance is rewritten in the format of equation 4.16:

$$\begin{aligned} \Delta H_{flue\ gas,1} - \Delta H_{flue\ gas,2} - \Delta H_{fuel,1} - \Delta H_{air,1} + \\ Q_{convection,1} + Q_{radiation,1} + \sigma A_0 (T_{G2}^4 - T_{G1}^4) = 0 \end{aligned} \quad (4.17a)$$

$$\begin{aligned} \Delta H_{flue\ gas,n} - \Delta H_{flue\ gas,n+1} - \Delta H_{fuel,n} - \Delta H_{air,n} + \\ Q_{convection,n} + Q_{radiation,n} + \sigma A_0 (T_{G(n-1)}^4 - T_{Gn}^4) + \sigma A_0 (T_{G(n+1)}^4 - T_{Gn}^4) = 0 \end{aligned} \quad (4.17b)$$

$$\begin{aligned} \Delta H_{flue\ gas,N} - \Delta H_{fuel,N} - \Delta H_{air,N} \\ + Q_{convection,i} + Q_{radiation,i} + \sigma A_0 (T_{G(N-1)}^4 - T_{GN}^4) = 0 \end{aligned} \quad (4.17c)$$

Chapter 5

Results

5.1 Implementation of the molecular mechanism

The validation of the constructed models is based on data from Li et al. [16]. The inputs used for the simulation are on table 5.1:

Table 5.1: Geometry parameters of the coil in the studied cases

Input	Value
Coil length (m)	400
Internal diameter (m)	0.1013
Tube wall thickness (m)	0.0065
Number of bends	19
Feed flowrate per coil (t/h)	21
Coil inlet temperature (°C)	260
Coil inlet pressure (kPa)	2355

The molecular mechanisms tested were from the above mentioned source, as well as the mechanisms from Kaggerud [13] and Dimian and Bildea [6]. These are based on the following reactions:



The kinetic parameters used for the simulation are on appendix A.

To test the different kinetic mechanisms, the one-dimensional tube model was used with the geometry from Li et al. [16] reported above. In these simulations, a constant heat flux was used, and the only input changed in the models was the kinetic parameters used. The results were then compared with plant data reported by Li et al. [16], as well as the profiles simulated by the author.

Firstly, the coil outlet temperature (COT) was assigned to the reported value of 756 K. The obtained results with the different mechanisms can be found in table 5.8 and the temperature and heat flux profile

in the coil for the different mechanism in figures 5.1 and 5.3.

Table 5.2: Simulation results using the geometry in Li et al. [16] and assigning a COT of 756 K

	Conversion (%)		Selectivity (%)		Pressure drop (bar)	
	Value	Difference	Value	Difference	Value	Difference
Mechanism by Li et al. [16]	61.9	13	94.2	-0.8	5.10	-7
Mechanism by Kaggerud [13]	17.6	-68	100	5.3	4.13	-25
Mechanism by Dimian and Bildea [6]	0.4	-99	100	5.3	3.81	-31
Plant data [16]	55	-	95	-	5.49	-

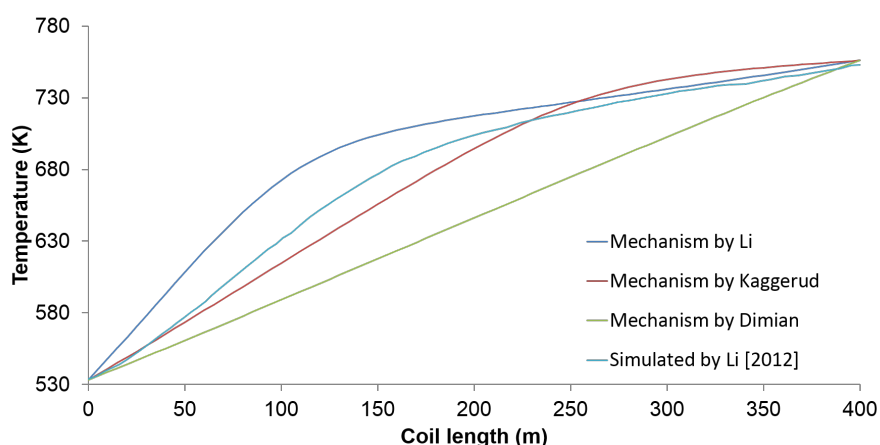


Figure 5.1: Temperature profile in the coil for different molecular mechanisms at a fixed COT of 756 K

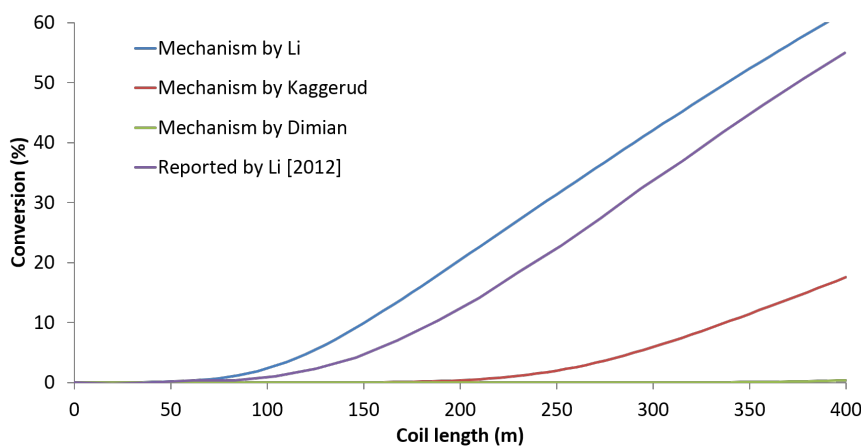


Figure 5.2: Conversion profile in the coil for different molecular mechanisms at a fixed COT of 756 K

It can be seen that none of the mechanisms can correctly predict the EDC conversion for the COT of the simulated case, with the mechanisms by Kaggerud [13] and Dimian and Bildea [6] underestimating EDC conversion and Li et al. [16] overestimating it.

Regarding the mechanism by Dimian and Bildea [6], it can be seen in figure 5.2 that the reaction doesn't significantly occur. In this mechanism, it is mentioned in the article that the main reactions starts only at 480 °C, which is a temperature much higher than reported by Li et al. [16].

Concerning the mechanism by Kaggerud [13], it can be seen in the conversion profile the cracking

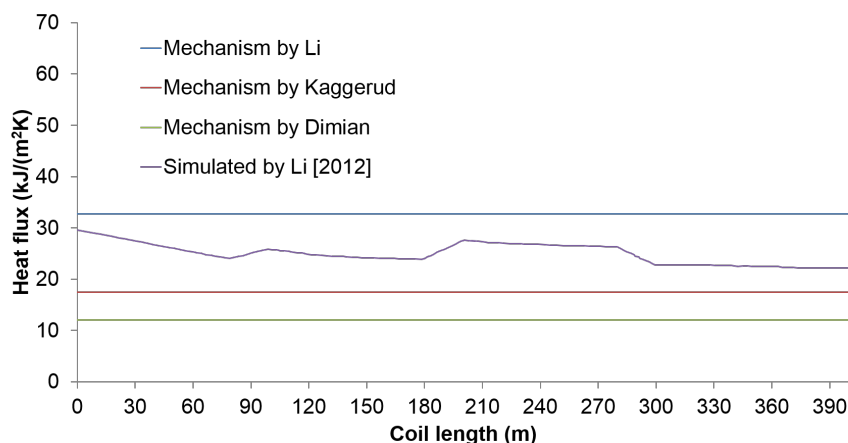


Figure 5.3: Heat flux profile in the coil for different molecular mechanisms at a fixed COT of 756 K

reaction starts only at 420 °C. However, it is also mentioned by Kaggerud [13] that cracking starts at lower temperatures, as using the commercial software EDC Crack[®], a 5% conversion at the entrance of the radiant section of the firebox was calculated, where temperatures are lower than 420 °C.

Analysing the conversion profile, it can be seen the conversion for the mechanism by Li et al. [16], the EDC cracking reaction starts at a lower coil length (around 90 m) than reported (around 120 m). This is due to the difference in the temperature profile, where for the simulated model the temperature increase is steeper, and cracking temperature (approximately 630 K) is reached faster than reported by Li et al. [16]. This explains the difference in the final conversion, where the simulation results predict a higher value. Also, since conversion is higher, a higher heat flux needs to be provided, to account for the energy needed in the endothermic reaction.

Regarding the difference in the temperature profiles between the different models, this is due to the heat flux calculated. For the mechanism by Li et al. [16], since the conversion at the assigned COT is higher, a higher heat flux is necessary in order to give the heat necessary for the endothermic cracking reactions, and consequently there is a quicker temperature increase at the beginning of the coil. For the mechanisms by Kaggerud [13] and Dimian and Bildea [6], since the conversion is lower, the heat flux is lower, and thus the temperature increase is also lower.

Regarding the selectivity, it can be seen that using the mechanism reported by Li et al. [16] the selectivity is similar to reported, albeit a little lower. This can be explained as conversion is also higher than expected, the concentration of vinyl chloride is higher than expected, and since VCM is the main reactant in by-product formation (through equation 5.1b), the reaction rate for the by-product formation increases and thus the selectivity is slightly lower.

Regarding the pressure drop, due to lack of information, it can be seen using the mechanisms from Li et al. [16] and Dimian and Bildea [6] the pressure drop is much lower than expected. This can be explained by the low conversion. Since the cracking reaction produces a higher number of molecules, the volumetric flow increases, which leads to a higher velocity in the coil. As showed in equation 4.6, higher velocities increase the pressure drop in the coil. However, it can also be seen the pressure drop using the mechanism by Li et al. [16] also underestimates the total pressure drop.

Alternatively, instead of assigning the COT, the EDC conversion can be fixed to the reported value. In this case, for the geometry reported by Li et al. [16], the simulation results are as follows:

Table 5.3: Simulation results using the geometry in Li et al. [16] and assigning a conversion of 55%

	COT (°C)		Selectivity (%)		Pressure drop (bar)	
	Value	Difference	Value	Difference	Value	Difference
Mechanism by Li et al. [16]	472.37	-2.2	95.4	0.4	4.98	-9.4
Mechanism by Kaggerud [13]	521.73	8.1	100	5.3	5.09	-7.3
Mechanism by Dimian and Bildea [6]	583.40	20.8	99.7	5.0	5.30	-3.4
Plant data [16]	482.85	-	95	-	5.49	-

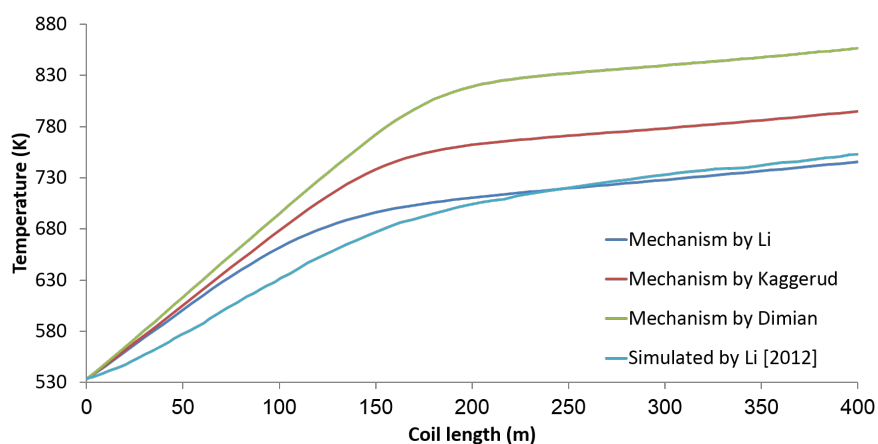


Figure 5.4: Temperature profile in the coil for different molecular mechanisms at a fixed conversion of 55%

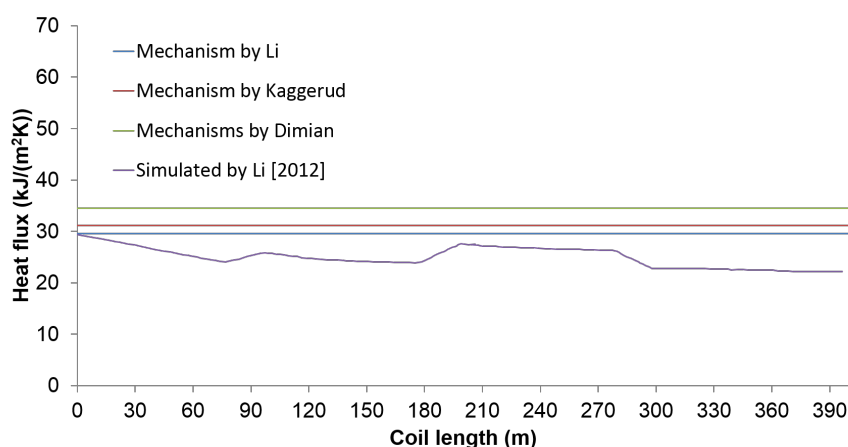


Figure 5.5: Heat flux profile in the coil for different molecular mechanisms at a fixed conversion of 55%

It can be seen in 5.4 that, for the mechanisms by Dimian and Bildea [6] and Kaggerud [13], the COT is clearly higher than reported. This is due to the high temperatures necessary for the cracking reaction to occur for these mechanisms, as was seen in the simulations using a fixed COT.

Regarding the mechanism used by Li et al. [16], again it can be seen that the initial temperature increase in the coil is higher than reported by Li et al. [16]. This is again due to the higher heat flux

calculated in the model. This higher heat flux is due to the higher heat capacity values estimated by Multiflash, which will be analysed further in section 5.4.1. It can be seen, despite this difference in the temperature profile in the beginning of the coil, the difference in the COT is lower than using the other mechanisms.

Regarding the selectivity, a higher selectivity using the mechanism by Li et al. [16] was obtained. This was expected, as the side reaction has higher activation energies. Since the simulated model has lower temperatures near the coil exit, the reaction rate for the side reaction is lower and thus selectivity is higher.

5.2 Firebox simulation

In this section, the firebox model is analysed. Firstly, the influence of using different correlations to estimate the flue gas emissivity is studied. It is also considered the use of a zone model for the firebox, where it is divided in several zones obtaining a temperature profile in the firebox. The data used in this simulation can be found on tables 5.4 and 5.5.

Table 5.4: Inputs used for the firebox model

Input	Value
Oxygen excess (% vol)	3
Furnace wall emissivity	0.75
Coil emissivity	0.85
Length (m)	20.898
Width (m)	1.900
Height (m)	6.700

Table 5.5: Composition of the fuel used

Component	% wt
C_4H_8	76.0
C_4H_6	20.0
C_4H_{10}	2.6
C_3H_8	0.7
H_2, C_1, C_2	0.7

Firstly, the single zone model was proposed to test the different correlations used to calculate the gas emissivities which were mentioned in the background (equations 2.10, 2.11, and 2.13). The coil profiles can be seen in figures 5.6 and 5.7, for a fixed conversion of 55%. It should be noted TMT refers to the tube metal temperature, which is the external temperature of the coil.

It can be seen that using a different emissivity correlation does not visibly affect the coil profiles, as expected. Since the conversion was fixed, the necessary heat flux, Q , in equation 2.5 is calculated in the coil model as the necessary energy for the reported conversion. Thus, a variation in the emissivity does not significantly change the coil profiles. However, a noticeable change can be seen between using the firebox model or assigning a constant heat flux. Since the flue gas temperature is constant in the single

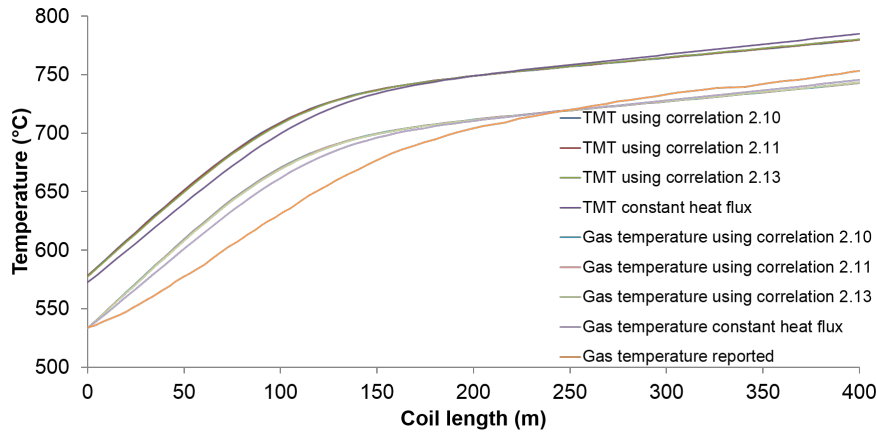


Figure 5.6: Temperature profile in the coil for different emissivity correlations in the firebox, for a fixed 55% conversion and geometry and kinetics by [16], using a single zone model

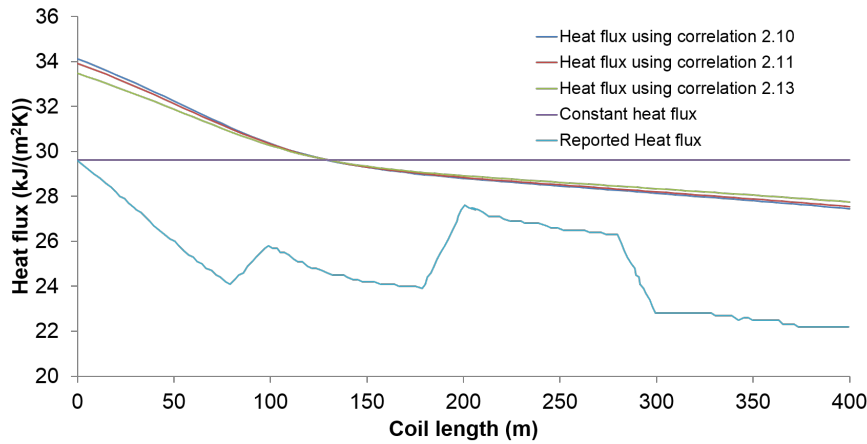


Figure 5.7: Heat flux profile in the coil for different emissivity correlations in the firebox, for a fixed 55% conversion and geometry and kinetics by [16], using a single zone model

zone model, it is expected that the heat flux is higher at the beginning of the coil, since the temperature gradient in equations 2.6 and 2.7 is higher. Thus, a higher heat flux and higher temperature increase can be seen in the first stages of the coil.

Regarding the firebox side, the results can be seen in table 5.7. It can be seen that, contrary to the coil side, the emissivity correlation used influences the firebox's results, as expected. The correlation by the VDI-Gesellschaft [28] estimates lower emissivities than the correlations by Perry et al. [23], and consequently higher values of flue gas temperature, to provide an equal amount of heat to the coil (according to equation 2.7, as lower emissivities decrease the radiation heat transfer area).

The flue gas temperature reported, however, is much lower than the results obtained in the simulations. The length of the coil used in the model (400 m) is longer than the value of 300 m usually mentioned in the literature. Thus, the simulated zone probably accounts for part of the shock or convection section, where heat transfer by convection is higher, and thus the transferred heat would increase. This would partly explain the higher flue gas temperature.

Regarding the fuel consumption, it can be seen all the models overestimate it. This is due to the

Table 5.6: Firebox results for the well-stirred furnace model
 Flue Gas temperature (K) Fuel Consumption (kg/t VCM)

	Value	Difference	Value	Difference	Gas emissivity
Correlation 2.10	1118	24%	77	6%	0.30
Correlation 2.11	1131	26%	77	7%	0.30
Correlation 2.13	1163	29%	79	10%	0.29
Constant heat flux	-	-	-	-	-
Plant data [16]	900	-	72	-	-

fact that, since the COT is higher than reported, the heat flux profile is higher (as can be seen in figure 5.7). This means more energy is required, and thus the fuel consumption is increased. Also, it should be noted that since the simulated flue gas temperature is higher, a greater amount of fuel is necessary, since the combustion of the fuel is less efficient. Comparing between the different correlations, since the required heat flux, Q , is the same for all simulations (since both the conversion and COT are the same), and the enthalpy of the flue gas leaving the firebox is higher (since the estimated flue gas temperature is higher), the fuel gas consumption is higher when the correlation from [28] is used.

It was also considered dividing the firebox. For this, the cases considered were of a well-stirred furnace (no divisions) and dividing the firebox in the number of coil passes. This is the maximum division without considering an angular temperature profile in the coil, as it considers each pass is enclosed in a zone of the firebox with constant properties.

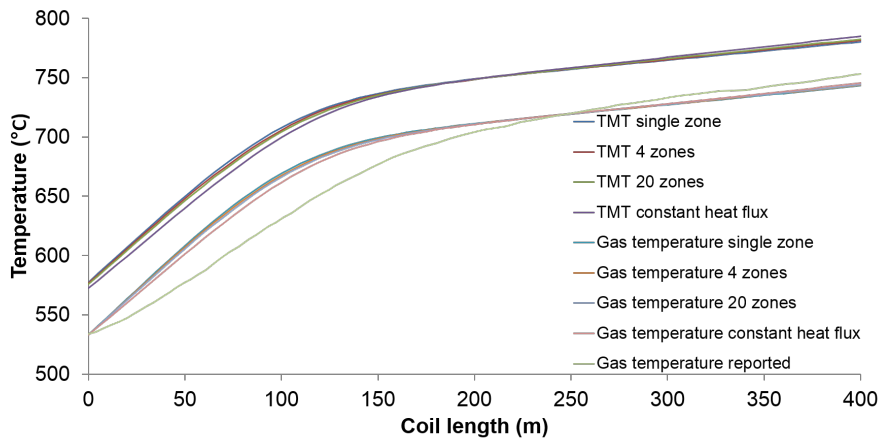


Figure 5.8: Temperature profile in the coil for different emissivity correlations in the firebox, for a fixed 55% conversion and geometry and kinetics by Li et al. [16], using a single zone model

It can be seen in figure 5.9 that, considering a higher number of zones, the heat flux profile along the coil is less steep, as the temperature in the firebox at the beginning of the coil is lower (as it corresponds to the exit of the firebox) and the temperature is higher at the end of the firebox. However, these changes in the heat flux profile do not seem to greatly influence the temperature profile in the coil.

Concerning the flue gas temperature leaving the furnace, it can be seen that increasing the number of zones in the firebox reduces the flue gas exit temperature. This is expected, as increasing the number of zones increases the temperature gradient in the coil. Also, since the flue gas temperature is lower when exiting the furnace, the fuel consumption decreases. However, despite this decrease, the fuel

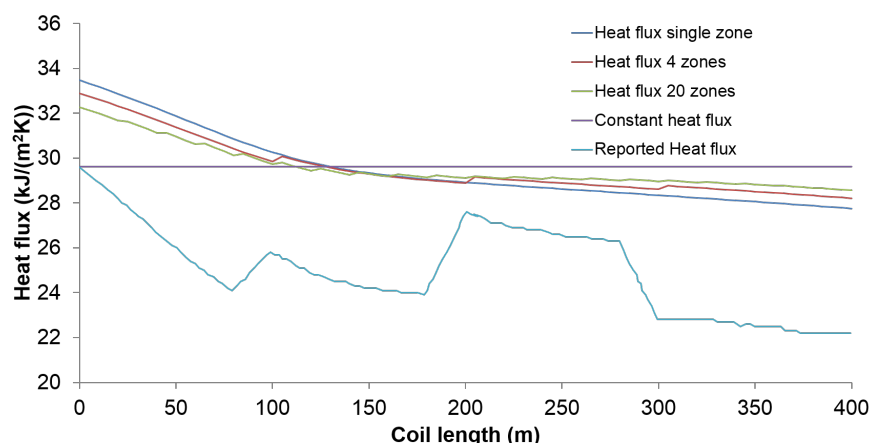


Figure 5.9: Heat flux profile in the coil for different emissivity correlations in the firebox, for a fixed 55% conversion and geometry and kinetics by Li et al. [16], using a single zone model

Table 5.7: Firebox results using different number of zones

	Flue Gas exit temperature (K)		Fuel Consumption (kg/t VCM)		Gas emissivity
	Value	Difference	Value	Difference	
Single zone	1163	29%	79	10%	0.29
4 zones	1156	28%	79	9%	0.29
20 zones	1141	27%	78	8%	0.29
Constant heat flux	-	-	-	-	-
Plant data [16]	900	-	72	-	-

consumption is still higher than what was reported by Li et al. [16].

5.3 Implementation of the radical mechanism

In this section, two radical mechanisms were tested: the one reported by Schirmeister [25], and by Borsa [2].

5.3.1 LSKM performance

To analyse the effect of compressing the kinetic mechanism, two simulations were considered, one where the LSKM foreign object was used and another where the matrices for the stoichiometric coefficients and forward and backward reaction orders were inserted in full in gPROMS. The simulations were performed in an Intel® Core™ i7-3770S CPU, with 16.0 GB of RAM.

Regarding the mechanism by Schirmeister et al. [25], the use of the LSKM FO did not seem to produce any visible results. This is due to the relatively small size of the problem, as the stoichiometric matrix has only 744 elements (composed of 24 species and 31 reactions). However, when the radical mechanism presented by Borsa [2], the stoichiometric matrix is composed of over 110,000 elements, the compression of the matrix significantly improves the run time of the simulation, as can be seen in figures 5.11–5.13.

```

System summary
Parameters:      248295
Variables:      158772
  User defined: 158258
  Eliminated:   -9486
Selectors:      19
Residual expressions: 158695
Jacobian expressions: 800544 in active branches, 800544 total
Performing Structural Analysis...

Structural analysis report
Variables:      158772
  Unknown:     158694
  Algebraic:   158693
  Differential: 1
  Known (assigned): 78
Equations:     158695
  Model equations: 158694
  Initial conditions: 1
Index of the problem: 1
Original problem is well posed

```

(a) Parameters and variables in the model using the LSKM FO

```

System summary
Parameters:      336071
Variables:      161190
  User defined: 170676
  Eliminated:   -9486
Selectors:      19
Residual expressions: 161113
Jacobian expressions: 915712 in active branches, 915712 total
Performing Structural Analysis...

Structural analysis report
Variables:      161190
  Unknown:     161112
  Algebraic:   161111
  Differential: 1
  Known (assigned): 78
Equations:     161113
  Model equations: 161112
  Initial conditions: 1
Index of the problem: 1
Original problem is well posed

```

(b) Parameters and variables in the model using the full stoichiometric matrix

Figure 5.10: Comparison of the number of parameters and variables using the mechanism by Borsa with and without compressing the stoichiometric matrix

```

Problem construction statistics...
Action          CPU: Total(s)  Sys(%) Memory: Delta(MB) After(MB)
-----
Parse (ObjectServer)  0.203    0.0    +13.1    22.4
Resolve parameters  5.507    3.7    +155.3   178.3
Write UnitTree data file  1.170   45.3    +0.1    178.4
Construct system    90.824   0.1    +531.3  709.7
Acquire licenses   0.016   100.0   +0.0    709.7
Run activity       556.721  0.5    +110.8   820.5

Peak memory usage: 1308.11 MB

Initialisation Procedure took 656 seconds.
Total CPU time: 654.299

```

(a) Run time using the LSKM FO

```

Problem construction statistics...
Action          CPU: Total(s)  Sys(%) Memory: Delta(MB) After(MB)
-----
Parse (ObjectServer)  4.040    3.9    +403.1   412.5
Resolve parameters  11.591   3.4    +232.2   644.6
Write UnitTree data file  1.607   35.9    +0.0    644.6
Construct system    169.479  0.2    +569.1  1213.7
Acquire licenses   0.000    0.0    +0.0    1213.7
Run activity       656.078  0.5    +137.7   1351.4

Peak memory usage: 1914.21 MB

Initialisation Procedure took 840 seconds.
Total CPU time: 838.802

```

(b) Run time using the full scheme

Figure 5.11: Comparison of the run time of the initialisation procedure with and without compressing the kinetic scheme

```

Problem construction statistics...
Action          CPU: Total(s)  Sys(%) Memory: Delta(MB) After(MB)
-----
Parse (ObjectServer)  0.156   10.0    +13.1    22.5
Resolve parameters  5.476    2.8    +151.3   174.6
Write UnitTree data file  1.217   26.9    +0.0    174.6
Construct system    94.147   0.3    +537.8  712.5
Acquire licenses   0.000    0.0    +0.0    712.5
Model pruning     12.714   0.2    +73.1    789.6
Run activity       8.642    4.5    +72.0    784.5

Peak memory usage: 1114.76 MB

Simulation took 124 seconds.
Total CPU time: 122.289

```

(a) Run time using the LSKM FO

```

Problem construction statistics...
Action          CPU: Total(s)  Sys(%) Memory: Delta(MB) After(MB)
-----
Parse (ObjectServer)  3.635    0.4    +403.0   412.4
Resolve parameters  10.967   0.7    +234.2   646.6
Write UnitTree data file  1.654   28.3    +0.1    646.7
Construct system    188.699  0.0    +563.5  1210.2
Acquire licenses   0.000    0.0    +0.0    1210.2
Model pruning     17.691   0.3    +88.3    1302.4
Run activity       33.181   1.6    +92.6    1302.8

Peak memory usage: 1655.99 MB

Simulation took 254 seconds.
Total CPU time: 252.285

```

(b) Run time using the full scheme

Figure 5.12: Comparison of the run time of the simulation using a saved variable set with and without compressing the kinetic scheme

As can be seen in figure 5.10, the compression of the matrix eliminates around one quarter of the parameters used in the simulation (from 336071 to 248295), which greatly reduces the simulation time of the model.

Figure 5.11 shows the run time for the initialisation procedure, a method used to obtain a first estimate of the variables. It can be seen that the use of the LSKM.FO does not greatly affect the overall run time of the simulation in this case. This is because when initialising the problem, the main task performed is the run activity of the system, and the LSKM.FO mainly reduces the time necessary to construct the

Problem construction statistics...					Problem construction statistics...				
Action	CPU: Total(s)	Sys(%)	Memory: Delta(MB)	After(MB)	Action	CPU: Total(s)	Sys(%)	Memory: Delta(MB)	After(MB)
Parse (ObjectServer)	0.156	0.0	+13.1	22.5	Parse (ObjectServer)	3.557	2.2	+402.7	412.1
Resolve parameters	5.288	2.1	+153.6	176.9	Resolve parameters	10.967	1.1	+230.9	643.0
Write UnitTree data file	1.201	32.5	+0.0	176.9	Write UnitTree data file	1.591	21.6	+0.0	643.1
Construct system	94.037	0.1	+535.6	712.4	Construct system	192.817	0.0	+567.2	1210.3
Acquire licenses	0.000	0.0	+0.0	712.4	Acquire licenses	0.000	0.0	+0.0	1210.3
Model pruning	12.698	0.0	+71.3	787.8	Model pruning	17.706	0.0	+88.0	1302.3
Run activity	48.002	1.1	+72.4	784.8	Run activity	79.763	1.1	+92.4	1302.7

Peak memory usage: 1157.58 MB

Simulation took 163 seconds.
Total CPU time: 161.352

Peak memory usage: 1698.12 MB

Simulation took 305 seconds.
Total CPU time: 302.907

(a) Run time using the LSKM FO

(b) Run time using the full scheme

Figure 5.13: Comparison of the run time of a simulation with a 10% variation of the assigned COT from the saved variable set with and without compressing the kinetic scheme

system (by eliminating the redundant stoichiometric coefficients).

As can be seen in figure 5.12, the simulation time using a saved variable set (obtained using the initialisation procedure) is reduced from 254 seconds to 124 seconds, and it can be seen that the greatest reduction in time is in the construction of the system. Running the simulation with a 10% change in the assigned COT regarding the saved variable set, the difference due to compressing the stoichiometric matrix becomes even greater, from 305 seconds to 163 seconds, as can be seen in figure 5.13.

Despite the improvement in the run time of the simulation, a greater improvement could be obtained should the matrices which contain the forward and backward reaction orders, n_f and n_r , were also compressed. This would lead to a further decrease in redundant parameters and decrease the time needed to construct the system.

5.3.2 Model performance

Using the LSKM FO, the following simulation results were obtained using the radical mechanisms mentioned above and the geometry reported by Li [16], for a fixed conversion of 55%:

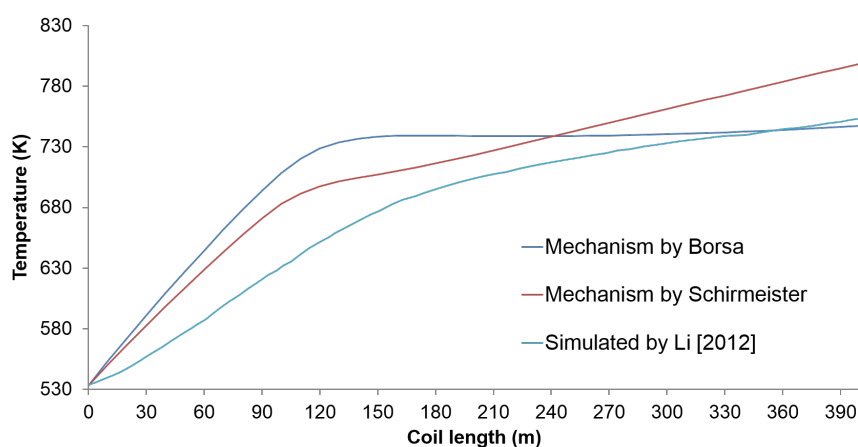


Figure 5.14: Temperature profiles using the geometry by Li and the radical mechanisms

It can be seen in 5.14 using the radical mechanism by Schirmeister et al. [25], the COT is over-estimated, which indicates the kinetic mechanism is not adequate for this geometry. Using the kinetic mechanism by Borsa, however, there is only a 2% deviation on the coil outlet temperature. It can also be

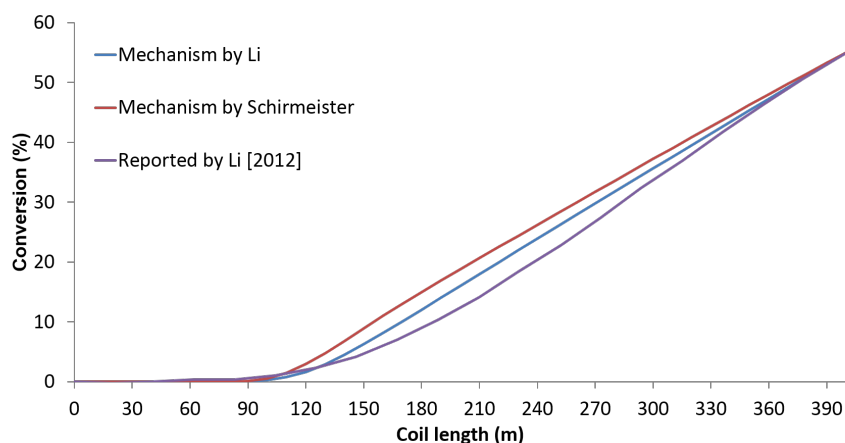


Figure 5.15: Conversion profiles using the geometry by Li et al. [16] and the radical mechanisms

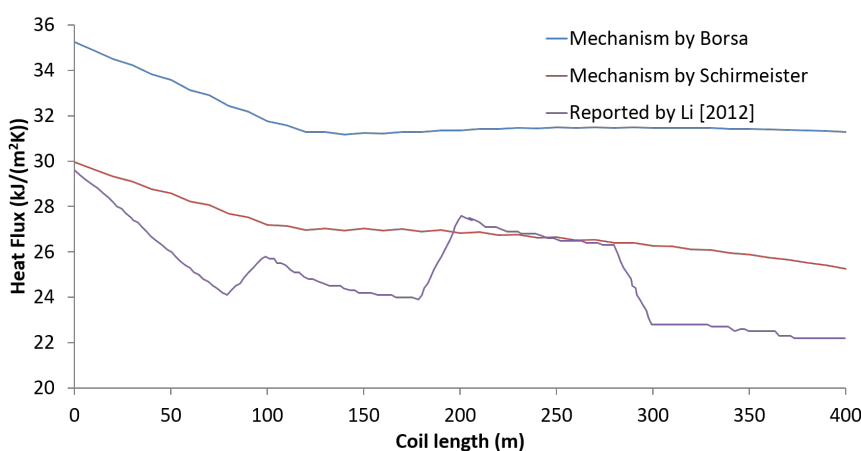


Figure 5.16: Heat flux profiles using the geometry by Li et al. [16] and the radical mechanisms

Table 5.8: Simulation results for the radical mechanisms using the geometry in Li et al. [16] and assigning a conversion of 55%

	Selectivity (%)		Pressure drop (bar)		Fuel consumption (kg/t VCM)	
	Value	Difference	Value	Difference	Value	Difference
Mechanism by Borsa [2]	95.9	1.0	4.99	-9	87.6	22
Mechanism by Schirmeister et al. [25]	98.6	3.8	5.07	-8	69.2	-4
Plant data [16]	95	-	5.49	-	72.0	-

seen in figure 5.15 that for all mechanisms the cracking reaction starts at the same coil length (around 120 m). This corresponds to a temperature of around 450 °C and 420 °C, respectively for the kinetic mechanism by Borsa and Schirmeister. These temperatures are higher than the one reported by Li et al. [16], where it starts at around 380 °C.

Concerning the heat flux, it can be seen that the heat flux using the mechanism by Schirmeister produces a heat flux close to the one reported in the article, while the heat flux using the mechanism by Borsa is higher. This is due to the lower selectivity: since the side reactions are endothermic, they require more energy, and thus the heat flux needed using the radical mechanism by Borsa is higher than

the one obtained when using the mechanism by Schirmeister.

Regarding the fuel gas consumed, as expected by analysing the heat flux, the consumption of fuel is higher in the mechanism by Borsa than what is reported.

Regarding the selectivity, Borsa's kinetic mechanism seems to produce a similar result to the one mentioned by [16], although a little higher. The mechanism by Schirmeister et al. [25], however, has a higher selectivity.

The coil outlet compositions for the used models can be seen in table 5.9. In this, the main by-products for both mechanisms are presented.

Table 5.9: Coil outlet compositions using the radical mechanisms

	Schirmeister et al. [25]	Borsa [2]
Ethylene dichloride	0.45	0.45
Vinyl chloride	0.3422	0.3332
Hydrogen chloride	0.2018	0.2066
1,1-dichloroethane	0.0038	2.38E-05
Acetylene	0.0003	0.0012
Benzene	1.1E-06	1.3E-08
Chloroprene (2-chlorabut-1,3-diene)	1.1E-06	0.0046
1,2-dichlorobut-3-ene	-	0.0015
1,2-trans-dichloroethylene	-	0.0011
3,4-dichlorobutene	0.0019	-

Since no experimental data is available on the outlet compositions, it is impossible to know which of these outlet concentrations better represents the real outlet coil composition. Regarding the mechanism by Schirmeister et al. [25], it can be seen that the main by-product is 1,1-dichloroethane, while for the mechanism by Borsa [2] the main by-product is chloroprene, followed by trans-dichloroethylene, acetylene, and 1,2-dichlorobut-3-ene.

5.4 Sensitivity analysis

In this section the model reported by Borsa [2] is tested to analyse the model's response to changing different process variables. In this model the furnace geometry reported by Li et al. [16] is used, with the radical mechanism by Borsa [2], as well as the firebox model using 20 divisions and the emissivity correlation reported in the VDI-Gesellschaft [28].

5.4.1 Analysis of the fluid properties

As mentioned in section 4.3.1, the calculation of the viscosity and thermal conductivity of the fluid was considered was performed using Multiflash considering only the main products. To analyse the effect of these properties on the overall results, a variation of 10% on these fluid properties were considered. The following results were obtained at the coil outlet's:

It can be seen that a 10% change in these properties does not affect the final results of the simulation.

Table 5.10: Results for the sensitivity analysis on the thermal conductivity and viscosity

	COT	Conversion	Selectivity	Pressure drop
Base case	482.85	66.0	93.9	5.24
-10% λ	482.85	66.0	93.9	5.25
+10% λ	482.85	66.0	93.9	5.25
-10% ν	482.85	66.0	93.9	5.24
+10% ν	482.85	66.0	93.9	5.25

Since selectivity is usually above 90%, the effect of not considering the viscosity and thermal conductivity of the by-products is not relevant on the overall results.

Regarding the heat capacity, the heat capacities from Multiflash and the ones obtained from Borsa were compared, as well as with data from Reid [24]. It can be seen in figures 5.17, 5.18, and 5.19 that the values obtained using Multiflash are higher than the ones calculated by Borsa [2] and Reid [24], which are closer to each other. This explains the steeper temperature increase in the radical mechanisms, since the heat capacity is lower, as well as the need for a higher heat flux when the molecular mechanism reported by Li et al. [16] is used (as was seen in figure 5.5).

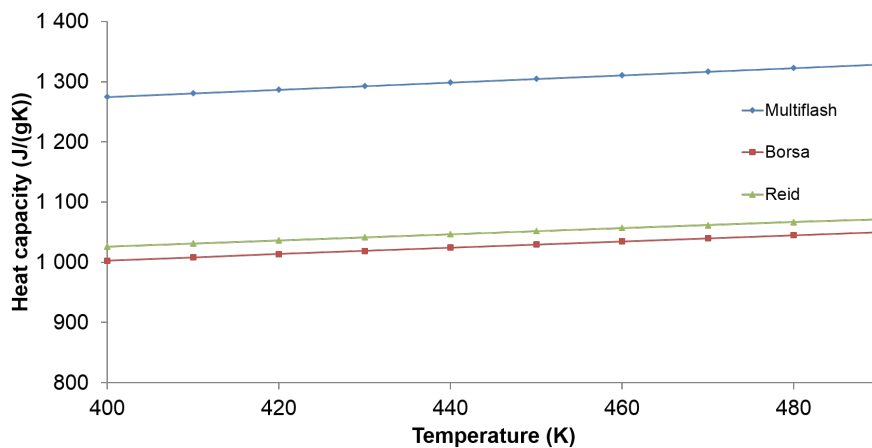


Figure 5.17: Estimation of the heat capacity for EDC

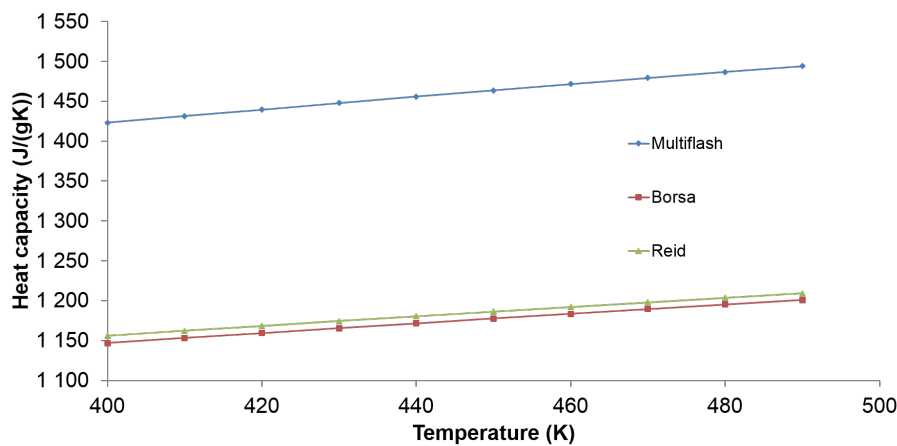


Figure 5.18: Estimation of the heat capacity for VCM

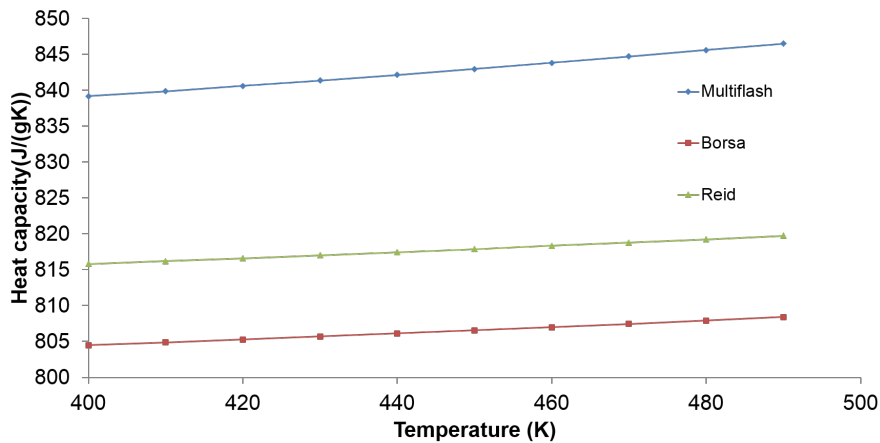


Figure 5.19: Estimation of the heat capacity for HCl

5.4.2 Analysis on the operating conditions

Fuel consumption

In this section, the effect of the fuel flowrate is analysed. The variation on the conversion is present in figure 5.20.

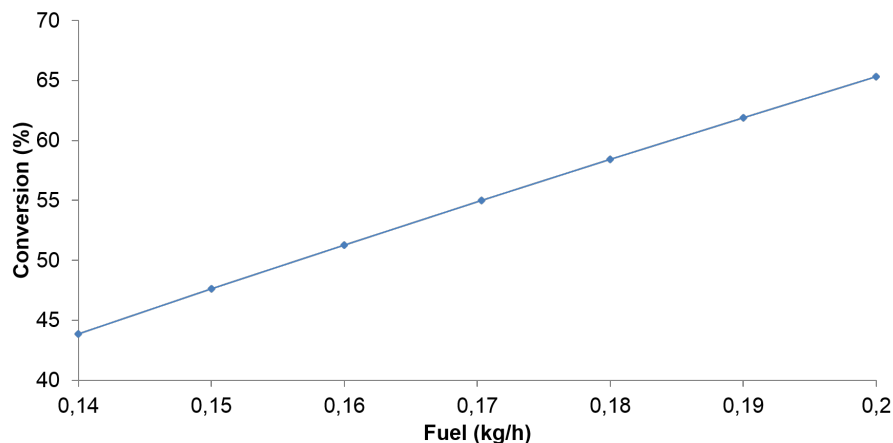


Figure 5.20: Influence of fuel flowrate on EDC conversion

It can be seen the conversion varies linearly with the fuel consumed. This is expected, as the increase of fuel increases the heat given to the coil, which in turn increases the reaction rate for the cracking reaction.

Regarding the coil outlet temperature, it can be seen in figure 5.21 that a small increase in the COT the conversion is greatly influenced. It can be seen that an increase on 1 °C makes an increase of 1.7% in conversion. This explains the fact that fixing COT grossly overestimates or underestimates conversion, as conversion is very sensitive to the COT.

Regarding the selectivity, it can be seen in figure 5.22 that the increase in conversion (due to higher fuel flowrate) decreases VCM selectivity. This was expected, as higher temperatures lead to more by-products formed. It can also be seen that this decrease is more accentuated at higher temperatures,

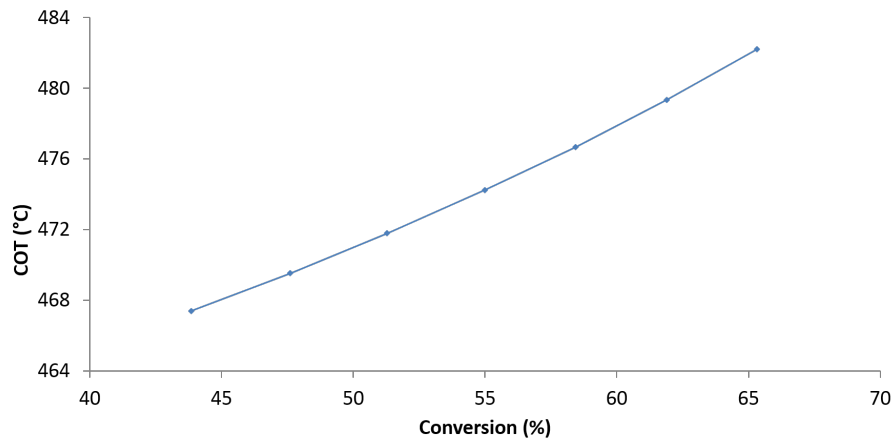


Figure 5.21: Relation between EDC and COT

which is expected as the temperature dependence in the reaction rate is exponential.

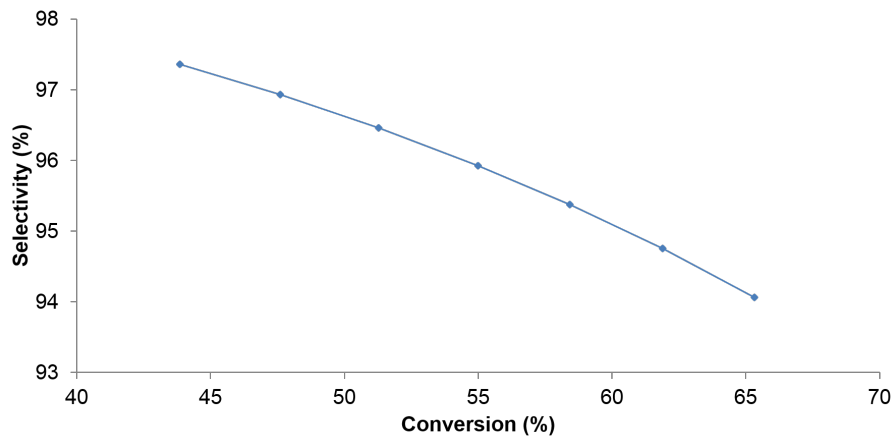


Figure 5.22: Variation of selectivity with conversion

The dependence of the specific fuel consumption (kg of fuel consumed per ton of VCM) with conversion is represented in figure 5.23. It can be seen there is a minimum of specific fuel consumption. This is due to the at lower conversions, less fuel is used; however, since the conversion is lower, less VCM is produced, and since the fuel consumption is expressed as kg of fuel per ton of VCM, less production of VCM represents in more specific fuel consumption. At high conversions, the increase of fuel consumed is greater than the increase in VCM production, and thus the specific fuel consumption increases.

Feed flowrate

The effect of the feed flowrate on the main operating conditions can be seen in figure 5.24. In these simulations a constant fuel flowrate was kept, and it can be seen that the conversion decreases with higher feed flowrates. This is expected, as a higher flowrate would need higher energy requirements to achieve the conversion needed with lower flowrates. The same can also be seen with the COT in figure 5.25.

Regarding the selectivity, it increases with higher flowrates. This is expected, because as was men-

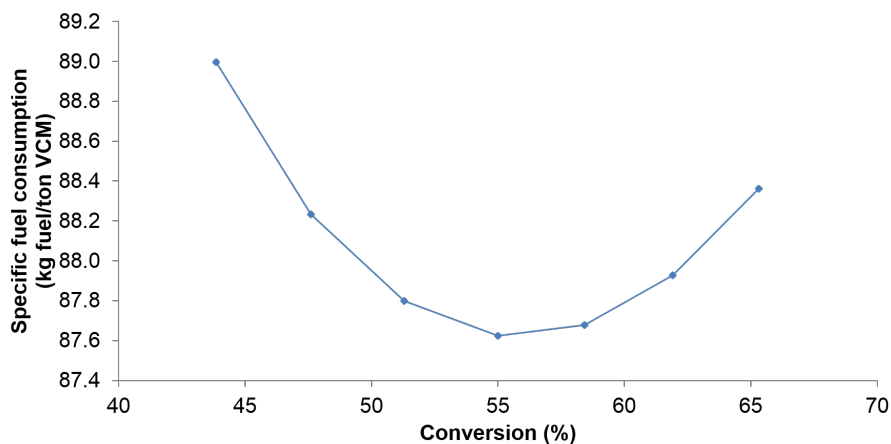


Figure 5.23: Variation of specific fuel consumption with conversion

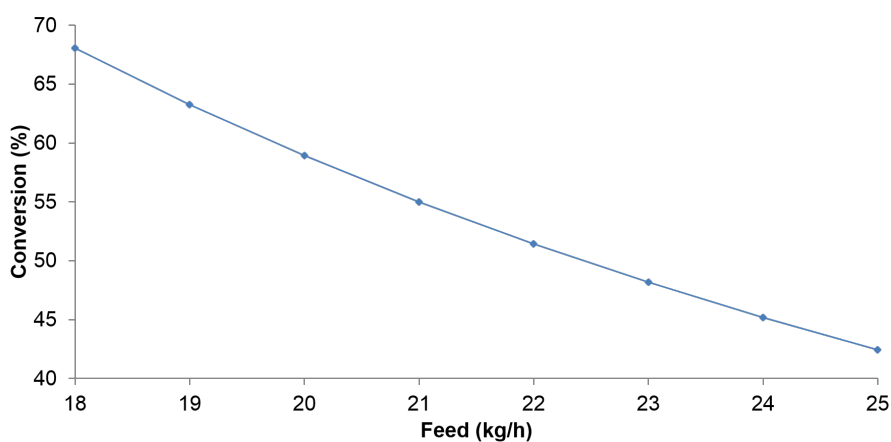


Figure 5.24: Variation of conversion with feed flowrate

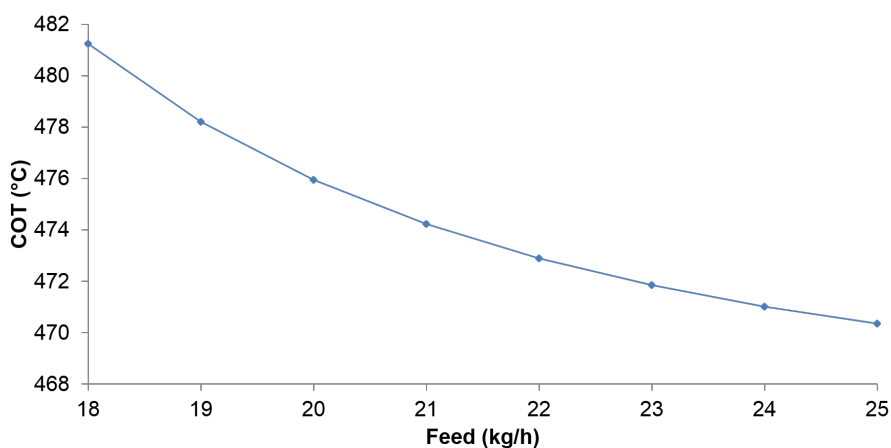


Figure 5.25: Variation of COT with feed flowrate

tioned, since the temperature in the coil is lower with increasing feed flowrate, the reaction rates for by-product formation decreases. It can also be seen in figure 5.27 the specific fuel consumption increases with higher feed flowrates. This again is due to the decrease in conversion, so the vinyl chloride produced decreases.

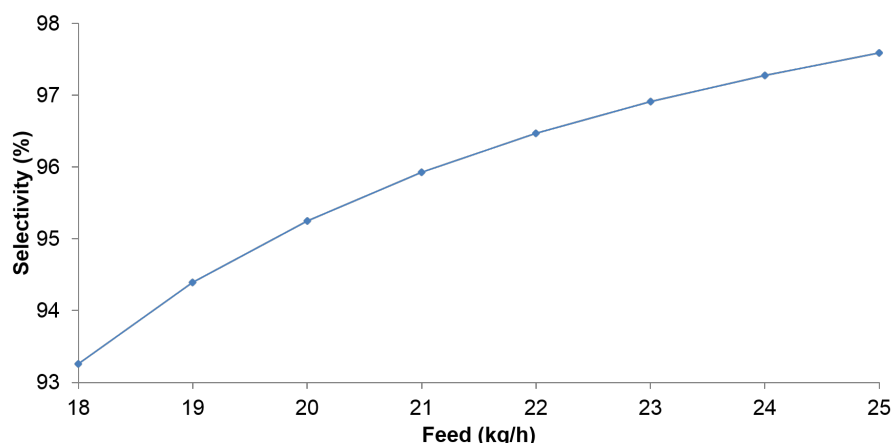


Figure 5.26: Variation of selectivity with feed flowrate

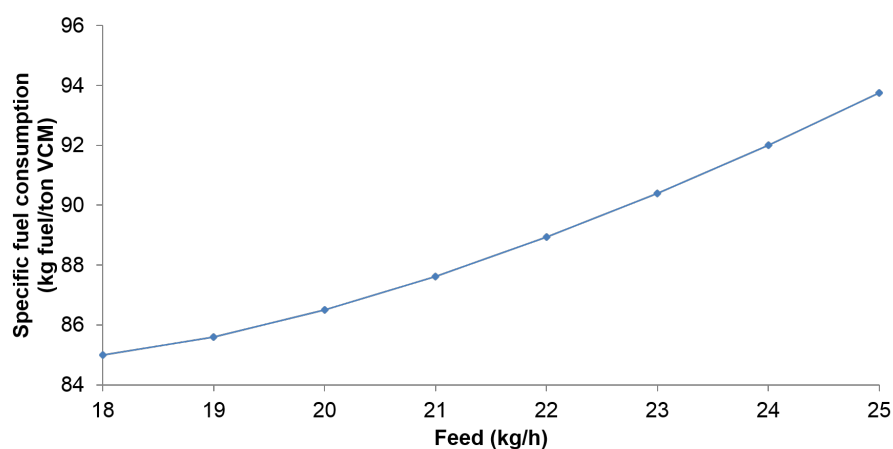


Figure 5.27: Variation of specific fuel consumption with feed flowrate

Coil inlet temperature

To analyse the influence of the coil inlet temperature (CIT), different CIT's were used in simulations with constant fuel flowrate.

The influence of the CIT on conversion can be seen in figure 5.28. It can be seen that higher CIT leads to higher conversions, which again is expected since the temperature profile in the coil will be higher. This also leads to a decrease in selectivity, as seen in figure 5.29.

Regarding the specific fuel consumption, it can be seen that it decreases with increasing CIT, which is expected because as was seen the conversion increases with higher CIT.

5.4.3 Promoters

As mentioned in section 2.7, the use of promoters for the cracking reaction can greatly increase the overall conversion, by acting either in the initiation or propagation of the radical reaction. This allows for lower coil temperatures, which reduces the fuel consumption. It should be noted however these promoters increase by-product formation and thus high concentrations might lead to problems in downstream separation.

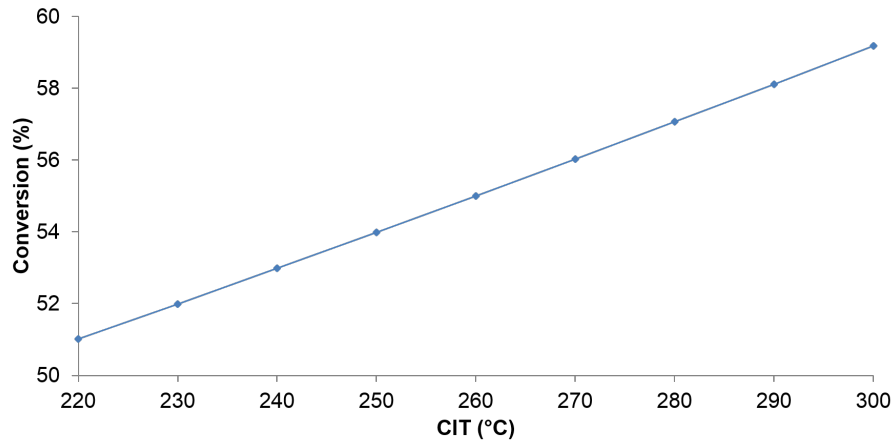


Figure 5.28: Variation of conversion with CIT

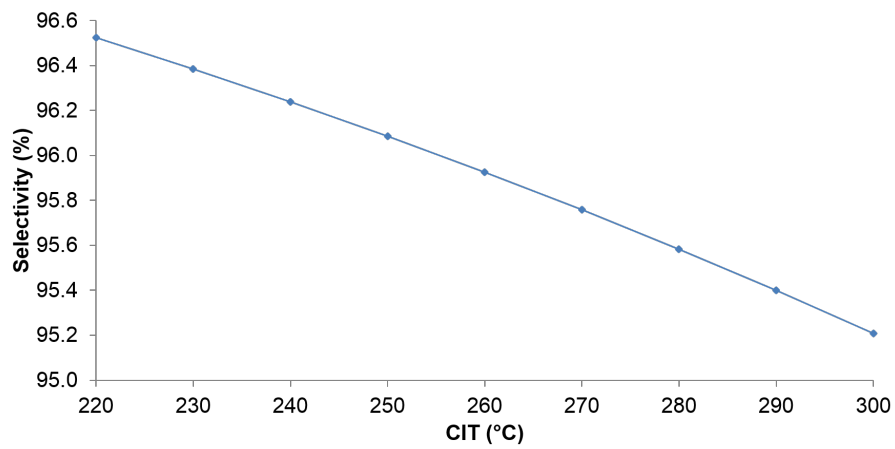


Figure 5.29: Variation of selectivity with CIT

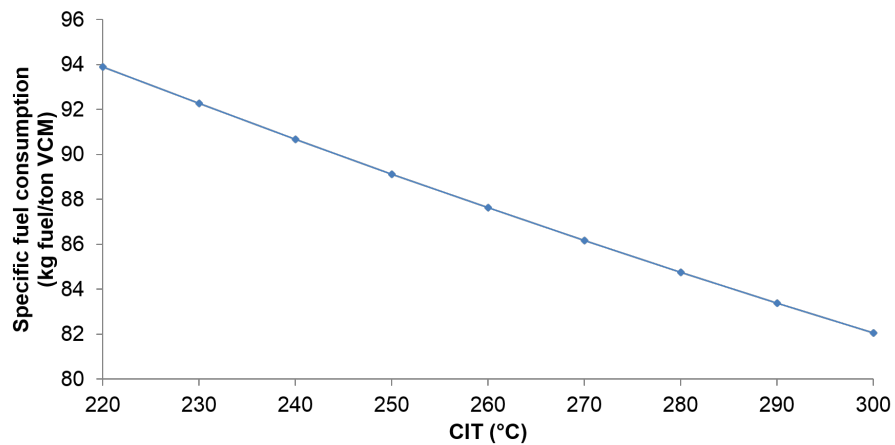


Figure 5.30: Variation of specific fuel consumption with CIT

For the simulations with the addition of promoters a constant conversion of 55% was assigned. It can be seen in figure 5.31 that the simulations using chlorine as a promoter reduce the coil outlet temperature, as expected. However, the same does not happen when using CCl_4 , where it can be seen that adding small quantities of carbon tetrachloride increases the COT by 4 °C. Adding higher quantities

of CCl_4 , however, slightly reduces the COT.

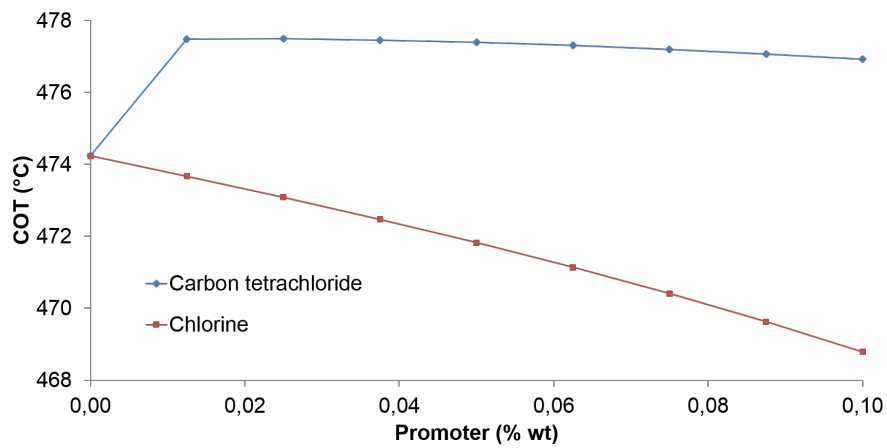


Figure 5.31: Influence of CCl_4 and Cl_2 on COT

Comparing the results with the results in the literature ([5], [17]) it can be seen that the mechanism by Borsa does not correctly predict the effect of carbon tetrachloride on the increase of conversion. For example, in [17], the addition of 200 ppm of CCl_4 is enough to increase the conversion by 2%. In [5], the addition of 1200 ppm increases conversion from around 52.4% to 65.4%. Thus, the reaction mechanism of CCl_4 cracking should be altered, in order to better represent its influence in EDC pyrolysis.

It can be seen that the addition of chlorine in the feed leads to an visible decrease in the COT. There is however, a sharp decrease in selectivity. This is consistent with the experimental results reported in [4], where the addition of 0.35 % wt of Cl_2 leads to a 100% EDC conversion at 465 °C.

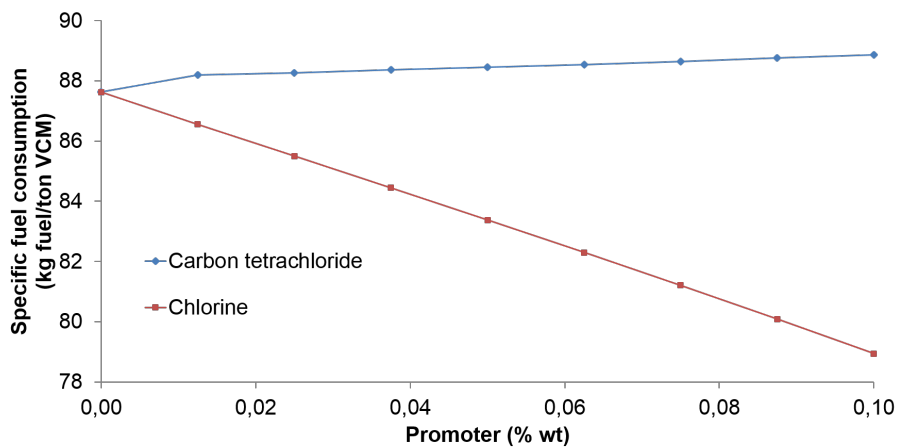


Figure 5.32: Influence of CCl_4 and Cl_2 on conversion

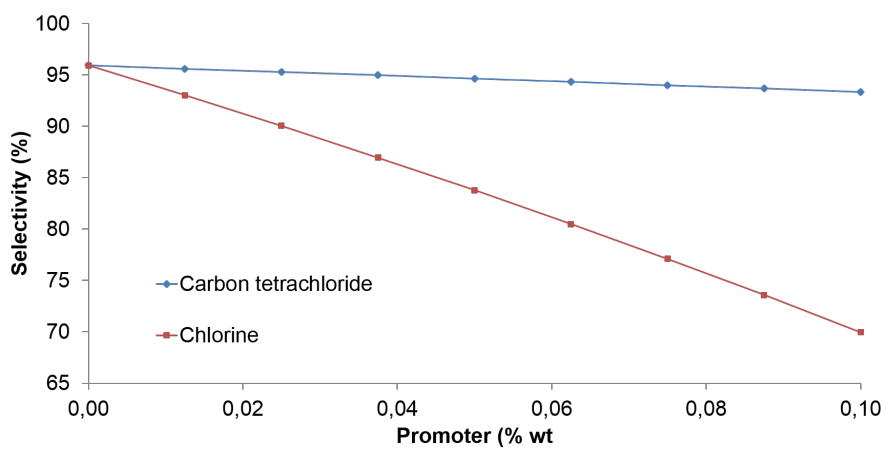


Figure 5.33: Influence of CCl_4 and Cl_2 on selectivity

Chapter 6

Conclusions

In this work a model was developed in order to simulate the process of ethylene dichloride (EDC) cracking to vinyl chloride (VCM). For this effect, a coil model was developed, where the EDC cracking mechanism was analysed, using different mechanisms available in the literature, molecular and radical. Besides the coil model, a model of the firebox was created, modelling the heat transfer of the flue gases to the coil by radiation. For this model, different correlations for estimating the flue gas emissivity were tested. It was also compared using a single zone firebox model with dividing the firebox in several zones. Finally, a sensitivity analysis was conducted on the main process variables.

Regarding the different molecular based kinetic mechanisms evaluated, it can be seen that different kinetics tested have different results on the COT needed to achieve the reported conversion of 55%, with some mechanisms clearly overestimating the needed COT. One of the tested mechanisms managed to predict the COT with a 2% error, even despite using a constant heat flux.

Regarding the radical kinetic mechanisms tested, two mechanisms were tested, one with 31 reactions and 24 species initially reported by Schirmeister et al. [25], and a detailed radical mechanism with 818 reactions and 135, of which 64 radical, reported by Borsa [2]. The most complex, reported by Borsa [2], estimates the COT with a 2% error, while the mechanism by Schirmeister et al. [25] overestimates the COT by 9%. Concerning the by-product formation, both models predict quite different outlet compositions, where for the mechanism by Borsa [2] the main by-products are chloroprene, dichlorobutene and acetylene, while for the mechanism by Schirmeister et al. [25] the main by-products are 1,1-dichloroethane and dichlorobutene.

To reduce the run time of the simulation using a radical mechanism, the stoichiometric matrix was compressed by eliminating the non-zero elements. When this is done, an overall reduction in the computing time can be seen, especially in the time needed to construct the system. The reduction is more considerable the bigger the kinetic mechanism used, as it was seen that using the mechanism by Schirmeister et al. [25] the computing time is not significantly reduced. When compressing the stoichiometric matrix of the mechanism by Borsa [2], the run time is halved. This allows using a more complex mechanism while still keeping a run time which allows for integration with other models, allowing for a detailed model of the full plant.

Regarding the firebox model, it can be seen using the models employed in this work the results do not seem to fit the available data regarding flue gas temperature and fuel consumption. This is in part due to the coil model overestimating the heat flux, which leads to a higher energy consumption and consequently higher fuel flowrates. The flue gas temperature exiting the firebox is also higher than reported, which may mean a problem in the modelling of the heat transfer in the firebox, namely on the heat transferred by convection.

Regarding the sensitivity analysis performed on the model, a minimum in fuel consumption per ton of produced VCM can be seen when the fuel flowrate is varied, for a conversion of 55%. However, special attention must be had when increasing fuel flowrate, as it leads to a decrease in selectivity which may cause problems on downstream separation.

The sensitivity analysis on the addition of CCl_4 on the feed showed that the kinetic mechanism by Borsa [2] does not correctly predict its effect, as adding it increases the temperature needed to achieve the desired conversion, contrary to what is reported in the literature. However, adding chlorine to the feed greatly reduces the COT as expected, but also decreases the selectivity, so more studies should be performed to analyse if its addition is beneficial to the process.

6.1 Achievements

This work was set out to test different kinetic mechanisms and to compare each other with plant data, extracted from Li et al. [16]. Taking that into account, a one-dimensional coil model was developed, with which several molecular and radical mechanisms were tested.

Moreover, when using a large scale kinetic mechanism, it was compressed using a scheme by Tewarson [26]. This allowed a significant time reduction even using mechanisms with a considerable size, which allows for a better prediction of by-product concentrations, which allow for a rigorous prediction of the coil outlet conditions.

A firebox model was developed which can use different correlations present in the literature to estimate the flue gases emissivity. This firebox model can be single zone, or it can be done in order to account for multiple zones, which discretise the firebox along its height. Using it, it was found that the different correlations used in estimating gas emissivity for flue gases produce very similar results, and that for the EDC cracker, dividing the furnace in several zones does not seem to have a great influence on the profiles along the coil.

6.2 Future Work

Despite the work done on this model, several improvements should be made in order to better describe the system. Firstly, the case study used to validate the model was the one reported by Li et al. [16], being the one with the most data required to fully compare the model results with plant data. However, more data is needed to further validate the model, such as rigorous inlet and outlet composition, as well as the temperature profile along the coil.

Regarding the firebox model further studies should be performed on the heat transfer between the different zones in the firebox. More complex heat transfer models can be applied, to analyse if they can reduce the difference in the flue gas outlet temperature, namely not considering the heat transfer between zones by radiation as the Stefan–Boltzmann equation, but considering the gas emissivity. Also, more work should be done to model the influence of convection on the process, to analyse its influence in the zones of the firebox which are at lower temperatures.

Other kinetic mechanisms should also be tested, to analyse the most appropriate kinetic mechanism to describe the series of reactions which happen in the coil, as well as the influence of reaction initiators and inhibitors.

One thing that should be better approached is the fluid properties' estimation. Although it can be seen that the conductivity and viscosity do not greatly influence the coil results, the same cannot be said about the heat capacity. Regarding the heat capacity, it can be seen that when using the data from Borsa [2] the temperature increase is steeper than using the heat capacities calculated by Multiflash. This is in part due to the higher heat capacity calculated by the Multiflash properties package. Thus, more work should be done on this, to assure a good prediction of the fluid's physical properties.

Another improvement that could be done would be to convert this model into a dynamic model, adding the coke formation in time. This is an essential part in the operating conditions of this cracking reactor, as coke formation leads to an increase in pressure drop and decrease of overall efficiency, eventually requiring the shutdown of the EDC cracker. For this effect, Schirmeister et al. [25] proposes a coking equation involving acetylene; however, a coking equation with chloroprene would be more adequate, since a relation between the formation of coke and outlet chloroprene concentration was found by Borsa et al. [4]. An optimisation of the run length would also be of great advantage, as it could lead to a more in–depth knowledge of the influence of certain factors in the overall performance of the cracker, such as higher temperatures or the use of initiators.

Finally, since there is a clear dependence of the hydrochlorination and EDC cracker due to the recycling of the HCl and EDC, proceeding to a rigorous full plant modelling and optimisation could lead to potential plant savings.

Bibliography

- [1] F. Benyahia. VCM process design. *Chemical Engineering Education Journal*, 39(1):62–67, 2005.
- [2] A. G. Borsa. *Industrial plant/laboratory investigation and computer modeling of 1,2-dichloroethane pyrolysis*. PhD thesis, Colorado School of Mines, 1999.
- [3] A. G. Borsa, A. M. Herring, J. T. McKinnon, R. L. McCormick, S. Yamamoto, Y. Teraoka, and Y. Natori. Characterization of Coke Formed in Vinyl Chloride Manufacture. *Ind. Eng. Chem. Res.*, 35(11):4259–4267, 1999.
- [4] A. G. Borsa, A. M. Herring, J. T. McKinnon, R. L. McCormick, and G. H. Ko. Coke and Byproduct Formation during 1,2-Dichloroethane Pyrolysis in a Laboratory Tubular Reactor. *Ind. Eng. Chem. Res.*, 40(11):2428–2436, 2001.
- [5] B.-S. Choi, J. S. Oh, S.-W. Lee, H. Kim, and J. Yi. Simulation of the Effects of ccl_4 on the Ethylene Dichloride Pyrolysis Process. *Ind. Eng. Chem. Res.*, 40(19):4040–4049, 2001.
- [6] A. C. Dimian and C. S. Bildea. *Chemical Process Design: Computer-Aided Case Studies*, chapter Vinyl Chloride Monomer Process, pages 201–230. Wiley–VCH, 2008.
- [7] E.-L. Dreher, T. R. Torkelson, and K. K. Beutel. Chloroethanes and Chloroethylenes. In *Ullman's Encyclopedia of Industrial Chemistry*. Wiley–VCH, 2012.
- [8] G. F. Froment and K. B. Bischoff. *Chemical Reactor Analysis and Design*. Wiley–VCH, second edition, 1990.
- [9] H. C. Hottel and A. F. Sarofim. *Radiative transfer*. McGraw–Hill, 1972.
- [10] K. E. Howlett. The pyrolysis of 1,2-dichloroethane. *Transactions of the Faraday society*, 48:25–34, 1952.
- [11] J. A. Incavo. A Detailed Quantitative Study of 1,2-Dichloroethane Cracking to Vinyl Chloride by a Gas Chromatographic Pyrolysis Device. *Ind. Eng. Chem. Res.*, 35:931–937, 1996.
- [12] D. Jo, J. Bae, J. Kim, B. Oh, and S. B. Ha. Method of inhibiting coke formation in ethylene dichloride pyrolysis cracker, Nov. 2006. Patent no. US 7,132,577 B2.
- [13] T. H. Kaggerud. Modeling and EDC Cracker using Computational Fluid Dynamics (CFD). Master's thesis, Norwegian University of Science and Technology, June 2007.

- [14] A. Lakshmanan, W. C. Tooney, and L. T. Biegler. A case study for reactor network synthesis: the vinyl chloride process. *Computers and Chemical Engineering*, 23:479–495, 1999.
- [15] K. Y. Lee. Numerical Simulations of the Pyrolysis of 1,2-Dichloroethane. *KSME International Journal*, 16(1):102–108, 2002.
- [16] C. Li, G. Hu, W. Zhong, H. Cheng, W. Du, and F. Qian. Comprehensive Simulation and Optimization of an Ethylene Dichloride Cracker Based on the One-Dimensional Lobo-Evans Method and Computational Fluid Dynamics. *Ind. Eng. Chem. Res.*, 52:645–657, 2012.
- [17] C. Li, G. Hu, W. Zhong, W. Du, and F. Qian. Coke Deposition Influence Based on a Run Length Simulation of a 1,2-Dichloroethane Cracker. *Ind. Eng. Chem. Res.*, 52:17501–17516, 2013.
- [18] D. T. T. Limited. PVC markets of Europe and South-East Asia: analysis of profitability and production cost. http://www.deloitte.com/assets/Dcom-Russia/Local%20Assets/Documents/Energy%20and%20Resources/dttl_PVC-markets-of-Europe-and-South-EastAsia_EN.pdf, October 2014.
- [19] D. Ma and G. Shahani. Improve the cracking of ethylene dichloride. *Hydrocarbon Processing*, pages 61–62, April 2014.
- [20] L. S. Marks, T. Baumeister, E. A. Avallone, and T. Baumeister III. *Marks' Standard Handbook for Mechanical Engineers*. McGraw-Hill, 1996.
- [21] I. Mochida, T. Tsunawaki, C. Sotowa, Y. Korai, and K. Higuchi. Coke Produced in the Commercial Pyrolysis of Ethylene Dichloride into Vinyl Chloride. *Ind. Eng. Chem. Res.*, 35(10):3803–3807, 1996.
- [22] P. Mullinger and B. Jenkins. *Industrial and Process Furnaces - Principles, design and operation*. Butterworth-Heinemann, first edition, 2008.
- [23] R. H. Perry, D. W. Green, and J. O. Maloney. *Perry's Chemical Engineers' Handbook*. McGraw-Hill International Editions, seventh edition, 1997.
- [24] R. C. Reid. *Parameters of the properties of gases & liquids*. McGraw-Hill, fourth edition, 1988.
- [25] R. Schirmeister, J. Kashnitz, and M. Träger. Influence of EDC Cracking Severity on the Marginal Costs of Vinyl Chloride Production. *American Chemical Society*, 2009.
- [26] R. P. Tewarson. Sparse Matrices. In *Mathematics in Science and Engineering*, volume 99. Academic Press Inc., 1973.
- [27] Y. Tong. Phosphine coke inhibitors for EDC-VCM furnaces, Sep. 2002. Patent no. US 6,454,995 B1.
- [28] VDI-Gesellschaft, editor. *VDI Heat Atlas*. Springer Reference, second edition, 2010.

Appendix A

Kinetics

A.1 Molecular kinetics

The molecular mechanisms are based on equations 5.1a, 5.1b, and 5.1c. The kinetic parameters, k_0 , E_a , and n , needed for equation 4.9a are on tables A.1, A.2, and A.3.

Table A.1: Kinetic parameters for the mechanism by Kaggerud [13]

	$k_0 \text{ mol/m}^3\text{s}$	$E_a \text{ J/mol}$	n
Reaction 5.1a	1.2×10^{12}	194.12×10^3	-0.05
Reaction 5.1b	0	0	
Reaction 5.1c	0	0	

Table A.2: Kinetic parameters for the mechanism by Li et al. [16]

	$k_0 \text{ mol/m}^3\text{s}$	$E_a \text{ J/mol}$	n
Reaction 5.1a	5.507×10^7	123.86×10^3	0
Reaction 5.1b	5.580×10^7	137.78×10^3	0
Reaction 5.1c	0	0	

Table A.3: Kinetic parameters for the mechanism by Dimian and Bildea [6]

	$k_0 \text{ mol/m}^3\text{s}$	$E_a \text{ J/mol}$	n
Reaction 5.1a	0.36×10^{14}	242.67×10^3	-0.05
Reaction 5.1b	0.5×10^{14}	288.70×10^3	0
Reaction 5.1c	1.0×10^{13}	301.25×10^3	0

A.2 Radical kinetics

For the mechanism by Schirmeister et al. [25], the following species were considered:

no.	reaction	frequency factor k_0 [(cm ³ /mol) ⁿ s ⁻¹]	n	activation energy E_a (kJ/mol)
1	EDC → R1 + R2	5.9×10^{15}	1	342
2	CCl4 → R1 + R8	2.2×10^{12}	1	230
3	EDC + R1 → HCl + R3	1.3×10^{13}	2	7
4	EDC + R5 → VCM + R3	1.2×10^{13}	2	34
5	EDC + R2 → EC + R3	1.0×10^{12}	2	42
6	EDC + R4 → 1,1 + R3	5.0×10^{11}	2	45
7	EDC + R6 → 1,1,2 + R3	2.0×10^{11}	2	48
8	EDC + R7 → 1,1,1,2 + R3	1.0×10^{11}	2	56
9	EDC + R8 → CHCl3 + R3	1.0×10^{12}	2	63
10	VCM + R1 → R4	9.1×10^{10}	2	0
11	VCM + R1 → HCl + R5	1.2×10^{14}	2	56
12	VCM + R5 → CP + R1	5.0×10^{11}	2	31
13	VCM + R4 → C4H6Cl2 + R1	2.0×10^{10}	2	30
14	VCM + R2 → EC + R5	3.0×10^{11}	2	61
15	R3 ↔ VCM + R1	2.1×10^{14}	1	84
16	R5 ↔ C2H2 + R1	5.0×10^{14}	1	90
17	R6 ↔ Di + R1	2.0×10^{13}	1	70
18	R7 ↔ Tri + R1	2.5×10^{13}	1	70
19	EC + R1 → HCl + R2	1.7×10^{13}	2	4
20	1,1 + R1 → HCl + R4	1.2×10^{13}	2	6
21	1,1,2 + R1 → HCl + R6	1.7×10^{13}	2	15
22	1,1,1,2 + R1 → HCl + R7	1.7×10^{13}	2	17
23	CHCl3 + R1 → HCl + R8	1.6×10^{13}	2	14
24	CCl4 + R5 → Di + R8	5.0×10^{11}	2	33
25	CCl4 + R4 → 112 + R8	1.0×10^{12}	2	33
26	CCl4 + R6 → 1112 + R8	5.0×10^{11}	2	33
27	R2 + R1 → VCM + HCl	1.0×10^{13}	2	13
28	R3 + R1 → Di + HCl	1.0×10^{13}	2	12
29	R6 + R8 → Di + CCl4	1.0×10^{13}	2	13
30	2C2H2 + R5 → C6H6 + R1	1.0×10^{14}	2	20
31	C2H2 + 2 R1 → 2C + 2 HCl	1.6×10^{14}	2	70

Figure A.1: List of species used on the mechanism by Schirmeister et al. [25]

The reactions for this mechanism are presented below:

no.	compound	short form
1	1,2-dichloroethane	EDC
2	vinylchlorid	VCM
3	hydrogen chloride	HCl
4	trichloromethane	CHCl3
5	tetrachloromethane	CCl4
6	ethylchloride	EC
7	1,1-dichloroethane	1,1
8	1,1,2-trichloroethane	1,1,2
9	1,1,1,2-/1,1,2,2-tetrachloroethane	1,1,1,2
10	1,1-/cis-/trans-dichloroethylene	Di
11	trichloroethylene	Tri
12	1-/2-chloroprene	CP
13	acetylene	C2H2
14	benzene	C6H6
15	3,4-dichlorobutene	C4H6Cl2
16	soot/coke	C
Radical		
1	Cl [*]	R1
2	CH ₂ Cl-CH ₂ [*] /CH ₃ -CHCl [*]	R2
3	CH ₂ Cl-CHCl [*]	R3
4	CHCl ₂ -CH ₂ [*]	R4
5	CHCl=CH [*] /CH ₂ =CCl [*]	R5
6	CH ₂ Cl-CCl ₂ [*] /CHCl ₂ -CHCl [*]	R6
7	CHCl ₂ -CCl ₂ [*] /CCl ₃ -CHCl [*]	R7
8	CCl ₃ [*]	R8

Figure A.2: List of species used on the mechanism by Schirmeister et al. [25]

For the mechanism by Borsa [2], the reaction list, along with the kinetic parameters for the forward reaction rate are presented on the following figures:

No.	Reaction	A (cm ³ -mol-s)	n	E _a (cal/mol)	Ref.
Molecular Elimination					
1.	CH ₃ CHCL ₂ =VCM+HCL	6.61E+13	-0.1	58000	E
2.	EDC=VCM+HCL	3.60E+13	0	58000	I
3.	VCM=C ₂ H ₂ +HCL	5.00E+13	0	69000	I
4.	C ₄ H ₅ CL ₃ _134D=C ₄ H ₄ CL ₂ _1413D+HCL	6.46E+10	0	47000	Ab
5.	C ₄ H ₆ CL ₂ _34D=C ₄ H ₅ CL_213D+HCL	6.46E+10	0	47000	Ab
6.	C ₄ H ₆ CL ₂ _34D=C ₄ H ₅ CL_113D+HCL	6.46E+10	0	47000	Ab
7.	C ₄ H ₅ CL ₃ _134D=C ₄ H ₄ CL ₂ _1313D+HCL	6.46E+10	0	47000	Ab
8.	CHCL ₃ =CCL ₂ +HCL	1.82E+12	0	54490	Ag
9.	CCL ₂ +EDC=C ₃ H ₄ CL ₄ _1223	1.80E+09	0	0	Ah
10.	C ₂ HCL ₃ =C ₂ CL ₂ +HCL	7.00E+15	0	84000	Ap
11.	CHCLCHCL_c=C ₂ HCL+HCL	3.63E+12	0	52700	Aq
12.	CHCLCHCL_t=C ₂ HCL+HCL	3.63E+12	0	52700	Aq
13.	CH ₂ CLCH ₃ =C ₂ H ₄ +HCL	3.00E+13	0	58000	I
14.	C ₂ H ₆ =C ₂ H ₄ +H ₂	1.20E+14	0	71000	I
15.	C ₂ H ₄ =C ₂ H ₂ +H ₂	1.00E+14	0	82000	I
16.	C ₄ H ₆ _13D=C ₂ H ₂ +C ₂ H ₄	5.00E+14	0	73000	I
17.	CH ₃ CCL ₃ =CHCLCHCL_t+HCL	5.80E+13	0	54000	I
18.	CH ₂ CLCHCL ₂ =CHCLCHCL_t+HCL	2.00E+13	0	59000	I
19.	CHCL ₂ CHCL ₂ =HCL+C ₂ HCL ₃	1.30E+13	0	58000	I
20.	CHCL ₂ CCL ₃ =HCL+C ₂ CL ₄	1.00E+13	0	58000	I
21.	C ₂ H ₄ +C ₂ H ₄ =C ₄ H ₆ _13D+H ₂	1.50E+07	0	39000	I
22.	C ₂ H ₄ +C ₄ H ₆ _13D=benzene+H ₂	3.00E+07	0	26500	I
23.	C ₂ H ₂ +C ₄ H ₆ _13D=benzene+H ₂	1.50E+08	0	22500	
Beta Scission					
24.	CH ₃ CHCL=C ₂ H ₄ +CL	1.00E+14	0	20500	I
25.	H+VCM=CH ₂ CLCH ₂	1.00E+13	0	0	I
26.	CL+C ₂ H ₄ =CH ₂ CLCH ₂	3.00E+13	0	0	I
27.	CL+VCM=CH ₂ CLCHCL	2.00E+13	0	0	I
28.	CL+C ₂ H ₂ =CHCLCH	5.00E+13	0	0	I
29.	C ₂ HCL+CL=CCL ₂ CH	1.39E+14	0	0	T
30.	C ₂ HCL+CL=CHCLCCL	1.39E+14	0	0	T
31.	C ₂ CL ₂ +CL=C ₂ CL ₃	1.39E+14	0	0	T
32.	CH ₂ CCL=C ₂ HCL+H	1.40E+13	0	50000	S
33.	C ₄ H ₆ CL ₃ _1134=C ₄ H ₅ CL ₃ _134D+H	3.50E+13	0	43200	R
34.	C ₄ H ₆ CL ₃ _1234=C ₄ H ₆ CL ₂ _34D+CL	3.90E+13	0	21698	R
35.	C ₄ H ₅ CL ₂ _434D=C ₄ H ₅ CL_113D+CL	3.90E+13	0	16000	R
36.	C ₄ H ₅ CL ₂ _334D=C ₄ H ₅ CL_213D+CL	3.90E+13	0	21698	R
37.	C ₄ H ₄ CL ₃ _4134D=C ₄ H ₄ CL ₂ _1413D+CL	3.90E+13	0	21698	R
38.	C ₄ H ₄ CL ₃ _3134D=C ₄ H ₄ CL ₂ _1313D+CL	3.90E+13	0	21698	R
39.	C ₄ H ₅ CL ₂ _413D=C ₄ H ₅ CL_113D+CL	3.90E+13	0	21698	R

Figure A.3: List of reactions used on the mechanism by Borsa [2]

No.	Reaction	A ($\text{cm}^3\text{-mol}^{-1}\text{s}^{-1}$)	n	E_a (cal/mol)	Ref.
40.	$\text{C4H5CL2_314D}=\text{C4H5CL_113D}+\text{CL}$	$3.90\text{E}+13$	0	21698	R
41.	$\text{C4H6CL_43D}=\text{C4H6_13D}+\text{CL}$	$3.90\text{E}+13$	0	21698	R
42.	$\text{C4H6CL_34D}=\text{C4H6_13D}+\text{CL}$	$3.90\text{E}+13$	0	21698	R
43.	$\text{C2HCL3}+\text{CL}=\text{CHCL2OCL2}$	$3.00\text{E}+13$	0	0	Aa
44.	$\text{C4H6CL_42D}=\text{C4H5CL_213D}+\text{H}$	$3.16\text{E}+13$	0	34800	K
45.	$\text{C4H8CL_14}=\text{C4H7CL_4D}+\text{H}$	$1.00\text{E}+14$	0	38300	Ak
46.	$\text{C4H7_4D}=\text{C4H6_13D}+\text{H}$	$3.16\text{E}+13$	0	34800	K
47.	$\text{C4H7CL2_134}=\text{C4H6CL2_34D}+\text{H}$	$1.00\text{E}+14$	0	38300	Ak
48.	$\text{C4H5CL2_423D}=\text{C4H5CL_213D}+\text{CL}$	$3.90\text{E}+12$	0	21698	R
Initiation/Termination (radical addition)					
49.	$\text{CHCL3}=\text{CHCL2}+\text{CL}$	$3.80\text{E}+16$	0	77000	B
50.	$\text{CH3CHCL2}=\text{CH3CHCL}+\text{CL}$	$3.00\text{E}+16$	0	81000	B
51.	$\text{CH3OCL3}=\text{CH3OCL2}+\text{CL}$	$1.50\text{E}+16$	0	76000	B
52.	$\text{CHCL2CHCL2}=\text{CCL3CH2}+\text{CL}$	$1.00\text{E}+16$	0	79100	B
53.	$\text{VCM}+\text{M}=\text{C2H3}+\text{CL}+\text{M}$	$2.50\text{E}+15$	0	78000	B
54.	$\text{CH3CL}=\text{CH3}+\text{CL}$	$9.98\text{E}+22$	-2.4	91540	B
55.	$\text{CH4}=\text{CH3}+\text{H}$	$1.10\text{E}+33$	-5.9	105150	B
56.	$\text{CH3}+\text{CH3}=\text{C2H5}+\text{H}$	$7.80\text{E}+11$	0	13039	B
57.	$\text{CH3}+\text{CH3}=\text{C2H4}+\text{H2}$	$1.00\text{E}+16$	0	31792	B
58.	$\text{CH3}+\text{CH2CL}=\text{C2H4}+\text{HCL}$	$2.31\text{E}+21$	-2.3	4905	B
59.	$\text{CH3}+\text{CH2CL}=\text{C2H5}+\text{CL}$	$1.57\text{E}+10$	1.1	4171	B
60.	$\text{CH2CL}+\text{CH2CL}=\text{VCM}+\text{HCL}$	$8.25\text{E}+24$	-3.5	8088	B
61.	$\text{CH2CL}+\text{CH2CL}=\text{CH2CLCH2}+\text{CL}$	$1.91\text{E}+17$	-1	9655	E
62.	$\text{C2H4}+\text{M}=\text{C2H3}+\text{H}+\text{M}$	$3.10\text{E}+17$	0	98160	B
63.	$\text{C2H4}+\text{M}=\text{C2H2}+\text{H2}+\text{M}$	$3.00\text{E}+17$	0	79800	B
64.	$\text{CH2CLCH2}+\text{CL}=\text{EDC}$	$1.50\text{E}+12$	0	0	K
65.	$\text{CL2}+\text{M}=\text{CL}+\text{CL}+\text{M}$	$2.34\text{E}+13$	0	47000	W
66.	$\text{CH2OCL}+\text{CL}=\text{CH2OCL2}$	$1.00\text{E}+13$	0	0	Y
67.	$\text{CH2CLCHCL2}=\text{CH2CLCHCL}+\text{CL}$	$1.00\text{E}+13$	0	69999	Ab
68.	$\text{CHCLCH}+\text{CL}=\text{CHCLCHCL}_c$	$1.00\text{E}+13$	0	0	Y
69.	$\text{CHCLCH}+\text{CL}=\text{CHCLCHCL}_i$	$1.00\text{E}+13$	0	0	Y
70.	$\text{CH2CLCHCL}+\text{CH2CLCHCL}=\text{C4H6CL4_1234}$	$1.00\text{E}+12$	0	0	W
71.	$\text{CH2CLCHCL}+\text{CH2CLCHCL}=\text{CH2CLCHCL2}+\text{VCM}$	$1.40\text{E}+12$	0	0	W
72.	$\text{OCL3}+\text{CH2CLCHCL}=\text{C3H3CL5_112}$	$1.00\text{E}+13$	0	0	Y
73.	$\text{VCM}=\text{C2H3}+\text{CL}$	$3.98\text{E}+15$	0	91701	Ad
74.	$\text{OCL3}+\text{CL}=\text{OCL4}$	$5.00\text{E}+11$	0	0	Ae
75.	$\text{CH2CLOCL2CHCL}=\text{C2HCL3}+\text{CH2CL}$	$1.20\text{E}+13$	0	27000	D
76.	$\text{C4H7CL_4D}=\text{C4H7_4D}+\text{CL}$	$1.00\text{E}+13$	0	70000	Ab
77.	$\text{EDC}=\text{CH2CL}+\text{CH2CL}$	$3.00\text{E}+16$	0	90000	I
78.	$\text{CH2CLCH3}=\text{C2H5}+\text{CL}$	$5.00\text{E}+15$	0	81000	I
79.	$\text{CH3CL}=\text{CH2CL}+\text{H}$	$1.00\text{E}+16$	0	102000	I
80.	$\text{CH3CL}+\text{M}=\text{CH3}+\text{CL}+\text{M}$	$2.00\text{E}+15$	0	75000	I
81.	$\text{CHCL3}+\text{M}=\text{CHCL2}+\text{CL}+\text{M}$	$2.00\text{E}+15$	0	75000	I

Figure A.4: List of reactions used on the mechanism by Borsa [2] (cont.)

No.	Reaction	A ($\text{cm}^3\text{-mol}^{-1}\text{s}^{-1}$)	n	E_a (cal/mol)	Ref.
82.	Cl+VCM=CHCL2CH2	1.00E+13	0	1000	I
83.	CH2CL+C2HCL=C3H3CL2_313D	1.50E+11	0	5000	I
84.	OCL3+C2H2=C3H2CL3_211D	1.50E+11	0	5000	I
85.	H+VCM=CH3CHCL	1.00E+13	0	0	I
86.	H+C2H4=C2H5	2.80E+13	0	2000	I
87.	H+C3H6=C2H4+CH3	2.00E+13	0	2000	I
88.	H+C2H2+M=C2H3+M	3.00E+11	0	-10000	I
89.	C2H3+C2H2=C4H5_113D	1.50E+11	0	4000	I
90.	CH3+VCM=C3H6+CL	2.00E+11	0	7600	I
91.	CH3+C2H2=C3H5_3D	1.00E+11	0	7600	I
92.	CH3+CH3=C2H6	2.00E+13	0	0	I
93.	CH3+CH2CL=CH2CLCH3	5.00E+13	0	0	I
94.	H+H=H2	1.00E+13	0	0	J
95.	H+CL=HCL	1.00E+13	0	0	J
96.	H+C2H3=C2H4	1.00E+13	0	0	J
97.	H+CH2CLCH2=CH2CLCH3	1.00E+13	0	0	J
98.	H+CH2CLCHCL=EDC	1.00E+13	0	0	J
99.	H+CHCLCH=VCM	1.00E+13	0	0	J
100.	H+OCL2=CHCL2	1.00E+13	0	0	J
101.	H+C2CL3=C2HCL3	1.00E+13	0	0	J
102.	H+CHCL2OCL2=CHCL2CHCL2	1.00E+13	0	0	J
103.	C3H4CL4_1223=H+CH2CLOCL2CHCL	1.58E+16	0	97500	Ak
104.	H+CH2OCL=VCM	1.00E+13	0	0	J
105.	H+C4H6CL3_1134=C4H7CL3_124	1.00E+13	0	0	J
106.	H+C4H5CL2_434D=C4H6CL2_34D	1.00E+13	0	0	J
107.	H+C4H5CL2_334D=C4H6CL2_34D	1.00E+13	0	0	J
108.	H+C4H4CL3_4134D=C4H5CL3_134D	1.00E+13	0	0	J
109.	H+C4H4CL3_3134D=C4H5CL3_134D	1.00E+13	0	0	J
110.	H+C4H5CL2_314D=C4H6CL2_14D	1.00E+13	0	0	J
111.	H+C4H6CL_34D=C4H7CL_4D	1.00E+13	0	0	J
112.	H+OCL2CH=CH2OCL2	1.00E+13	0	0	J
113.	H+CHCLOCL=CHCLCHCL_c	1.00E+13	0	0	J
114.	H+CHCLOCL=CHCLCHCL_t	1.00E+13	0	0	J
115.	Cl+OCL2=OCL3	1.00E+13	0	0	J
116.	Cl+CH2CL=CH2CL2	1.00E+13	0	0	J
117.	Cl+C2CL3=C2CL4	1.00E+13	0	0	J
118.	Cl+CHCL2OCL2=CHCL2OCL3	1.00E+13	0	0	J
119.	Cl+CH2CLOCL2CHCL=C3H3CL5_113	5.00E+13	0	0	V
120.	Cl+C4H5_213D=C4H5CL_213D	1.00E+13	0	0	J
121.	Cl+C4H5_113D=C4H5CL_113D	1.00E+13	0	0	J
122.	Cl+C4H6CL3_1234=C4H6CL4_1234	1.00E+13	0	0	J
123.	Cl+C4H5CL2_314D=C4H5CL3_134D	1.00E+13	0	0	J
124.	Cl+C4H6CL_43D=C4H6CL2_34D	1.00E+13	0	0	J
125.	Cl+C4H6CL_34D=C4H6CL2_34D	1.00E+13	0	0	J

Figure A.5: List of reactions used on the mechanism by Borsa [2] (cont.)

No.	Reaction	A (cm ³ -mol-s)	n	E _a (cal/mol)	Ref.
126.	Cl+C4H5Cl2_413D=C4H5Cl3_134D	1.00E+13	0	0	J
127.	Cl+C4H7Cl2_134=C4H7Cl3_124	1.00E+13	0	0	J
128.	Cl+OCl2CH=C2HCl3	1.00E+13	0	0	J
129.	Cl+CHClOCl=C2HCl3	1.00E+13	0	0	J
130.	C2H3+CH2ClCH2=C4H7Cl_4D	1.00E+13	0	0	J
131.	C2H3+CH2ClCHCl=C4H6Cl2_34D	1.00E+13	0	0	J
132.	C2H3+CHClCH=C4H5Cl_113D	1.00E+13	0	0	J
133.	C3H3Cl3_333D=C2H3+OCl3	8.00E+16	0	100000	Ak
134.	C2H3+CH2Cl=C3H5Cl_3D	1.00E+15	0	0	J
135.	C2H3+CH2OCl=C4H5Cl_213D	1.00E+13	0	0	J
136.	CH2ClCH2+CH2ClCHCl=C4H7Cl3_124	1.00E+13	0	0	J
137.	CH2ClCH2+CHClCH=C4H6Cl2_14D	1.00E+13	0	0	J
138.	C3H4Cl4_1113=C2ClCH2+OCl3	5.00E+15	0	85653	Aq
139.	C3H6Cl2_13=C2ClCH2+CH2Cl	5.00E+15	0	85653	Aq
140.	CH2ClCH2+CH2OCl=C4H6Cl2_24D	1.00E+13	0	0	J
141.	CH2ClCHCl+CHClCH=C4H5Cl3_134D	1.00E+13	0	0	J
142.	C3H5Cl3_123=C2ClCHCl+CH2Cl	5.00E+15	0	85653	Aq
143.	CHClCH+CHClCH=C4H4Cl2_1413D	1.00E+13	0	0	J
144.	C3H2Cl4_12D=CHClCH+OCl3	8.00E+16	0	100000	Ak
145.	C3H4Cl2_13D=CHClCH+CH2Cl	8.00E+16	0	100000	Ak
146.	C3Cl6_D=OCl3+C2Cl3	8.00E+16	0	100000	Ak
147.	C3H2Cl4_11D=OCl3+CH2OCl	8.00E+16	0	100000	Ak
148.	C3HCl5_2D=OCl3+OCl2CH	8.00E+16	0	100000	Ak
149.	C3HCl5_1D=OCl3+CHClOCl	8.00E+16	0	100000	Ak
150.	OCl2+OCl2=C2Cl4	1.00E+13	0	0	Ak
151.	C3H2Cl4_33D=CH2Cl+C2Cl3	8.00E+16	0	100000	Ak
152.	C3H4Cl2_23D=CH2Cl+CH2OCl	8.00E+16	0	100000	Ak
153.	C3H3Cl3_113D=CH2Cl+OCl2CH	8.00E+16	0	100000	Ak
154.	C3H3Cl3_123D=CH2Cl+CHClOCl	8.00E+16	0	100000	Ak
155.	H+C4H6_13D=C2H3+C2H4	2.00E+13	0	2000	I
156.	C2H3+C2H3=C4H6_13D	4.94E+13	0	0	A
157.	C4H6_13D=C4H5_213D+H	8.00E+15	0	110000	C
158.	C4H5_113D+H=C4H6_13D	2.00E+14	0	1814	C
159.	CHCl2+CHCl2=CHCl2CHCl2	1.50E+10	0	0	Q
160.	CH2ClCH2+CH2ClCH2=C4H4Cl2_1313D+H2+H2	1.00E+10	0	0	Q
161.	CH3CHCl+CH3CHCl=C4H4Cl2_1313D+H2+H2	5.00E+09	0	0	Q
162.	CH2OCl+CH2OCl=C4H4Cl2_1313D	1.00E+10	0	0	Q
163.	Cl+H+M=HCl+M	1.00E+10	0	-10000	Q
164.	Cl+CHCl2CH2=CH2ClCHCl2	4.00E+10	0	0	Q
165.	Cl+CH2OCl=CHClCHCl_1	6.00E+10	0	0	Q
166.	CH3+CHCl2=CH3CHCl2	3.50E+10	0	0	Q
167.	CH3+OCl3=CH3OCl3	3.00E+10	0	0	Q
168.	CH3+CH2ClCHCl=C3H6Cl2_13	2.00E+10	0	0	Q
169.	CH3+CH3OCl2=C3H6Cl2_13	2.00E+10	0	0	Q

Figure A.6: List of reactions used on the mechanism by Borsa [2] (cont.)

No.	Reaction	A (cm ³ -mol-s)	n	E _a (cal/mol)	Ref.
170.	CH ₃ +CHCl ₂ CH ₂ =C ₃ H ₆ Cl ₂ _13	2.00E+10	0	0	Q
171.	CH ₃ +CH ₂ OCl=C ₃ H ₅ Cl_3D	3.00E+10	0	0	Q
172.	CH ₂ Cl+CHCl ₂ =CH ₂ ClCHCl ₂	3.00E+10	0	0	Q
173.	CH ₂ Cl+OCl ₃ =CHCl ₂ CHCl ₂	2.40E+10	0	0	Q
174.	CH ₂ Cl+CH ₃ CHCl=C ₃ H ₆ Cl ₂ _13	1.70E+10	0	0	Q
175.	CH ₂ Cl+CH ₂ OCl=C ₃ H ₄ Cl ₂ _13D	2.40E+10	0	0	Q
176.	CHCl ₂ +H=CH ₂ Cl ₂	1.00E+11	0	0	Q
177.	CHCl ₂ +OCl ₃ =CHCl ₂ OCl ₃	2.40E+10	0	0	Q
178.	CHCl ₂ +C ₂ H ₅ =C ₃ H ₆ Cl ₂ _13	2.00E+10	0	0	Q
179.	CHCl ₂ +C ₂ H ₃ =C ₃ H ₄ Cl ₂ _13D	2.40E+10	0	0	Q
180.	OCl ₃ +H=CHCl ₃	5.00E+10	0	0	Q
Disproportionation					
181.	C ₄ H ₆ Cl_42D+Cl=C ₄ H ₆ Cl ₂ _24D	1.00E+13	0	0	Y
182.	C ₄ H ₇ _4D+C ₂ H ₃ =C ₄ H ₆ _13D+C ₂ H ₄	1.40E+12	0	0	W
183.	C ₄ H ₇ _4D+CH ₂ ClCH ₂ =C ₄ H ₆ _13D+CH ₂ ClCH ₃	1.40E+12	0	0	W
184.	C ₄ H ₆ Cl_43D+CH ₂ OCl=C ₄ H ₆ _13D+CH ₂ OCl ₂	1.40E+12	0	0	W
185.	C ₄ H ₆ Cl_43D+CHClCH=C ₄ H ₆ _13D+CHClCHCl_c	1.40E+12	0	0	W
186.	C ₄ H ₆ Cl_43D+CHClCH=C ₄ H ₆ _13D+CHClCHCl_t	1.40E+12	0	0	W
187.	C ₄ H ₆ Cl_43D+CH ₂ ClCHCl=C ₄ H ₆ _13D+CH ₂ ClCHCl ₂	1.40E+12	0	0	W
188.	C ₄ H ₆ Cl_34D+CH ₂ OCl=C ₄ H ₆ _13D+CH ₂ OCl ₂	1.40E+12	0	0	W
189.	C ₄ H ₆ Cl_34D+CHClCH=C ₄ H ₆ _13D+CHClCHCl_c	1.40E+12	0	0	W
190.	C ₄ H ₆ Cl_34D+CHClCH=C ₄ H ₆ _13D+CHClCHCl_t	1.40E+12	0	0	W
191.	C ₄ H ₆ Cl_34D+CH ₂ ClCHCl=C ₄ H ₆ _13D+CH ₂ ClCHCl ₂	1.40E+12	0	0	W
192.	C ₄ H ₅ Cl ₂ _423D+CH ₂ OCl=C ₄ H ₅ Cl_213D+CH ₂ OCl ₂	1.40E+12	0	0	W
193.	C ₄ H ₅ Cl ₂ _423D+CHClCH=C ₄ H ₅ Cl_213D+CHClCHCl_c	1.40E+12	0	0	W
194.	C ₄ H ₅ Cl ₂ _423D+CHClCH=C ₄ H ₅ Cl_213D+CHClCHCl_t	1.40E+12	0	0	W
195.	C ₄ H ₅ Cl ₂ _423D+CH ₂ ClCHCl=C ₄ H ₅ Cl_213D+CH ₂ ClCHCl ₂	1.40E+12	0	0	W
196.	H+CHClCH=C ₂ H ₂ +HCl	1.21E+13	0	0	J
197.	H+C ₂ Cl ₃ =C ₂ Cl ₂ +HCl	1.00E+13	0	0	J
198.	H+CHCl ₂ OCl ₂ =C ₂ HCl ₃ +HCl	1.00E+12	0	0	J
199.	H+CH ₂ ClOCl ₂ CHCl=C ₃ H ₃ Cl ₃ _123D+HCl	1.00E+12	0	0	D
200.	H+CH ₂ OCl=C ₂ HCl+H ₂	1.00E+13	0	0	J
201.	H+C ₄ H ₅ _213D=C ₄ H ₄ _DT+H ₂	1.00E+12	0	0	J
202.	H+C ₄ H ₅ _113D=C ₄ H ₄ _DT+H ₂	1.00E+12	0	0	J
203.	H+C ₄ H ₆ Cl ₃ _1134=C ₄ H ₅ Cl ₃ _134D+H ₂	1.00E+12	0	0	J
204.	H+C ₄ H ₆ Cl ₃ _1234=C ₄ H ₆ Cl ₂ _34D+HCl	1.00E+12	0	0	J
205.	H+C ₄ H ₅ Cl ₂ _434D=C ₄ H ₅ Cl_113D+HCl	1.00E+12	0	0	J
206.	H+C ₄ H ₅ Cl ₂ _334D=C ₄ H ₅ Cl_213D+HCl	1.00E+12	0	0	J
207.	H+C ₄ H ₄ Cl ₃ _4134D=C ₄ H ₄ Cl ₂ _1413D+HCl	1.00E+12	0	0	J
208.	H+C ₄ H ₅ Cl ₂ _314D=C ₄ H ₅ Cl_113D+HCl	1.00E+12	0	0	J
209.	H+C ₄ H ₆ Cl_43D=C ₄ H ₆ _13D+HCl	1.00E+12	0	0	J
210.	H+C ₄ H ₆ Cl_34D=C ₄ H ₆ _13D+HCl	1.00E+12	0	0	J
211.	H+C ₄ H ₅ Cl ₂ _413D=C ₄ H ₅ Cl_113D+HCl	1.00E+12	0	0	J

Figure A.7: List of reactions used on the mechanism by Borsa [2] (cont.)

No.	Reaction	A (cm ³ -mol-s)	n	E _a [∞] (cal/mol)	Ref.
212.	H+C4H6CL_42D=C4H5CL_213D+H2	1.00E+12	0	0	J
213.	H+C4H8CL_14=C4H7CL_4D+H2	1.00E+12	0	0	J
214.	H+C4H7_4D=C4H6_13D+H2	1.00E+12	0	0	J
215.	H+C4H7CL2_134=C4H6CL2_34D+H2	1.00E+12	0	0	J
216.	H+C4H5CL2_423D=C4H5CL_213D+HCL	1.00E+12	0	0	J
217.	H+OCL2CH=C2HCL+HCL	1.00E+13	0	0	J
218.	H+CHCLOCL=C2CL2+H2	1.00E+13	0	0	J
219.	CL+CH2CLCH2=C2H4+CL2	1.00E+12	0	0	J
220.	CL+CH2CLCHCL=VCM+CL2	1.00E+12	0	0	J
221.	CL+CHCLCH=C2H2+CL2	1.21E+13	0	0	J
222.	CL+C2CL3=C2CL2+CL2	1.00E+13	0	0	J
223.	CL+CHCL2CCL2=C2HCL3+CL2	1.00E+12	0	0	J
224.	CL+CH2CLOCL2CHCL=C3H3CL3_123D+CL2	1.00E+12	0	0	D
225.	CL+CH2OCL=C2HCL+HCL	1.00E+13	0	0	J
226.	CL+C4H5_213D=C4H4_DT+HCL	1.00E+12	0	0	J
227.	CL+C4H5_113D=C4H4_DT+HCL	1.00E+12	0	0	J
228.	CL+C4H6CL3_1134=C4H5CL3_134D+HCL	1.00E+12	0	0	J
229.	CL+C4H6CL3_1234=C4H6CL2_34D+CL2	1.00E+12	0	0	J
230.	CL+C4H5CL2_434D=C4H5CL_113D+CL2	1.00E+12	0	0	J
231.	CL+C4H5CL2_334D=C4H5CL_213D+CL2	1.00E+12	0	0	J
232.	CL+C4H4CL3_4134D=C4H4CL2_1413D+CL2	1.00E+12	0	0	J
233.	CL+C4H4CL3_3134D=C4H4CL2_1313D+CL2	1.00E+12	0	0	J
234.	CL+C4H5CL2_314D=C4H5CL_113D+CL2	1.00E+12	0	0	J
235.	CL+C4H6CL_43D=C4H6_13D+CL2	1.00E+12	0	0	J
236.	CL+C4H6CL_34D=C4H6_13D+CL2	1.00E+12	0	0	J
237.	CL+C4H5CL2_413D=C4H5CL_113D+CL2	1.00E+12	0	0	J
238.	CL+C4H6CL_42D=C4H5CL_213D+HCL	1.00E+12	0	0	J
239.	CL+C4H8CL_14=C4H7CL_4D+HCL	1.00E+12	0	0	J
240.	CL+C4H7_4D=C4H6_13D+HCL	1.00E+12	0	0	J
241.	CL+C4H7CL2_134=C4H6CL2_34D+HCL	1.00E+12	0	0	J
242.	CL+C4H5CL2_423D=C4H5CL_213D+CL2	1.00E+12	0	0	J
243.	CL+OCL2CH=C2HCL+CL2	1.00E+13	0	0	J
244.	CL+CHCLOCL=C2CL2+HCL	1.00E+13	0	0	J
245.	C2H3+C2H3=C2H2+C2H4	9.64E+11	0	0	J
246.	C2H3+CH2CLCH2=C2H4+VCM	1.00E+12	0	0	J
247.	C2H3+CH2CLCHCL=VCM+VCM	1.00E+12	0	0	J
248.	C2H3+CHCLCH=C2H2+VCM	9.64E+11	0	0	J
249.	C2H3+C2CL3=C2CL2+VCM	9.64E+11	0	0	J
250.	C2H3+CHCL2CCL2=C2HCL3+VCM	1.00E+12	0	0	J
251.	C2H3+CH2CLOCL2CHCL=C3H3CL3_123D+VCM	1.00E+12	0	0	D
252.	C2H3+CH2OCL=C2HCL+C2H4	9.64E+11	0	0	J
253.	C2H3+C4H5_213D=C4H4_DT+C2H4	1.00E+12	0	0	J
254.	C2H3+C4H5_113D=C4H4_DT+C2H4	1.00E+12	0	0	J
255.	C2H3+C4H6CL3_1134=C4H5CL3_134D+C2H4	1.00E+12	0	0	J

Figure A.8: List of reactions used on the mechanism by Borsa [2] (cont.)

No.	Reaction	A ($\text{cm}^3\text{-mol}^{-1}\text{s}^{-1}$)	n	E_a (cal/mol)	Ref.
256.	C2H3+C4H6CL3_1234=C4H6CL2_34D+VCM	1.00E+12	0	0	J
257.	C2H3+C4H5CL2_434D=C4H5CL_113D+VCM	1.00E+12	0	0	J
258.	C2H3+C4H5CL2_334D=C4H5CL_213D+VCM	1.00E+12	0	0	J
259.	C2H3+C4H4CL3_4134D=C4H4CL2_1413D+VCM	1.00E+12	0	0	J
260.	C2H3+C4H4CL3_3134D=C4H4CL2_1313D+VCM	1.00E+12	0	0	J
261.	C2H3+C4H5CL2_314D=C4H5CL_113D+VCM	1.00E+12	0	0	J
262.	C2H3+C4H6CL_43D=C4H6_13D+VCM	1.00E+12	0	0	J
263.	C2H3+C4H6CL_34D=C4H6_13D+VCM	1.00E+12	0	0	J
264.	C2H3+C4H5CL2_413D=C4H5CL_113D+VCM	1.00E+12	0	0	J
265.	C2H3+C4H6CL_42D=C4H5CL_213D+C2H4	1.00E+12	0	0	J
266.	C2H3+C4H8CL_14=C4H7CL_4D+C2H4	1.00E+12	0	0	J
267.	C2H3+C4H7CL2_134=C4H6CL2_34D+C2H4	1.00E+12	0	0	J
268.	C2H3+C4H5CL2_423D=C4H5CL_213D+VCM	1.00E+12	0	0	J
269.	C2H3+OCL2CH=C2HCL+VCM	9.64E+11	0	0	J
270.	C2H3+CHCLOCL=C2CL2+C2H4	9.64E+11	0	0	J
271.	CH2CLCH2+CH2CLCH2=C2H4+EDC	1.00E+10	0	0	J
272.	CH2CLCH2+CH2CLCHCL=VCM+EDC	1.00E+10	0	0	J
273.	CH2CLCH2+CHCLCH=C2H2+EDC	1.00E+10	0	0	J
274.	CH2CLCH2+C2CL3=C2CL2+EDC	1.00E+10	0	0	J
275.	CH2CLCH2+CHCL2OCL2=C2HCL3+EDC	1.00E+10	0	0	J
276.	CH2CLCH2+CH2CLOCL2CHCL=C3H3CL3_123D+EDC	1.00E+10	0	0	D
277.	CH2CLCH2+CH2OCL=C2HCL+CH2CLCH3	1.00E+12	0	0	J
278.	CH2CLCH2+C4H5_213D=C4H4_DT+CH2CLCH3	1.00E+12	0	0	J
279.	CH2CLCH2+C4H5_113D=C4H4_DT+CH2CLCH3	1.00E+12	0	0	J
280.	CH2CLCH2+C4H6CL3_1134=C4H5CL3_134D+CH2CLCH3	1.00E+12	0	0	J
281.	CH2CLCH2+C4H6CL3_1234=C4H6CL2_34D+EDC	1.00E+10	0	0	J
282.	CH2CLCH2+C4H5CL2_434D=C4H5CL_113D+EDC	1.00E+10	0	0	J
283.	CH2CLCH2+C4H5CL2_334D=C4H5CL_213D+EDC	1.00E+10	0	0	J
284.	CH2CLCH2+C4H4CL3_4134D=C4H4CL2_1413D+EDC	1.00E+10	0	0	J
285.	CH2CLCH2+C4H4CL3_3134D=C4H4CL2_1313D+EDC	1.00E+10	0	0	J
286.	CH2CLCH2+C4H5CL2_314D=C4H5CL_113D+EDC	1.00E+10	0	0	J
287.	CH2CLCH2+C4H6CL_43D=C4H6_13D+EDC	1.00E+10	0	0	J
288.	CH2CLCH2+C4H6CL_34D=C4H6_13D+EDC	1.00E+10	0	0	J
289.	CH2CLCH2+C4H5CL2_413D=C4H5CL_113D+EDC	1.00E+10	0	0	J
290.	CH2CLCH2+C4H6CL_42D=C4H5CL_213D+CH2CLCH3	1.00E+12	0	0	J
291.	CH2CLCH2+C4H8CL_14=C4H7CL_4D+CH2CLCH3	1.00E+12	0	0	J
292.	CH2CLCH2+C4H7CL2_134=C4H6CL2_34D+CH2CLCH3	1.00E+12	0	0	J
293.	CH2CLCH2+C4H5CL2_423D=C4H5CL_213D+EDC	1.00E+10	0	0	J
294.	CH2CLCH2+OCL2CH=C2HCL+EDC	1.00E+10	0	0	J
295.	CH2CLCH2+CHCLOCL=C2CL2+CH2CLCH3	1.00E+12	0	0	J
296.	CH2CLCHCL+CHCLCH=C2H2+CH2CLCHCL2	1.00E+12	0	0	J
297.	CH2CLCHCL+C2CL3=C2CL2+CH2CLCHCL2	1.00E+12	0	0	J
298.	CH2CLCHCL+CHCL2OCL2=C2HCL3+CH2CLCHCL2	1.00E+12	0	0	J
299.	CH2CLCHCL+CH2CLOCL2CHCL=C3H3CL3_123D+CH2CLCHCL2	1.00E+12	0	0	J

Figure A.9: List of reactions used on the mechanism by Borsa [2] (cont.)

No.	Reaction	A (cm ³ -mol ^{-s})	n	E _a (cal/mol)	Ref.
300.	CH2CLCHCL+CH2OCL=C2HCL+EDC	1.00E+10	0	0	J
301.	CH2CLCHCL+C4H5_213D=C4H4_DT+EDC	1.00E+10	0	0	J
302.	CH2CLCHCL+C4H5_113D=C4H4_DT+EDC	1.00E+10	0	0	J
303.	CH2CLCHCL+C4H6CL3_1134=C4H5CL3_134D+EDC	1.00E+10	0	0	J
304.	CH2CLCHCL+C4H6CL3_1234=C4H6CL2_34D+CH2CLCHCL2	1.00E+12	0	0	J
305.	CH2CLCHCL+C4H5CL2_434D=C4H5CL_113D+CH2CLCHCL2	1.00E+12	0	0	J
306.	CH2CLCHCL+C4H5CL2_334D=C4H5CL_213D+CH2CLCHCL2	1.00E+12	0	0	J
307.	CH2CLCHCL+C4H4CL3_4134D=C4H4CL2_1413D+CH2CLCHCL2	1.00E+12	0	0	J
308.	CH2CLCHCL+C4H4CL3_3134D=C4H4CL2_1313D+CH2CLCHCL2	1.00E+12	0	0	J
309.	CH2CLCHCL+C4H5CL2_314D=C4H5CL_113D+CH2CLCHCL2	1.00E+12	0	0	J
310.	CH2CLCHCL+C4H5CL2_413D=C4H5CL_113D+CH2CLCHCL2	1.00E+12	0	0	J
311.	CH2CLCHCL+C4H6CL_42D=C4H5CL_213D+EDC	1.00E+10	0	0	J
312.	CH2CLCHCL+C4H8CL_14=C4H7CL_4D+EDC	1.00E+10	0	0	J
313.	CH2CLCHCL+C4H7_4D=C4H6_13D+EDC	1.00E+10	0	0	J
314.	CH2CLCHCL+C4H7CL2_134=C4H6CL2_34D+EDC	1.00E+10	0	0	J
315.	CH2CLCHCL+OCL2CH=C2HCL+CH2CLCHCL2	1.00E+12	0	0	J
316.	CH2CLCHCL+CHCLOCL=C2CL2+EDC	1.00E+10	0	0	J
317.	CHCLCH+CHCLCH=C2H2+CHCLCHCL_c	1.00E+12	0	0	J
318.	CHCLCH+C2CL3=C2CL2+CHCLCHCL_c	1.00E+12	0	0	J
319.	CHCLCH+CHCL2OCL2=C2HCL3+CHCLCHCL_c	1.00E+12	0	0	J
320.	CHCLCH+CH2CLOCL2CHCL=C3H3CL3_123D+CHCLCHCL_c	1.00E+12	0	0	D
321.	CHCLCH+CH2OCL=C2HCL+VCM	1.00E+12	0	0	J
322.	CHCLCH+C4H5_213D=C4H4_DT+VCM	1.00E+12	0	0	J
323.	CHCLCH+C4H5_113D=C4H4_DT+VCM	1.00E+12	0	0	J
324.	CHCLCH+C4H6CL3_1134=C4H5CL3_134D+VCM	1.00E+12	0	0	J
325.	CHCLCH+C4H6CL3_1234=C4H6CL2_34D+CHCLCHCL_c	1.00E+12	0	0	J
326.	CHCLCH+C4H5CL2_434D=C4H5CL_113D+CHCLCHCL_c	1.00E+12	0	0	J
327.	CHCLCH+C4H5CL2_334D=C4H5CL_213D+CHCLCHCL_c	1.00E+12	0	0	J
328.	CHCLCH+C4H4CL3_4134D=C4H4CL2_1413D+CHCLCHCL_c	1.00E+12	0	0	J
329.	CHCLCH+C4H4CL3_3134D=C4H4CL2_1313D+CHCLCHCL_c	1.00E+12	0	0	J
330.	CHCLCH+C4H5CL2_314D=C4H5CL_113D+CHCLCHCL_c	1.00E+12	0	0	J
331.	CHCLCH+C4H5CL2_413D=C4H5CL_113D+CHCLCHCL_c	1.00E+12	0	0	J
332.	CHCLCH+C4H6CL_42D=C4H5CL_213D+VCM	1.00E+12	0	0	J
333.	CHCLCH+C4H8CL_14=C4H7CL_4D+VCM	1.00E+12	0	0	J
334.	CHCLCH+C4H7_4D=C4H6_13D+VCM	1.00E+12	0	0	J
335.	CHCLCH+C4H7CL2_134=C4H6CL2_34D+VCM	1.00E+12	0	0	J
336.	CHCLCH+OCL2CH=C2HCL+CHCLCHCL_c	1.00E+12	0	0	J
337.	CHCLCH+CHCLOCL=C2CL2+VCM	1.00E+12	0	0	J
338.	C2CL3+C2CL3=C2CL2+C2CL4	1.00E+12	0	0	J
339.	C2CL3+CHCL2OCL2=C2HCL3+C2CL4	1.00E+12	0	0	J
340.	C2CL3+CH2CLOCL2CHCL=C3H3CL3_123D+C2CL4	1.00E+12	0	0	D
341.	C2CL3+CH2OCL=C2HCL+C2HCL3	1.00E+12	0	0	J
342.	C2CL3+C4H5_213D=C4H4_DT+C2HCL3	1.00E+12	0	0	J
343.	C2CL3+C4H5_113D=C4H4_DT+C2HCL3	1.00E+12	0	0	J

Figure A.10: List of reactions used on the mechanism by Borsa [2] (cont.)

No.	Reaction	A ($\text{cm}^3\text{-mol}^{-1}\text{s}^{-1}$)	n	E_a (cal/mol)	Ref.
344.	C2CL3+C4H6CL3_1134=C4H5CL3_134D+C2HCL3	1.00E+12	0	0	J
345.	C2CL3+C4H6CL3_1234=C4H6CL2_34D+C2CL4	1.00E+12	0	0	J
346.	C2CL3+C4H5CL2_434D=C4H5CL_113D+C2CL4	1.00E+12	0	0	J
347.	C2CL3+C4H5CL2_334D=C4H5CL_213D+C2CL4	1.00E+12	0	0	J
348.	C2CL3+C4H4CL3_4134D=C4H4CL2_1413D+C2CL4	1.00E+12	0	0	J
349.	C2CL3+C4H4CL3_3134D=C4H4CL2_1313D+C2CL4	1.00E+12	0	0	J
350.	C2CL3+C4H5CL2_314D=C4H5CL_113D+C2CL4	1.00E+12	0	0	J
351.	C2CL3+C4H6CL_43D=C4H6_13D+C2CL4	1.00E+12	0	0	J
352.	C2CL3+C4H6CL_34D=C4H6_13D+C2CL4	1.00E+12	0	0	J
353.	C2CL3+C4H5CL2_413D=C4H5CL_113D+C2CL4	1.00E+12	0	0	J
354.	C2CL3+C4H6CL_42D=C4H5CL_213D+C2HCL3	1.00E+12	0	0	J
355.	C2CL3+C4H8CL_14=C4H7CL_4D+C2HCL3	1.00E+12	0	0	J
356.	C2CL3+C4H7_4D=C4H6_13D+C2HCL3	1.00E+12	0	0	J
357.	C2CL3+C4H7CL2_134=C4H6CL2_34D+C2HCL3	1.00E+12	0	0	J
358.	C2CL3+C4H5CL2_423D=C4H5CL_213D+C2CL4	1.00E+12	0	0	J
359.	C2CL3+CCL2CH=C2HCL+C2CL4	1.00E+12	0	0	J
360.	C2CL3+CHCLOCL=C2CL2+C2HCL3	1.00E+12	0	0	J
361.	CH2OCL+CH2OCL=C2HCL+VCM	1.00E+12	0	0	J
362.	CH2OCL+C4H5_213D=C4H4_DT+VCM	1.00E+12	0	0	J
363.	CH2OCL+C4H5_113D=C4H4_DT+VCM	1.00E+12	0	0	J
364.	CH2OCL+C4H6CL3_1134=C4H5CL3_134D+VCM	1.00E+12	0	0	J
365.	CH2OCL+C4H6CL3_1234=C4H6CL2_34D+CH2OCL2	1.00E+12	0	0	J
366.	CH2OCL+C4H5CL2_434D=C4H5CL_113D+CH2OCL2	1.00E+12	0	0	J
367.	CH2OCL+C4H5CL2_334D=C4H5CL_213D+CH2OCL2	1.00E+12	0	0	J
368.	CH2OCL+C4H4CL3_4134D=C4H4CL2_1413D+CH2OCL2	1.00E+12	0	0	J
369.	CH2OCL+C4H4CL3_3134D=C4H4CL2_1313D+CH2OCL2	1.00E+12	0	0	J
370.	CH2OCL+C4H5CL2_314D=C4H5CL_113D+CH2OCL2	1.00E+12	0	0	J
371.	CH2OCL+C4H5CL2_413D=C4H5CL_113D+CH2OCL2	1.00E+12	0	0	J
372.	CH2OCL+C4H6CL_42D=C4H5CL_213D+VCM	1.00E+12	0	0	J
373.	CH2OCL+C4H8CL_14=C4H7CL_4D+VCM	1.00E+12	0	0	J
374.	CH2OCL+C4H7_4D=C4H6_13D+VCM	1.00E+12	0	0	J
375.	CH2OCL+C4H7CL2_134=C4H6CL2_34D+VCM	1.00E+12	0	0	J
376.	CH2OCL+CCL2CH=C2HCL+CH2OCL2	1.00E+12	0	0	J
377.	CH2OCL+CHCLOCL=C2CL2+VCM	1.00E+12	0	0	J
378.	OCL2CH+CCL2CH=C2HCL3+C2HCL	1.00E+12	0	0	J
379.	OCL2CH+CHCLOCL=CH2OCL2+C2CL2	1.00E+12	0	0	J
380.	CHCL2OCL2+CHCL2OCL2=CHCL2OCL3+C2HCL3	1.00E+12	0	0	J
381.	CHCL2OCL2+CH2CLOCL2CHCL=C3H3CL3_123D+CHCL2OCL3	1.00E+12	0	0	D
382.	CHCL2OCL2+CH2OCL=CHCL2CHCL2+C2HCL	1.00E+12	0	0	J
383.	CHCL2OCL2+C4H5_213D=CHCL2CHCL2+C4H4_DT	1.00E+12	0	0	J
384.	CHCL2OCL2+C4H5_113D=CHCL2CHCL2+C4H4_DT	1.00E+12	0	0	J
385.	CHCL2OCL2+C4H6CL3_1134=CHCL2CHCL2+C4H5CL3_134D	1.00E+12	0	0	J
386.	CHCL2OCL2+C4H6CL3_1234=CHCL2OCL3+C4H6CL2_34D	1.00E+12	0	0	J
387.	CHCL2OCL2+C4H5CL2_434D=CHCL2OCL3+C4H5CL_113D	1.00E+12	0	0	J

Figure A.11: List of reactions used on the mechanism by Borsa [2] (cont.)

No.	Reaction	A (cm ² -mol-s)	n	E _a (cal/mol)	Ref.
388.	CHCL2OCL2+C4H5CL2_334D=CHCL2OCL3+C4H5CL_213D	1.00E+12	0	0	J
389.	CHCL2OCL2+C4H4CL3_4134D=CHCL2OCL3+C4H4CL2_1413D	1.00E+12	0	0	J
390.	CHCL2OCL2+C4H4CL3_3134D=CHCL2OCL3+C4H4CL2_1313D	1.00E+12	0	0	J
391.	CHCL2OCL2+C4H5CL2_314D=CHCL2OCL3+C4H5CL_113D	1.00E+12	0	0	J
392.	CHCL2OCL2+C4H6CL_43D=CHCL2OCL3+C4H6_13D	1.00E+12	0	0	J
393.	CHCL2OCL2+C4H6CL_34D=CHCL2OCL3+C4H6_13D	1.00E+12	0	0	J
394.	CHCL2OCL2+C4H5CL2_413D=CHCL2OCL3+C4H5CL_113D	1.00E+12	0	0	J
395.	CHCL2OCL2+C4H6CL_42D=CHCL2CHCL2+C4H5CL_213D	1.00E+12	0	0	J
396.	CHCL2OCL2+C4H8CL_14=CHCL2CHCL2+C4H7CL_4D	1.00E+12	0	0	J
397.	CHCL2OCL2+C4H7_4D=CHCL2CHCL2+C4H6_13D	1.00E+12	0	0	J
398.	CHCL2OCL2+C4H7CL2_134=CHCL2CHCL2+C4H6CL2_34D	1.00E+12	0	0	J
399.	CHCL2OCL2+C4H5CL2_423D=CHCL2OCL3+C4H5CL_213D	1.00E+12	0	0	J
400.	CHCL2OCL2+OCL2CH=CHCL2OCL3+C2HCL	1.00E+12	0	0	J
401.	CHCL2OCL2+CHCLOCL=CHCL2CHCL2+C2CL2	1.00E+12	0	0	J
Hydrogen Abstraction					
402.	H+H2=H2+H	1.20E+13	0	9000	Q
403.	H+CH2CL2=H2+CHCL2	1.20E+13	0	9000	Q
404.	H+CHCL3=H2+OCL3	1.20E+13	0	9000	Q
405.	H+CH2CLCHCL2=H2+CHCLCHCL_1+CL	1.20E+13	0	9000	Q
406.	H+CHCL2CHCL2=H2+C2HCL3+CL	1.20E+13	0	9000	Q
407.	H+CHCL2OCL3=H2+C2CL4+CL	1.20E+13	0	9000	Q
408.	H+CH3OCL3=H2+OCL3CH2	1.20E+13	0	9000	Q
409.	CH2CL+CH3CL=CH3CL+CH2CL	2.40E+11	0	10000	Q
410.	CH2CL+CH2CL2=CH3CL+CHCL2	2.40E+11	0	10000	Q
411.	CH2CL+CHCL3=CH3CL+OCL3	2.40E+11	0	10000	Q
412.	CH2CL+CH2CLCHCL2=CH3CL+CHCLCHCL_1+CL	2.40E+11	0	10000	Q
413.	CH2CL+CHCL2CHCL2=CH3CL+C2HCL3+CL	2.40E+11	0	10000	Q
414.	CH2CL+CHCL2OCL3=CH3CL+C2CL4+CL	2.40E+11	0	10000	Q
415.	CH2CL+CH3OCL3=CH3CL+OCL3CH2	2.40E+11	0	10000	Q
416.	CHCL2+CH4=CH2CL2+CH3	3.02E+11	0	13000	Q
417.	CHCL2+CH2CL2=CH2CL2+CHCL2	3.02E+11	0	13000	Q
418.	CHCL2+CHCL3=CH2CL2+OCL3	3.02E+11	0	13000	Q
419.	CHCL2+C2H6=CH2CL2+C2H5	3.02E+11	0	13000	Q
420.	CHCL2+EDC=CH2CL2+CH2CLCHCL	3.02E+11	0	13000	Q
421.	CHCL2+CH3CHCL2=CH2CL2+CH3OCL2	3.02E+11	0	13000	Q
422.	CHCL2+CH3CHCL2=CH2CL2+CHCL2CH2	3.02E+11	0	13000	Q
423.	CHCL2+CH2CLCHCL2=CH2CL2+CHCLCHCL_1+CL	3.02E+11	0	13000	Q
424.	CHCL2+CHCL2CHCL2=CH2CL2+C2HCL3+CL	3.02E+11	0	13000	Q
425.	CHCL2+CHCL2OCL3=CH2CL2+C2CL4+CL	3.02E+11	0	13000	Q
426.	CHCL2+C2H4=CH2CL2+C2H5	3.02E+11	0	13000	Q
427.	CHCL2+VCM=CH2CL2+CH2OCL	3.02E+11	0	13000	Q
428.	CHCL2+CH3OCL3=CH2CL2+OCL3CH2	3.02E+11	0	13000	Q
429.	OCL3+CH4=CHCL3+CH3	5.01E+11	0	14000	Q

Figure A.12: List of reactions used on the mechanism by Borsa [2] (cont.)

No.	Reaction	A ($\text{cm}^3\text{-mol}^{-1}\text{s}^{-1}$)	n	E_a (cal/mol)	Ref.
430.	$\text{OCL}_3 + \text{CHCL}_3 \rightarrow \text{CHCL}_3 + \text{OCL}_3$	5.01E+11	0	14000	Q
431.	$\text{OCL}_3 + \text{C}_2\text{H}_6 \rightarrow \text{CHCL}_3 + \text{C}_2\text{H}_5$	5.01E+11	0	14000	Q
432.	$\text{OCL}_3 + \text{CH}_3\text{CHCL}_2 \rightarrow \text{CHCL}_3 + \text{CH}_3\text{OCL}_2$	5.01E+11	0	14000	Q
433.	$\text{OCL}_3 + \text{CH}_3\text{CHCL}_2 \rightarrow \text{CHCL}_3 + \text{CHCL}_2\text{CH}_2$	5.01E+11	0	14000	Q
434.	$\text{OCL}_3 + \text{CH}_2\text{CLCHCL}_2 \rightarrow \text{CHCL}_3 + \text{CHCLCHCL}_2 + \text{CL}$	5.01E+11	0	14000	Q
435.	$\text{OCL}_3 + \text{CHCL}_2\text{CHCL}_2 \rightarrow \text{CHCL}_3 + \text{C}_2\text{HCL}_3 + \text{CL}$	5.01E+11	0	14000	Q
436.	$\text{OCL}_3 + \text{CHCL}_2\text{OCL}_3 \rightarrow \text{CHCL}_3 + \text{C}_2\text{CL}_4 + \text{CL}$	5.01E+11	0	14000	Q
437.	$\text{OCL}_3 + \text{C}_2\text{H}_4 \rightarrow \text{CHCL}_3 + \text{C}_2\text{H}_3$	5.01E+11	0	14000	Q
438.	$\text{OCL}_3 + \text{VCM} \rightarrow \text{CHCL}_3 + \text{CH}_2\text{OCL}$	5.01E+11	0	14000	Q
439.	$\text{OCL}_3 + \text{CH}_3\text{OCL}_3 \rightarrow \text{CHCL}_3 + \text{OCL}_3\text{CH}_2$	5.01E+11	0	14000	Q
440.	$\text{CH}_2\text{CLCHCL} + \text{C}_2\text{H}_6 \rightarrow \text{EDC} + \text{C}_2\text{H}_5$	3.02E+11	0	14500	Q
441.	$\text{CH}_2\text{CLCHCL} + \text{EDC} \rightarrow \text{EDC} + \text{CH}_2\text{CLCHCL}$	3.02E+11	0	14500	Q
442.	$\text{CH}_2\text{CLCHCL} + \text{CH}_3\text{CHCL}_2 \rightarrow \text{EDC} + \text{CH}_3\text{OCL}_2$	3.02E+11	0	14500	Q
443.	$\text{CH}_2\text{CLCHCL} + \text{CH}_3\text{CHCL}_2 \rightarrow \text{EDC} + \text{CHCL}_2\text{CH}_2$	3.02E+11	0	14500	Q
444.	$\text{CH}_2\text{CLCHCL} + \text{CH}_2\text{CLCHCL}_2 \rightarrow \text{EDC} + \text{CHCLCHCL}_2 + \text{CL}$	3.02E+11	0	14500	Q
445.	$\text{CH}_2\text{CLCHCL} + \text{CHCL}_2\text{CHCL}_2 \rightarrow \text{EDC} + \text{C}_2\text{HCL}_3 + \text{CL}$	3.02E+11	0	14500	Q
446.	$\text{CH}_2\text{CLCHCL} + \text{CHCL}_2\text{OCL}_3 \rightarrow \text{EDC} + \text{C}_2\text{CL}_4 + \text{CL}$	3.02E+11	0	14500	Q
447.	$\text{CH}_2\text{CLCHCL} + \text{CH}_3\text{OCL}_3 \rightarrow \text{EDC} + \text{OCL}_3\text{CH}_2$	3.02E+11	0	14500	Q
448.	$\text{CH}_3\text{CHCL} + \text{CH}_2\text{CL}_2 \rightarrow \text{CH}_2\text{CLCH}_3 + \text{CHCL}_2$	3.02E+11	0	14500	Q
449.	$\text{CH}_3\text{CHCL} + \text{CHCL}_3 \rightarrow \text{CH}_2\text{CLCH}_3 + \text{OCL}_3$	3.02E+11	0	14500	Q
450.	$\text{CH}_3\text{CHCL} + \text{C}_2\text{H}_6 \rightarrow \text{CH}_2\text{CLCH}_3 + \text{C}_2\text{H}_5$	3.02E+11	0	14500	Q
451.	$\text{CH}_3\text{CHCL} + \text{EDC} \rightarrow \text{CH}_2\text{CLCH}_3 + \text{CH}_2\text{CLCHCL}$	3.02E+11	0	14500	Q
452.	$\text{CH}_3\text{CHCL} + \text{CH}_3\text{CHCL}_2 \rightarrow \text{CH}_2\text{CLCH}_3 + \text{CH}_3\text{OCL}_2$	3.02E+11	0	14500	Q
453.	$\text{CH}_3\text{CHCL} + \text{CH}_3\text{CHCL}_2 \rightarrow \text{CH}_2\text{CLCH}_3 + \text{CHCL}_2\text{CH}_2$	3.02E+11	0	14500	Q
454.	$\text{CH}_3\text{CHCL} + \text{CH}_2\text{CLCHCL}_2 \rightarrow \text{CH}_2\text{CLCH}_3 + \text{CHCLCHCL}_2 + \text{CL}$	3.02E+11	0	14500	Q
455.	$\text{CH}_3\text{CHCL} + \text{CHCL}_2\text{CHCL}_2 \rightarrow \text{CH}_2\text{CLCH}_3 + \text{C}_2\text{HCL}_3 + \text{CL}$	3.02E+11	0	14500	Q
456.	$\text{CH}_3\text{CHCL} + \text{CHCL}_2\text{OCL}_3 \rightarrow \text{CH}_2\text{CLCH}_3 + \text{C}_2\text{CL}_4 + \text{CL}$	3.02E+11	0	14500	Q
457.	$\text{CH}_3\text{CHCL} + \text{C}_2\text{H}_4 \rightarrow \text{CH}_2\text{CLCH}_3 + \text{C}_2\text{H}_3$	3.02E+11	0	14500	Q
458.	$\text{CH}_3\text{CHCL} + \text{VCM} \rightarrow \text{CH}_2\text{CLCH}_3 + \text{CH}_2\text{OCL}$	3.02E+11	0	14500	Q
459.	$\text{CH}_3\text{CHCL} + \text{CH}_3\text{OCL}_3 \rightarrow \text{CH}_2\text{CLCH}_3 + \text{OCL}_3\text{CH}_2$	3.02E+11	0	14500	Q
460.	$\text{CH}_2\text{OCL} + \text{C}_2\text{H}_6 \rightarrow \text{VCM} + \text{C}_2\text{H}_5$	3.02E+11	0	11000	Q
461.	$\text{CH}_2\text{OCL} + \text{CH}_3\text{CHCL}_2 \rightarrow \text{VCM} + \text{CH}_3\text{OCL}_2$	3.02E+11	0	11000	Q
462.	$\text{CH}_2\text{OCL} + \text{CH}_3\text{CHCL}_2 \rightarrow \text{VCM} + \text{CHCL}_2\text{CH}_2$	3.02E+11	0	11000	Q
463.	$\text{CH}_2\text{OCL} + \text{CH}_2\text{CLCHCL}_2 \rightarrow \text{VCM} + \text{CHCLCHCL}_2 + \text{CL}$	3.02E+11	0	11000	Q
464.	$\text{CH}_2\text{OCL} + \text{CHCL}_2\text{CHCL}_2 \rightarrow \text{VCM} + \text{C}_2\text{HCL}_3 + \text{CL}$	3.02E+11	0	11000	Q
465.	$\text{CH}_2\text{OCL} + \text{CHCL}_2\text{OCL}_3 \rightarrow \text{VCM} + \text{C}_2\text{CL}_4 + \text{CL}$	3.02E+11	0	11000	Q
466.	$\text{CH}_2\text{OCL} + \text{C}_2\text{H}_4 \rightarrow \text{VCM} + \text{C}_2\text{H}_3$	3.02E+11	0	11000	Q
467.	$\text{CH}_2\text{OCL} + \text{VCM} \rightarrow \text{VCM} + \text{CH}_2\text{OCL}$	3.02E+11	0	11000	Q
468.	$\text{CH}_2\text{OCL} + \text{CH}_3\text{OCL}_3 \rightarrow \text{VCM} + \text{OCL}_3\text{CH}_2$	3.02E+11	0	11000	Q
469.	$\text{CH}_2\text{CLCH}_2 + \text{CH}_2\text{CL}_2 \rightarrow \text{CH}_2\text{CLCH}_3 + \text{CHCL}_2$	3.02E+11	0	14500	Q
470.	$\text{CH}_2\text{CLCH}_2 + \text{CHCL}_3 \rightarrow \text{CH}_2\text{CLCH}_3 + \text{OCL}_3$	3.02E+11	0	14500	Q
471.	$\text{CH}_2\text{CLCH}_2 + \text{C}_2\text{H}_6 \rightarrow \text{CH}_2\text{CLCH}_3 + \text{C}_2\text{H}_5$	3.02E+11	0	14500	Q
472.	$\text{CH}_2\text{CLCH}_2 + \text{CH}_3\text{CHCL}_2 \rightarrow \text{CH}_2\text{CLCH}_3 + \text{CH}_3\text{OCL}_2$	3.02E+11	0	14500	Q
473.	$\text{CH}_2\text{CLCH}_2 + \text{CH}_3\text{CHCL}_2 \rightarrow \text{CH}_2\text{CLCH}_3 + \text{CHCL}_2\text{CH}_2$	3.02E+11	0	14500	Q

Figure A.13: List of reactions used on the mechanism by Borsa [2] (cont.)

No.	Reaction	A ($\text{cm}^3\text{-mol}^{-1}\text{-s}$)	n	E_a (cal/mol)	Ref.
474.	$\text{CH}_2\text{ClCH}_2+\text{CH}_2\text{ClCHCl}_2=\text{CH}_2\text{ClCH}_3+\text{CHClCHCl}_1+\text{Cl}$	$3.02\text{E}+11$	0	14500	Q
475.	$\text{CH}_2\text{ClCH}_2+\text{CHCl}_2\text{CHCl}_2=\text{CH}_2\text{ClCH}_3+\text{C}_2\text{HCl}_3+\text{Cl}$	$3.02\text{E}+11$	0	14500	Q
476.	$\text{CH}_2\text{ClCH}_2+\text{CHCl}_2\text{OCl}_3=\text{CH}_2\text{ClCH}_3+\text{C}_2\text{Cl}_4+\text{Cl}$	$3.02\text{E}+11$	0	14500	Q
477.	$\text{CH}_2\text{ClCH}_2+\text{C}_2\text{H}_4=\text{CH}_2\text{ClCH}_3+\text{C}_2\text{H}_3$	$3.02\text{E}+11$	0	14500	Q
478.	$\text{CH}_2\text{ClCH}_2+\text{VCM}=\text{CH}_2\text{ClCH}_3+\text{CH}_2\text{OCl}$	$3.02\text{E}+11$	0	14500	Q
479.	$\text{CH}_2\text{ClCH}_2+\text{CH}_3\text{OCl}_3=\text{CH}_2\text{ClCH}_3+\text{OCl}_3\text{CH}_2$	$3.02\text{E}+11$	0	14500	Q
480.	$\text{CH}_3+\text{CH}_4=\text{CH}_4+\text{CH}_3$	$3.02\text{E}+11$	0	12400	Q
481.	$\text{CH}_3+\text{CH}_2\text{ClCHCl}_2=\text{CH}_4+\text{CHClCHCl}_1+\text{Cl}$	$3.02\text{E}+11$	0	12400	Q
482.	$\text{CH}_3+\text{CHCl}_2\text{CHCl}_2=\text{CH}_4+\text{C}_2\text{HCl}_3+\text{Cl}$	$3.02\text{E}+11$	0	12400	Q
483.	$\text{CH}_3+\text{CHCl}_2\text{OCl}_3=\text{CH}_4+\text{C}_2\text{Cl}_4+\text{Cl}$	$3.02\text{E}+11$	0	12400	Q
484.	$\text{CH}_3+\text{CH}_3\text{OCl}_3=\text{CH}_4+\text{OCl}_3\text{CH}_2$	$3.02\text{E}+11$	0	12400	Q
485.	$\text{C}_2\text{H}_5+\text{C}_2\text{H}_6=\text{C}_2\text{H}_6+\text{C}_2\text{H}_5$	$3.02\text{E}+11$	0	14800	Q
486.	$\text{C}_2\text{H}_5+\text{CH}_3\text{CHCl}_2=\text{C}_2\text{H}_6+\text{CH}_3\text{OCl}_2$	$3.02\text{E}+11$	0	14800	Q
487.	$\text{C}_2\text{H}_5+\text{CH}_3\text{CHCl}_2=\text{C}_2\text{H}_6+\text{CHCl}_2\text{CH}_2$	$3.02\text{E}+11$	0	14800	Q
488.	$\text{C}_2\text{H}_5+\text{CH}_2\text{ClCHCl}_2=\text{C}_2\text{H}_6+\text{CHClCHCl}_1+\text{Cl}$	$3.02\text{E}+11$	0	14800	Q
489.	$\text{C}_2\text{H}_5+\text{CHCl}_2\text{CHCl}_2=\text{C}_2\text{H}_6+\text{C}_2\text{HCl}_3+\text{Cl}$	$3.02\text{E}+11$	0	14800	Q
490.	$\text{C}_2\text{H}_5+\text{CHCl}_2\text{OCl}_3=\text{C}_2\text{H}_6+\text{C}_2\text{Cl}_4+\text{Cl}$	$3.02\text{E}+11$	0	14800	Q
491.	$\text{C}_2\text{H}_5+\text{C}_2\text{H}_4=\text{C}_2\text{H}_6+\text{C}_2\text{H}_3$	$3.02\text{E}+11$	0	14800	Q
492.	$\text{C}_2\text{H}_5+\text{CH}_3\text{OCl}_3=\text{C}_2\text{H}_6+\text{OCl}_3\text{CH}_2$	$3.02\text{E}+11$	0	14800	Q
493.	$\text{C}_2\text{H}_3+\text{CH}_3\text{CHCl}_2=\text{C}_2\text{H}_4+\text{CH}_3\text{OCl}_2$	$6.03\text{E}+11$	0	11200	Q
494.	$\text{C}_2\text{H}_3+\text{CH}_3\text{CHCl}_2=\text{C}_2\text{H}_4+\text{CHCl}_2\text{CH}_2$	$6.03\text{E}+11$	0	11200	Q
495.	$\text{C}_2\text{H}_3+\text{CH}_2\text{ClCHCl}_2=\text{C}_2\text{H}_4+\text{CHClCHCl}_1+\text{Cl}$	$6.03\text{E}+11$	0	11200	Q
496.	$\text{C}_2\text{H}_3+\text{CHCl}_2\text{CHCl}_2=\text{C}_2\text{H}_4+\text{C}_2\text{HCl}_3+\text{Cl}$	$6.03\text{E}+11$	0	11200	Q
497.	$\text{C}_2\text{H}_3+\text{CHCl}_2\text{OCl}_3=\text{C}_2\text{H}_4+\text{C}_2\text{Cl}_4+\text{Cl}$	$6.03\text{E}+11$	0	11200	Q
498.	$\text{C}_2\text{H}_3+\text{C}_2\text{H}_4=\text{C}_2\text{H}_4+\text{C}_2\text{H}_3$	$6.03\text{E}+11$	0	11200	Q
499.	$\text{C}_2\text{H}_3+\text{CH}_3\text{OCl}_3=\text{C}_2\text{H}_4+\text{OCl}_3\text{CH}_2$	$6.03\text{E}+11$	0	11200	Q
500.	$\text{CH}_3\text{OCl}_2+\text{CH}_3\text{CHCl}_2=\text{CH}_3\text{CHCl}_2+\text{CH}_3\text{OCl}_2$	$3.63\text{E}+11$	0	16800	Q
501.	$\text{CH}_3\text{OCl}_2+\text{CH}_3\text{CHCl}_2=\text{CH}_3\text{CHCl}_2+\text{CHCl}_2\text{CH}_2$	$3.63\text{E}+11$	0	16800	Q
502.	$\text{CH}_3\text{OCl}_2+\text{CH}_2\text{ClCHCl}_2=\text{CH}_3\text{CHCl}_2+\text{CHClCHCl}_1+\text{Cl}$	$3.63\text{E}+11$	0	16800	Q
503.	$\text{CH}_3\text{OCl}_2+\text{CHCl}_2\text{CHCl}_2=\text{CH}_3\text{CHCl}_2+\text{C}_2\text{HCl}_3+\text{Cl}$	$3.63\text{E}+11$	0	16800	Q
504.	$\text{CH}_3\text{OCl}_2+\text{CHCl}_2\text{OCl}_3=\text{CH}_3\text{CHCl}_2+\text{C}_2\text{Cl}_4+\text{Cl}$	$3.63\text{E}+11$	0	16800	Q
505.	$\text{CH}_3\text{OCl}_2+\text{CH}_3\text{OCl}_3=\text{CH}_3\text{CHCl}_2+\text{OCl}_3\text{CH}_2$	$3.63\text{E}+11$	0	16800	Q
506.	$\text{CHCl}_2\text{CH}_2+\text{CH}_3\text{CHCl}_2=\text{CH}_3\text{CHCl}_2+\text{CHCl}_2\text{CH}_2$	$3.02\text{E}+11$	0	14000	Q
507.	$\text{CHCl}_2\text{CH}_2+\text{CH}_2\text{ClCHCl}_2=\text{CH}_3\text{CHCl}_2+\text{CHClCHCl}_1+\text{Cl}$	$3.02\text{E}+11$	0	14000	Q
508.	$\text{CHCl}_2\text{CH}_2+\text{CHCl}_2\text{CHCl}_2=\text{CH}_3\text{CHCl}_2+\text{C}_2\text{HCl}_3+\text{Cl}$	$3.02\text{E}+11$	0	14000	Q
509.	$\text{CHCl}_2\text{CH}_2+\text{CHCl}_2\text{OCl}_3=\text{CH}_3\text{CHCl}_2+\text{C}_2\text{Cl}_4+\text{Cl}$	$3.02\text{E}+11$	0	14000	Q
510.	$\text{CHCl}_2\text{CH}_2+\text{CH}_3\text{OCl}_3=\text{CH}_3\text{CHCl}_2+\text{OCl}_3\text{CH}_2$	$3.02\text{E}+11$	0	14000	Q
511.	$\text{OCl}_3\text{CH}_2+\text{CH}_2\text{ClCHCl}_2=\text{CH}_3\text{OCl}_3+\text{CHClCHCl}_1+\text{Cl}$	$3.02\text{E}+11$	0	14000	Q
512.	$\text{OCl}_3\text{CH}_2+\text{CHCl}_2\text{CHCl}_2=\text{CH}_3\text{OCl}_3+\text{C}_2\text{HCl}_3+\text{Cl}$	$3.02\text{E}+11$	0	14000	Q
513.	$\text{OCl}_3\text{CH}_2+\text{CHCl}_2\text{OCl}_3=\text{CH}_3\text{OCl}_3+\text{C}_2\text{Cl}_4+\text{Cl}$	$3.02\text{E}+11$	0	14000	Q
514.	$\text{OCl}_3\text{CH}_2+\text{CH}_3\text{OCl}_3=\text{CH}_3\text{OCl}_3+\text{OCl}_3\text{CH}_2$	$3.02\text{E}+11$	0	14000	Q
515.	$\text{CH}_4+\text{H}=\text{CH}_3+\text{H}_2$	$5.50\text{E}+07$	2	11207	B
516.	$\text{CH}_4+\text{Cl}=\text{CH}_3+\text{HCl}$	$5.16\text{E}+06$	2.1	1580	B
517.	$\text{CH}_3\text{Cl}+\text{Cl}=\text{CH}_2\text{Cl}+\text{HCl}$	$3.16\text{E}+13$	0	330	B

Figure A.14: List of reactions used on the mechanism by Borsa [2] (cont.)

No.	Reaction	A ($\text{cm}^3 \cdot \text{mol}^{-1} \cdot \text{s}^{-1}$)	n	E_a (cal/mol)	Ref.
518.	$\text{CH}_3\text{Cl} + \text{H} = \text{CH}_3 + \text{HCl}$	3.72E+13	0	9300	B
519.	$\text{CH}_3\text{Cl} + \text{H} = \text{CH}_2\text{Cl} + \text{H}_2$	1.00E+13	0	9000	B
520.	$\text{CH}_3\text{Cl} + \text{CH}_3 = \text{CH}_2\text{Cl} + \text{CH}_4$	1.51E+10	0.5	9330	B
521.	$\text{C}_2\text{H}_6 + \text{H} = \text{C}_2\text{H}_5 + \text{H}_2$	5.40E+02	3.5	5210	B
522.	$\text{C}_2\text{H}_6 + \text{Cl} = \text{C}_2\text{H}_5 + \text{HCl}$	4.64E+13	0	179	B
523.	$\text{C}_2\text{H}_6 + \text{CH}_3 = \text{C}_2\text{H}_5 + \text{CH}_4$	5.50E-01	4	8294	B
524.	$\text{C}_2\text{H}_6 + \text{CH}_2\text{Cl} = \text{C}_2\text{H}_5 + \text{CH}_3\text{Cl}$	1.00E+12	0	8500	B
525.	$\text{CH}_2\text{ClCH}_3 + \text{H} = \text{C}_2\text{H}_5 + \text{HCl}$	6.31E+13	0	8600	B
526.	$\text{CH}_2\text{ClCH}_3 + \text{H} = \text{CH}_2\text{ClCH}_2 + \text{H}_2$	3.00E+13	0	10000	E
527.	$\text{CH}_2\text{ClCH}_3 + \text{H} = \text{CH}_3\text{CHCl} + \text{H}_2$	2.00E+13	0	10000	E
528.	$\text{CH}_2\text{ClCH}_3 + \text{Cl} = \text{CH}_2\text{ClCH}_2 + \text{HCl}$	8.46E+12	0	616	E
529.	$\text{CH}_2\text{ClCH}_3 + \text{Cl} = \text{CH}_3\text{CHCl} + \text{HCl}$	5.64E+12	0	616	E
530.	$\text{CH}_2\text{ClCH}_3 + \text{CH}_3 = \text{CH}_2\text{ClCH}_2 + \text{CH}_4$	6.00E+11	0	8500	E
531.	$\text{CH}_2\text{ClCH}_3 + \text{CH}_3 = \text{CH}_3\text{CHCl} + \text{CH}_4$	4.00E+11	0	8500	E
532.	$\text{CH}_2\text{ClCH}_3 + \text{CH}_2\text{Cl} = \text{CH}_2\text{ClCH}_2 + \text{CH}_3\text{Cl}$	1.90E+12	0	9000	E
533.	$\text{CH}_2\text{ClCH}_3 + \text{CH}_2\text{Cl} = \text{CH}_3\text{CHCl} + \text{CH}_3\text{Cl}$	1.26E+12	0	9000	E
534.	$\text{CH}_3\text{CHCl}_2 + \text{H} = \text{CH}_3\text{CCl}_2 + \text{H}_2$	1.25E+13	0	10000	E
535.	$\text{CH}_3\text{CHCl}_2 + \text{H} = \text{CHCl}_2\text{CH}_2 + \text{H}_2$	3.75E+13	0	10000	E
536.	$\text{EDC} + \text{H} = \text{CH}_2\text{ClCHCl} + \text{H}_2$	5.00E+13	0	10000	E
537.	$\text{CH}_3\text{CHCl}_2 + \text{Cl} = \text{CH}_3\text{CCl}_2 + \text{HCl}$	6.27E+12	0	3100	E
538.	$\text{CH}_3\text{CHCl}_2 + \text{Cl} = \text{CHCl}_2\text{CH}_2 + \text{HCl}$	1.88E+13	0	3100	E
539.	$\text{CH}_3\text{CHCl}_2 + \text{CH}_3 = \text{CH}_3\text{CCl}_2 + \text{CH}_4$	2.50E+11	0	8500	E
540.	$\text{CH}_3\text{CHCl}_2 + \text{CH}_3 = \text{CHCl}_2\text{CH}_2 + \text{CH}_4$	7.50E+11	0	8500	E
541.	$\text{EDC} + \text{CH}_3 = \text{CH}_2\text{ClCHCl} + \text{CH}_4$	1.00E+12	0	8500	E
542.	$\text{CH}_3\text{CHCl}_2 + \text{CH}_2\text{Cl} = \text{CH}_3\text{CCl}_2 + \text{CH}_3\text{Cl}$	7.90E+11	0	9000	E
543.	$\text{CH}_3\text{CHCl}_2 + \text{CH}_2\text{Cl} = \text{CHCl}_2\text{CH}_2 + \text{CH}_3\text{Cl}$	2.37E+12	0	9000	E
544.	$\text{CH}_2\text{ClCH}_2 + \text{Cl} = \text{VCM} + \text{HCl}$	1.00E+13	0	3000	E
545.	$\text{CH}_3\text{CHCl} + \text{Cl} = \text{VCM} + \text{HCl}$	1.00E+13	0	3000	E
546.	$\text{CHCl}_2\text{CH}_2 + \text{H} = \text{VCM} + \text{HCl}$	1.00E+13	0	1000	E
547.	$\text{CH}_2\text{ClCHCl} + \text{H} = \text{VCM} + \text{HCl}$	1.00E+13	0	1000	E
548.	$\text{VCM} + \text{H} = \text{CHClCH} + \text{H}_2$	6.67E+13	0	10000	E
549.	$\text{VCM} + \text{H} = \text{CH}_2\text{OCl} + \text{H}_2$	3.33E+13	0	10000	E
550.	$\text{VCM} + \text{CH}_3 = \text{CHClCH} + \text{CH}_4$	6.67E+11	0	11000	E
551.	$\text{VCM} + \text{CH}_3 = \text{CH}_2\text{OCl} + \text{CH}_4$	3.33E+11	0	11000	E
552.	$\text{VCM} + \text{CH}_2\text{Cl} = \text{CHClCH} + \text{CH}_3\text{Cl}$	6.66E+11	0	12000	E
553.	$\text{VCM} + \text{CH}_2\text{Cl} = \text{CH}_2\text{OCl} + \text{CH}_3\text{Cl}$	3.33E+11	0	12000	E
554.	$\text{C}_2\text{H}_5 + \text{H} = \text{C}_2\text{H}_4 + \text{H}_2$	1.90E+12	0	0	B
555.	$\text{C}_2\text{H}_5 + \text{Cl} = \text{C}_2\text{H}_4 + \text{HCl}$	2.00E+12	0	0	B
556.	$\text{C}_2\text{H}_4 + \text{H} = \text{C}_2\text{H}_3 + \text{H}_2$	7.00E+14	0	14500	B
557.	$\text{C}_2\text{H}_4 + \text{CH}_3 = \text{C}_2\text{H}_3 + \text{CH}_4$	3.97E+11	0	7988	B
558.	$\text{C}_2\text{H}_4 + \text{CH}_2\text{Cl} = \text{C}_2\text{H}_3 + \text{CH}_3\text{Cl}$	2.00E+12	0	12000	B
559.	$\text{VCM} + \text{H} = \text{C}_2\text{H}_3 + \text{HCl}$	1.00E+14	0	4500	B
560.	$\text{C}_2\text{H}_3 + \text{H} = \text{C}_2\text{H}_2 + \text{H}_2$	1.00E+13	0	0	B
561.	$\text{C}_2\text{H}_3 + \text{Cl} = \text{C}_2\text{H}_2 + \text{HCl}$	1.00E+13	0	0	B

Figure A.15: List of reactions used on the mechanism by Borsa [2] (cont.)

No.	Reaction	A (cm ³ -mol-s)	n	E _a (cal/mol)	Ref.
562.	EDC+CL=CH2CLCHCL+HCL	1.33E+13	0	1576	Ac
563.	VCM+CL=CHCLCH+HCL	1.20E+14	0	13312	X
564.	VCM+CL=CH2OCL+HCL	6.00E+13	0	9300	X
565.	CHCLCH+EDC=VCM+CH2CLCHCL	1.20E+13	0	8000	U
566.	CH2OCL+EDC=VCM+CH2CLCHCL	1.20E+13	0	10000	U
567.	CH2CLCH2+EDC=CH2CLCH3+CH2CLCHCL	2.00E+12	0	10000	V
568.	C2H4+CL=C2H3+HCL	1.00E+14	0	7001	K
569.	C4H6CL2_34D+CL=C4H5CL2_434D+HCL	7.00E+12	0	1576	Ac
570.	C4H6CL2_34D+CL=C4H5CL2_334D+HCL	3.50E+12	0	1576	Ac
571.	C4H5CL3_134D+CL=C4H4CL3_4134D+HCL	7.00E+12	0	1576	Ac
572.	C4H5CL3_134D+CL=C4H4CL3_3134D+HCL	3.50E+12	0	1576	Ac
573.	C4H5CL3_134D+CH2CLCHCL=C4H4CL3_4134D+EDC	1.00E+12	0	14000	D
574.	C4H5CL3_134D+CH2CLCHCL=C4H4CL3_3134D+EDC	5.00E+11	0	14000	D
575.	C4H6CL2_34D+CH2CLCHCL=C4H5CL2_434D+EDC	1.00E+12	0	14000	D
576.	C4H6CL2_34D+CH2CLCHCL=C4H5CL2_334D+EDC	5.00E+11	0	14000	D
577.	OCL3+EDC=CHCL3+CH2CLCHCL	1.00E+12	0	15000	G
578.	CHCL3+CL=OCL3+HCL	6.90E+12	0	3348	Af
579.	C2HCL3+CL=C2CL3+HCL	1.00E+12	0	2000	Ac
580.	C3H4CL4_1223+CL=CH2CLOCL2CHCL+HCL	1.33E+13	0	1576	Ac
581.	C4H5_213D+EDC=CH2CLCHCL+C4H6_13D	1.00E+13	0	8000	U
582.	CL+C2H2=C2H+HCL	1.58E+14	0	16900	K
583.	CL+C2HCL=C2CL+HCL	1.58E+14	0	16900	K
584.	OCL3+C2H2=C2H+CHCL3	1.38E+14	0	16900	K
585.	OCL3+C2HCL=C2CL+CHCL3	1.58E+14	0	16900	K
586.	CH2CLCHCL+C2H2=EDC+C2H	1.58E+14	0	16900	K
587.	CH2CLCHCL+C2HCL=EDC+C2CL	1.58E+14	0	16900	K
588.	CH2OCL+C2H2=VCM+C2H	1.58E+14	0	16900	K
589.	CH2OCL+C2HCL=VCM+C2CL	1.58E+14	0	16900	K
590.	C2CL3+C2H2=C2HCL3+C2H	1.58E+14	0	16900	K
591.	C2CL3+C2HCL=C2HCL3+C2CL	1.58E+14	0	16900	K
592.	C2H+CH2CLCHCL2=C2H2+CHCL2CHCL	1.00E+13	0	4000	N
593.	C2H+CH3CHCL2=C2H2+CHCL2CH2	7.00E+12	0	3000	O
594.	C2CL+CH2CLCHCL2=C2HCL+CHCL2CHCL	1.00E+13	0	4000	N
595.	C2CL+CH3CHCL2=C2HCL+CHCL2CH2	7.00E+12	0	3000	O
596.	C2H+CH3OCL3=C2H2+OCL3CH2	2.00E+13	0	26000	L
597.	C2CL+CH3OCL3=C2HCL+OCL3CH2	2.00E+13	0	26000	L
598.	CH3OCL2+C2H2=C2H+CH3CHCL2	6.14E+12	0	1264	P
599.	CH3OCL2+C2HCL=C2CL+CH3CHCL2	6.14E+12	0	1264	P
600.	CL+C3H3CL3_123D=HCL+C3H2CL3_313D	2.00E+14	0	0	F
601.	CL+C3H3CL3_113D=HCL+C3H2CL3_323D	2.00E+14	0	0	F
602.	CL+C3H4CL2_23D=HCL+C3H3CL2_323D	2.00E+14	0	0	F
603.	CL+C3H2CL4_33D=HCL+C3HCL4_33D	2.00E+14	0	0	F
604.	CL+C3H4CL2_13D=HCL+C3H3CL2_313D	2.00E+14	0	0	F
605.	CL+C3H5CL_3D=HCL+C3H4CL_33D	2.00E+14	0	0	F

Figure A.16: List of reactions used on the mechanism by Borsa [2] (cont.)

No.	Reaction	A (cm ³ -mol-s)	n	E _a (cal/mol)	Ref.
606.	CL+C3H2CL4_12D=HCL+C3HCL4_21D	2.00E+14	0	0	F
607.	CL+C3H3CL3_333D=HCL+C3H2CL3_211D	2.00E+14	0	0	F
608.	CL+C3H3CL5_112=HCL+C3H2CL5_211	2.00E+14	0	0	F
609.	OCL3+C3H3CL3_123D=CHCL3+C3H2CL3_313D	2.00E+11	0	10000	G
610.	OCL3+C3H3CL3_113D=CHCL3+C3H2CL3_323D	2.00E+11	0	10000	G
611.	OCL3+C3H4CL2_23D=CHCL3+C3H3CL2_323D	2.00E+11	0	10000	G
612.	OCL3+C3H2CL4_33D=CHCL3+C3HCL4_33D	2.00E+11	0	10000	G
613.	OCL3+C3H4CL2_13D=CHCL3+C3H3CL2_313D	2.00E+11	0	10000	G
614.	OCL3+C3H5CL_3D=CHCL3+C3H4CL_33D	2.00E+11	0	10000	G
615.	OCL3+C3H2CL4_12D=CHCL3+C3HCL4_21D	2.00E+11	0	10000	G
616.	OCL3+C3H3CL3_333D=CHCL3+C3H2CL3_211D	2.00E+11	0	10000	G
617.	OCL3+C3H3CL5_112=CHCL3+C3H2CL5_211	2.00E+11	0	10000	G
618.	OCL3+C3H4CL4_1223=CHCL3+CH2CLOCL2CHCL	2.00E+11	0	10000	G
619.	CH3OCL2+C3H3CL3_123D=CH3CHCL2+C3H2CL3_313D	2.00E+11	0	10000	G
620.	CH3OCL2+C3H3CL3_113D=CH3CHCL2+C3H2CL3_323D	2.00E+11	0	10000	G
621.	CH3OCL2+C3H4CL2_23D=CH3CHCL2+C3H3CL2_323D	2.00E+11	0	10000	G
622.	CH3OCL2+C3H2CL4_33D=CH3CHCL2+C3HCL4_33D	2.00E+11	0	10000	G
623.	CH3OCL2+C3H4CL2_13D=CH3CHCL2+C3H3CL2_313D	2.00E+11	0	10000	G
624.	CH3OCL2+C3H5CL_3D=CH3CHCL2+C3H4CL_33D	2.00E+11	0	10000	G
625.	CH3OCL2+C3H2CL4_12D=CH3CHCL2+C3HCL4_21D	2.00E+11	0	10000	G
626.	CH3OCL2+C3H3CL3_333D=CH3CHCL2+C3H2CL3_211D	2.00E+11	0	10000	G
627.	CH3OCL2+C3H3CL5_112=CH3CHCL2+C3H2CL5_211	2.00E+11	0	10000	G
628.	CH3OCL2+C3H4CL4_1223=CH3CHCL2+CH2CLOCL2CHCL	2.00E+11	0	10000	G
629.	CH2CLCHCL+C3H3CL3_123D=EDC+C3H2CL3_313D	2.00E+11	0	10000	G
630.	CH2CLCHCL+C3H3CL3_113D=EDC+C3H2CL3_323D	2.00E+11	0	10000	G
631.	CH2CLCHCL+C3H4CL2_23D=EDC+C3H3CL2_323D	2.00E+11	0	10000	G
632.	CH2CLCHCL+C3H2CL4_33D=EDC+C3HCL4_33D	2.00E+11	0	10000	G
633.	CH2CLCHCL+C3H4CL2_13D=EDC+C3H3CL2_313D	2.00E+11	0	10000	G
634.	CH2CLCHCL+C3H5CL_3D=EDC+C3H4CL_33D	2.00E+11	0	10000	G
635.	CH2CLCHCL+C3H2CL4_12D=EDC+C3HCL4_21D	2.00E+11	0	10000	G
636.	CH2CLCHCL+C3H3CL3_333D=EDC+C3H2CL3_211D	2.00E+11	0	10000	G
637.	CH2CLCHCL+C3H3CL5_112=EDC+C3H2CL5_211	2.00E+11	0	10000	G
638.	CH2CLCHCL+C3H4CL4_1223=EDC+CH2CLOCL2CHCL	2.00E+11	0	10000	G
639.	CH2OCL+C3H3CL3_123D=VCM+C3H2CL3_313D	2.00E+11	0	10000	G
640.	CH2OCL+C3H3CL3_113D=VCM+C3H2CL3_323D	2.00E+11	0	10000	G
641.	CH2OCL+C3H4CL2_23D=VCM+C3H3CL2_323D	2.00E+11	0	10000	G
642.	CH2OCL+C3H2CL4_33D=VCM+C3HCL4_33D	2.00E+11	0	10000	G
643.	CH2OCL+C3H4CL2_13D=VCM+C3H3CL2_313D	2.00E+11	0	10000	G
644.	CH2OCL+C3H5CL_3D=VCM+C3H4CL_33D	2.00E+11	0	10000	G
645.	CH2OCL+C3H2CL4_12D=VCM+C3HCL4_21D	2.00E+11	0	10000	G
646.	CH2OCL+C3H3CL3_333D=VCM+C3H2CL3_211D	2.00E+11	0	10000	G
647.	CH2OCL+C3H3CL5_112=VCM+C3H2CL5_211	2.00E+11	0	10000	G
648.	CH2OCL+C3H4CL4_1223=VCM+CH2CLOCL2CHCL	2.00E+11	0	10000	G
649.	C3H3CL2_312D+EDC=CH2CLCHCL+C3H4CL2_12D	2.00E+11	0	10000	G

Figure A.17: List of reactions used on the mechanism by Borsa [2] (cont.)

No.	Reaction	A (cm ² -mol-s)	n	E _a (cal/mol)	Ref.
650.	C3H3CL2_311D+EDC=CH2CLCHCL+C3H4CL2_11D	2.00E+11	0	10000	G
651.	C3H4CL_32D+EDC=CH2CLCHCL+C3H5CL_2D	2.00E+11	0	10000	G
652.	C3H2CL3_333D+EDC=CH2CLCHCL+C3H3CL3_112D	2.00E+11	0	10000	G
653.	C3H4CL_31D+EDC=CH2CLCHCL+C3H5CL_1D	2.00E+11	0	10000	G
654.	C3H5_3D+EDC=CH2CLCHCL+C3H6	2.00E+14	0	10000	G
655.	C3H2CL3_312D+EDC=CH2CLCHCL+C3H3CL3_133D	2.00E+11	0	10000	G
656.	C3H3CL2_333D+EDC=CH2CLCHCL+C3H4CL2_33D	2.00E+11	0	10000	G
657.	C3H3CL2_312D+VCM=CHCLCH+C3H4CL2_12D	2.00E+11	0	10000	G
658.	C3H3CL2_311D+VCM=CHCLCH+C3H4CL2_11D	2.00E+11	0	10000	G
659.	C3H4CL_32D+VCM=CHCLCH+C3H5CL_2D	2.00E+11	0	10000	G
660.	C3H2CL3_333D+VCM=CHCLCH+C3H3CL3_112D	2.00E+11	0	10000	G
661.	C3H4CL_31D+VCM=CHCLCH+C3H5CL_1D	2.00E+11	0	10000	G
662.	C3H5_3D+VCM=CHCLCH+C3H6	2.00E+10	0	10000	G
663.	C3H2CL3_312D+VCM=CHCLCH+C3H3CL3_133D	2.00E+11	0	10000	G
664.	C3H3CL2_333D+VCM=CHCLCH+C3H4CL2_33D	2.00E+11	0	10000	G
665.	C3H3CL2_312D+CH3CHCL2=CHCL2CH2+C3H4CL2_12D	2.00E+11	0	10000	G
666.	C3H3CL2_311D+CH3CHCL2=CHCL2CH2+C3H4CL2_11D	2.00E+11	0	10000	G
667.	C3H4CL_32D+CH3CHCL2=CHCL2CH2+C3H5CL_2D	2.00E+11	0	10000	G
668.	C3H2CL3_333D+CH3CHCL2=CHCL2CH2+C3H3CL3_112D	2.00E+11	0	10000	G
669.	C3H4CL_31D+CH3CHCL2=CHCL2CH2+C3H5CL_1D	2.00E+11	0	10000	G
670.	C3H5_3D+CH3CHCL2=CHCL2CH2+C3H6	2.00E+14	0	10000	G
671.	C3H2CL3_312D+CH3CHCL2=CHCL2CH2+C3H3CL3_133D	2.00E+11	0	10000	G
672.	C3H3CL2_333D+CH3CHCL2=CHCL2CH2+C3H4CL2_33D	2.00E+11	0	10000	G
673.	C3H4CL_33D+VCM=C3H5CL_3D+CHCLCH	2.00E+11	0	10000	G
Chlorine Abstraction					
674.	HCL+H=CL+H2	5.00E+10	0	4600	Q
675.	CL+CH2CLCHCL2=HCL+CHCLCHCL_1+CL	2.00E+10	0	3100	Q
676.	CL+CHCL2CHCL2=HCL+C2HCL3+CL	1.50E+10	0	3100	Q
677.	CL+CHCL2OCL3=HCL+C2CL4+CL	7.50E+09	0	3100	Q
678.	CL+CH2CL2=HCL+CHCL2	2.70E+10	0	3000	Q
679.	CL+CH3OCL3=HCL+OCL3CH2	2.50E+09	0	3600	Q
680.	CL+HCL=CL2+H	2.00E+11	0	49000	Q
681.	CL+CH3CL=CL2+CH3	1.00E+11	0	25000	Q
682.	CL+CH2CL2=CL2+CH2CL	1.00E+11	0	21400	Q
683.	CL+CHCL3=CL2+CHCL2	1.00E+11	0	21000	Q
684.	CL+OCL4=CL2+OCL3	8.50E+10	0	20000	Q
685.	CL+CH2CLCH3=CL2+C2H5	2.00E+11	0	21500	Q
686.	CL+EDC=CL2+CH2CLCH2	2.00E+11	0	21300	Q
687.	CL+CH3OCL3=CL2+CH3OCL2	1.50E+11	0	21800	Q
688.	EDC+H=CH2CLCH2+HCL	6.31E+13	0	8400	E
689.	CH3CHCL2+H=CH3CHCL+HCL	6.31E+13	0	8400	E
690.	CH2CLCH2+H=C2H4+HCL	3.16E+12	0	0	E
691.	CHCLCH+EDC=CHCLCHCL_c+CH2CLCH2	6.00E+12	0	10000	U

Figure A.18: List of reactions used on the mechanism by Borsa [2] (cont.)

No.	Reaction	A (cm ³ -mol ⁻¹ -s)	n	E _a (cal/mol)	Ref.
692.	CH ₂ OCL+EDC=CH ₂ OCL ₂ +CH ₂ CLCH ₂	6.00E+11	0	8000	U
693.	CH ₂ CLCHCL+EDC=CH ₂ CLCHCL ₂ +CH ₂ CLCH ₂	1.00E+12	0	18000	V
694.	C ₂ H ₃ +EDC=VCM+CH ₂ CLCH ₂	1.20E+14	0	13312	X
695.	CH ₂ CLCHCL+CL ₂ =CH ₂ CLCHCL ₂ +CL	1.00E+13	0	0	Z
696.	CH ₂ OCL+CL ₂ =CH ₂ OCL ₂ +CL	1.00E+13	0	0	Z
697.	CHCLCH+CL ₂ =CHCLCHCL _c +CL	1.00E+13	0	0	Z
698.	C ₄ H ₅ CL ₃ _134D+CH ₂ CLCHCL=C ₄ H ₅ CL ₂ _413D+CH ₂ CLCHCL ₂	1.00E+12	0	18000	V
699.	C ₄ H ₅ CL ₃ _134D+CH ₂ CLCHCL=C ₄ H ₅ CL ₂ _314D+CH ₂ CLCHCL ₂	1.00E+12	0	18000	V
700.	C ₄ H ₆ CL ₂ _34D+CH ₂ CLCHCL=C ₄ H ₆ CL_43D+CH ₂ CLCHCL ₂	1.00E+12	0	6300	V
701.	C ₄ H ₆ CL ₂ _34D+CH ₂ CLCHCL=C ₄ H ₆ CL_34D+CH ₂ CLCHCL ₂	1.00E+12	0	6300	V
702.	CCL ₄ +CH ₂ CLCHCL=CCL ₃ +CH ₂ CLCHCL ₂	1.00E+12	0	8000	V
703.	CHCLCH+CL ₂ =CHCLCHCL _f +CL	1.00E+13	0	0	Z
704.	CHCLCH+EDC=CHCLCHCL _f +CH ₂ CLCH ₂	6.00E+12	0	10000	U
705.	CH ₂ CL+EDC=CH ₂ CL+CH ₂ CLCHCL	2.00E+12	0	13000	Y
706.	C ₄ H ₇ CL_4D+CH ₂ OCL=C ₄ H ₇ _4D+CH ₂ OCL ₂	1.00E+12	0	18000	R
707.	C ₄ H ₇ CL_4D+CHCLCH=C ₄ H ₇ _4D+CHCLCHCL _c	1.00E+12	0	18000	R
708.	C ₄ H ₇ CL_4D+CHCLCH=C ₄ H ₇ _4D+CHCLCHCL _f	1.00E+12	0	18000	R
709.	C ₄ H ₇ CL_4D+CH ₂ CLCHCL=C ₄ H ₇ _4D+CH ₂ CLCHCL ₂	1.00E+12	0	18000	R
710.	C ₄ H ₆ CL ₂ _34D+CH ₂ OCL=C ₄ H ₆ CL_34D+CH ₂ OCL ₂	1.00E+12	0	18300	R
711.	C ₄ H ₆ CL ₂ _34D+CHCLCH=C ₄ H ₆ CL_34D+CHCLCHCL _c	1.00E+12	0	18300	R
712.	C ₄ H ₆ CL ₂ _34D+CHCLCH=C ₄ H ₆ CL_34D+CHCLCHCL _f	1.00E+12	0	18300	R
713.	C ₄ H ₆ CL ₂ _34D+CH ₂ OCL=C ₄ H ₆ CL_43D+CH ₂ OCL ₂	1.00E+12	0	18300	R
714.	C ₄ H ₆ CL ₂ _34D+CHCLCH=C ₄ H ₆ CL_43D+CHCLCHCL _c	1.00E+12	0	18300	R
715.	C ₄ H ₆ CL ₂ _34D+CHCLCH=C ₄ H ₆ CL_43D+CHCLCHCL _f	1.00E+12	0	18300	R
716.	C ₄ H ₅ CL_213D+CH ₂ OCL=C ₄ H ₅ _213D+CH ₂ OCL ₂	1.00E+12	0	8300	Y
717.	C ₄ H ₅ CL_213D+CHCLCH=C ₄ H ₅ _213D+CHCLCHCL _c	1.00E+12	0	8300	Y
718.	C ₄ H ₅ CL_213D+CHCLCH=C ₄ H ₅ _213D+CHCLCHCL _f	1.00E+12	0	8300	Y
719.	C ₄ H ₅ CL_213D+CH ₂ CLCHCL=C ₄ H ₅ _213D+CH ₂ CLCHCL ₂	1.00E+12	0	8300	Y
720.	C ₂ HCL+H=C ₂ H+HCL	1.00E+15	0	14872	M
721.	C ₂ CL ₂ +H=C ₂ CL+HCL	1.00E+15	0	14872	M
722.	C ₂ HCL+OCL ₃ =C ₂ H+OCL ₄	1.00E+15	0	14872	M
723.	C ₂ CL ₂ +OCL ₃ =C ₂ CL+OCL ₄	1.00E+15	0	14872	M
724.	CH ₂ CLCHCL+C ₂ HCL=C ₂ H+CH ₂ CLCHCL ₂	1.00E+15	0	14872	M
725.	CH ₂ CLCHCL+C ₂ CL ₂ =C ₂ CL+CH ₂ CLCHCL ₂	1.00E+15	0	14872	M
726.	CH ₂ OCL+C ₂ HCL=C ₂ H+CH ₂ OCL ₂	1.00E+15	0	14872	M
727.	CH ₂ OCL+C ₂ CL ₂ =C ₂ CL+CH ₂ OCL ₂	1.00E+15	0	14872	M
728.	C ₂ CL ₃ +C ₂ HCL=C ₂ H+C ₂ CL ₄	1.00E+15	0	14872	M
729.	C ₂ CL ₃ +C ₂ CL ₂ =C ₂ CL+C ₂ CL ₄	1.00E+15	0	14872	M
730.	C ₂ H+CHCL ₃ =C ₂ HCL+CHCL ₂	2.00E+13	0	26000	L
731.	C ₂ H+EDC=C ₂ HCL+CH ₂ CLCH ₂	2.00E+13	0	26000	L
732.	C ₂ H+VCM=C ₂ HCL+C ₂ H ₃	3.98E+13	0	9298	Aa
733.	C ₂ H+CH ₃ CHCL ₂ =C ₂ HCL+CH ₃ CHCL	2.00E+13	0	26000	L
734.	C ₂ H+C ₂ HCL ₃ =C ₂ HCL+CHCL ₂ OCL	3.47E+13	0	0	Aa
735.	C ₂ CL+CHCL ₃ =C ₂ CL ₂ +CHCL ₂	2.00E+13	0	26000	L

Figure A.19: List of reactions used on the mechanism by Borsa [2] (cont.)

No.	Reaction	A (cm ³ -mol-s)	n	E _a (cal/mol)	Ref.
736.	C2CL+EDC=C2CL2+CH2CLCH2	2.00E+13	0	26000	L
737.	C2CL+VCM=C2CL2+C2H3	3.98E+13	0	9298	As
738.	C2CL+CH3CHCL2=C2CL2+CH3CHCL	2.00E+13	0	26000	L
739.	C2CL+C2HCL3=C2CL2+CHCLOCL	2.00E+13	0	26000	L
740.	CH3OCL2+C2HCL=C2H+CH3OCL3	1.20E+15	0	14873	At
741.	CH3OCL2+C2CL2=C2CL+CH3OCL3	1.20E+15	0	14873	At
742.	OCL3+C3H3CL3_123D=OCL4+C3H3CL2_312D	5.00E+11	0	5000	H
743.	OCL3+C3H3CL3_113D=OCL4+C3H3CL2_311D	5.00E+11	0	5000	H
744.	OCL3+C3H4CL2_23D=OCL4+C3H4CL_32D	5.00E+11	0	5000	H
745.	OCL3+C3H2CL4_33D=OCL4+C3H2CL3_333D	5.00E+11	0	5000	H
746.	OCL3+C3H4CL2_13D=OCL4+C3H4CL_31D	5.00E+11	0	5000	H
747.	OCL3+C3H5CL_3D=OCL4+C3H5_3D	5.00E+11	0	5000	H
748.	OCL3+C3H2CL4_12D=OCL4+C3H2CL3_312D	5.00E+11	0	5000	H
749.	OCL3+C3H3CL3_333D=OCL4+C3H3CL2_333D	5.00E+11	0	5000	H
750.	OCL3+C3H3CL5_112=OCL4+C3H3CL4_3112	5.00E+11	0	5000	H
751.	OCL3+C3H4CL4_1223=OCL4+C3H4CL3_2123	5.00E+11	0	5000	H
752.	CH3OCL2+C3H3CL3_123D=CH3OCL3+C3H3CL2_312D	5.00E+11	0	5000	H
753.	CH3OCL2+C3H3CL3_113D=CH3OCL3+C3H3CL2_311D	5.00E+11	0	5000	H
754.	CH3OCL2+C3H4CL2_23D=CH3OCL3+C3H4CL_32D	5.00E+11	0	5000	H
755.	CH3OCL2+C3H2CL4_33D=CH3OCL3+C3H2CL3_333D	5.00E+11	0	5000	H
756.	CH3OCL2+C3H4CL2_13D=CH3OCL3+C3H4CL_31D	5.00E+11	0	5000	H
757.	CH3OCL2+C3H5CL_3D=CH3OCL3+C3H5_3D	5.00E+14	0	5000	H
758.	CH3OCL2+C3H2CL4_12D=CH3OCL3+C3H2CL3_312D	5.00E+11	0	5000	H
759.	CH3OCL2+C3H3CL3_333D=CH3OCL3+C3H3CL2_333D	5.00E+11	0	5000	H
760.	CH3OCL2+C3H3CL5_112=CH3OCL3+C3H3CL4_3112	5.00E+11	0	5000	H
761.	CH3OCL2+C3H4CL4_1223=CH3OCL3+C3H4CL3_2123	5.00E+11	0	5000	H
762.	CH2CLCHCL+C3H3CL3_123D=CH2CLCHCL2+C3H3CL2_312D	5.00E+11	0	5000	H
763.	CH2CLCHCL+C3H3CL3_113D=CH2CLCHCL2+C3H3CL2_311D	5.00E+11	0	5000	H
764.	CH2CLCHCL+C3H4CL2_23D=CH2CLCHCL2+C3H4CL_32D	5.00E+11	0	5000	H
765.	CH2CLCHCL+C3H2CL4_33D=CH2CLCHCL2+C3H2CL3_333D	5.00E+11	0	5000	H
766.	CH2CLCHCL+C3H4CL2_13D=CH2CLCHCL2+C3H4CL_31D	5.00E+11	0	5000	H
767.	CH2CLCHCL+C3H5CL_3D=CH2CLCHCL2+C3H5_3D	5.00E+14	0	5000	H
768.	CH2CLCHCL+C3H2CL4_12D=CH2CLCHCL2+C3H2CL3_312D	5.00E+11	0	5000	H
769.	CH2CLCHCL+C3H3CL3_333D=CH2CLCHCL2+C3H3CL2_333D	5.00E+11	0	5000	H
770.	CH2CLCHCL+C3H3CL5_112=CH2CLCHCL2+C3H3CL4_3112	5.00E+11	0	5000	H
771.	CH2CLCHCL+C3H4CL4_1223=CH2CLCHCL2+C3H4CL3_2123	5.00E+11	0	5000	H
772.	CH2OCL+C3H3CL3_123D=CH2OCL2+C3H3CL2_312D	5.00E+11	0	5000	H
773.	CH2OCL+C3H3CL3_113D=CH2OCL2+C3H3CL2_311D	5.00E+11	0	5000	H
774.	CH2OCL+C3H4CL2_23D=CH2OCL2+C3H4CL_32D	5.00E+11	0	5000	H
775.	CH2OCL+C3H2CL4_33D=CH2OCL2+C3H2CL3_333D	5.00E+11	0	5000	H
776.	CH2OCL+C3H4CL2_13D=CH2OCL2+C3H4CL_31D	5.00E+11	0	5000	H
777.	CH2OCL+C3H5CL_3D=CH2OCL2+C3H5_3D	5.00E+14	0	5000	H
778.	CH2OCL+C3H2CL4_12D=CH2OCL2+C3H2CL3_312D	5.00E+11	0	5000	H
779.	CH2OCL+C3H3CL3_333D=CH2OCL2+C3H3CL2_333D	5.00E+11	0	5000	H

Figure A.20: List of reactions used on the mechanism by Borsa [2] (cont.)

No.	Reaction	A ($\text{cm}^3\text{-mol-s}$)	n	E_a (cal/mol)	Ref.
780.	$\text{CH}_2\text{OCL}+\text{C}_3\text{H}_3\text{CL}_5 \rightarrow 112\text{-CH}_2\text{OCL}_2+\text{C}_3\text{H}_3\text{CL}_4$ 3112	5.00E+11	0	5000	H
781.	$\text{CH}_2\text{OCL}+\text{C}_3\text{H}_4\text{CL}_4 \rightarrow 1223\text{-CH}_2\text{OCL}_2+\text{C}_3\text{H}_4\text{CL}_3$ 2123	5.00E+11	0	5000	H
782.	$\text{C}_3\text{H}_2\text{CL}_3 \rightarrow 313\text{D}+\text{EDC}=\text{CH}_2\text{CLCH}_2+\text{C}_3\text{H}_2\text{CL}_4$ 13D	5.00E+11	0	5000	H
783.	$\text{C}_3\text{H}_2\text{CL}_3 \rightarrow 323\text{D}+\text{EDC}=\text{CH}_2\text{CLCH}_2+\text{C}_3\text{H}_2\text{CL}_4$ 23D	5.00E+11	0	5000	H
784.	$\text{C}_3\text{H}_3\text{CL}_2 \rightarrow 323\text{D}+\text{EDC}=\text{CH}_2\text{CLCH}_2+\text{C}_3\text{H}_3\text{CL}_3$ 233D	5.00E+11	0	5000	H
785.	$\text{C}_3\text{HCL}_4 \rightarrow 33\text{D}+\text{EDC}=\text{CH}_2\text{CLCH}_2+\text{C}_3\text{HCL}_5$ 3D	5.00E+11	0	5000	H
786.	$\text{C}_3\text{H}_3\text{CL}_2 \rightarrow 313\text{D}+\text{EDC}=\text{CH}_2\text{CLCH}_2+\text{C}_3\text{H}_3\text{CL}_3$ 133D	5.00E+11	0	5000	H
787.	$\text{C}_3\text{H}_4\text{CL} \rightarrow 33\text{D}+\text{EDC}=\text{CH}_2\text{CLCH}_2+\text{C}_3\text{H}_4\text{CL}_2$ 33D	5.00E+11	0	5000	H
788.	$\text{C}_3\text{HCL}_4 \rightarrow 21\text{D}+\text{EDC}=\text{CH}_2\text{CLCH}_2+\text{C}_3\text{HCL}_5$ 1D	5.00E+11	0	5000	H
789.	$\text{C}_3\text{H}_2\text{CL}_3 \rightarrow 211\text{D}+\text{EDC}=\text{CH}_2\text{CLCH}_2+\text{C}_3\text{H}_2\text{CL}_4$ 11D	5.00E+11	0	5000	H
790.	$\text{C}_3\text{H}_2\text{CL}_3 \rightarrow 313\text{D}+\text{VCM}=\text{C}_2\text{H}_3+\text{C}_3\text{H}_2\text{CL}_4$ 13D	5.00E+11	0	5000	H
791.	$\text{C}_3\text{H}_2\text{CL}_3 \rightarrow 323\text{D}+\text{VCM}=\text{C}_2\text{H}_3+\text{C}_3\text{H}_2\text{CL}_4$ 23D	5.00E+11	0	5000	H
792.	$\text{C}_3\text{H}_3\text{CL}_2 \rightarrow 323\text{D}+\text{VCM}=\text{C}_2\text{H}_3+\text{C}_3\text{H}_3\text{CL}_3$ 233D	5.00E+11	0	5000	H
793.	$\text{CL}+\text{CL}=\text{CL}_2$	2.51E+14	0	1800	Aa
794.	$\text{C}_3\text{HCL}_4 \rightarrow 33\text{D}+\text{VCM}=\text{C}_2\text{H}_3+\text{C}_3\text{HCL}_5$ 3D	5.00E+11	0	5000	H
795.	$\text{C}_3\text{H}_3\text{CL}_2 \rightarrow 313\text{D}+\text{VCM}=\text{C}_2\text{H}_3+\text{C}_3\text{H}_3\text{CL}_3$ 133D	5.00E+11	0	5000	H
796.	$\text{C}_3\text{H}_4\text{CL} \rightarrow 33\text{D}+\text{VCM}=\text{C}_2\text{H}_3+\text{C}_3\text{H}_4\text{CL}_2$ 33D	5.00E+11	0	5000	H
797.	$\text{C}_3\text{HCL}_4 \rightarrow 21\text{D}+\text{VCM}=\text{C}_2\text{H}_3+\text{C}_3\text{HCL}_5$ 1D	5.00E+11	0	5000	H
798.	$\text{C}_3\text{H}_2\text{CL}_3 \rightarrow 211\text{D}+\text{VCM}=\text{C}_2\text{H}_3+\text{C}_3\text{H}_2\text{CL}_4$ 11D	5.00E+11	0	5000	H
Molecular Weight Growth					
799.	$\text{CL}+\text{C}_2\text{H}_2=\text{CH}_2\text{OCL}$	5.00E+10	0	0	Q
800.	$\text{CL}+\text{VCM}=\text{CH}_3\text{OCL}_2$	1.00E+10	0	1000	Q
801.	$\text{CL}+\text{CHCLCHCL} \rightarrow \text{CCL}_3\text{CH}_2$	4.00E+08	0	0	Q
802.	$\text{C}_2\text{H}_3+\text{C}_3\text{H}_6=\text{C}_4\text{H}_6$ 13D+ CH_3	2.50E+08	0	6000	Q
803.	$\text{C}_2\text{H}_3+\text{C}_4\text{H}_6 \rightarrow 13\text{D}=\text{benzene}+\text{H}+\text{H}_2$	3.50E+08	0	5000	Q
804.	$\text{CH}_2\text{OCL}+\text{C}_2\text{H}_4=\text{C}_4\text{H}_6$ 13D+ CL	1.00E+08	0	9000	Q
805.	$\text{CH}_2\text{CLCHCL}+\text{VCM}=\text{C}_4\text{H}_6\text{CL}_3$ 1134	1.40E+11	0	10150	Aa
806.	$\text{CH}_2\text{CLCHCL}+\text{VCM}=\text{C}_4\text{H}_6\text{CL}_3$ 1234	2.08E+10	0	8130	Aa
807.	$\text{CH}_2\text{CLCHCL}+\text{VCM}=\text{C}_4\text{H}_6\text{CL}_2$ 34D+ CL	7.82E+11	0	13900	Aj
808.	$\text{CH}_2\text{CLCHCL}+\text{VCM}=\text{C}_4\text{H}_5\text{CL}_3$ 134D+ H	1.82E+12	0	30800	Aj
809.	$\text{CH}_2\text{OCL}+\text{C}_2\text{H}_4=\text{C}_4\text{H}_5\text{CL}$ 213D+ H	5.00E+11	0	7300	An
810.	$\text{CH}_2\text{OCL}+\text{C}_2\text{H}_4=\text{C}_4\text{H}_6\text{CL}$ 42D	2.00E+11	0	2000	K
811.	$\text{CH}_2\text{CLCH}_2+\text{C}_2\text{H}_4=\text{C}_4\text{H}_8\text{CL}$ 14	1.60E+11	0	7300	Aa
812.	$\text{CH}_2\text{CLCH}_2+\text{C}_2\text{H}_4=\text{C}_4\text{H}_7\text{CL}$ 4D+ H	5.20E+07	0	0	Al
813.	$\text{VCM}+\text{C}_2\text{H}_3=\text{C}_4\text{H}_6\text{CL}$ 43D	2.00E+11	0	2000	K
814.	$\text{VCM}+\text{C}_2\text{H}_3=\text{C}_4\text{H}_6$ 13D+ CL	6.30E+11	0	3000	Am

Figure A.21: List of reactions used on the mechanism by Borsa [2] (cont.)

No.	Reaction	A (cm ³ -mol-s)	n	E ₀ (cal/mol)	Ref.
815.	CH2CLCHCL+C2H4=C4H7CL2_134	1.60E+11	0	7300	Am
816.	CH2CLCHCL+C2H4=C4H6CL2_34D+H	5.20E+07	0	0	Al
817.	VCM+CH2CCL=C4H5CL2_423D	2.00E+11	0	3000	K
818.	VCM+CH2CCL=C4H5CL_213D+CL	5.00E+11	0	7300	Am

A: estimated from Degout (1991), B: Karra (1988), C: Shi (1994), D: estimated from Tsang (1988), E: Fisher (1990), F: estimated from Wallington (1988), G: estimated from Matheson (1982), H: estimated from Timonen (1986), I: Ranzi (1990), J: estimated with method of Ranzi (1994), K: estimated from Weissman (1984), L: estimated from Bell (1977), M: estimated from Tsang (1991), N: estimated from Tschuikow-Roux (1986), O: estimated from Tschuikow-Roux (1985), P: estimated from Tschuikow-Roux (1985), Q: Bertolini (1992), R: estimated from Barat (1992), S: estimated from Barat (1992) by decreasing E₀ by 8kcal, T: estimated from Atkinson (1992), U: estimated from C2H3+C2H4 in Mallard (1993), V: estimated from C2H5+C3H8 in Mallard (1993), X: estimated from Schneider (1986), Y: estimated, Z: estimated from Timonen (1988), Aa: estimated from Kerr (1972), Ab: estimated from Howlett (1952), Ac: estimated from Wine (1983), Ad: estimated from Manion (1986), Ae: estimated from Shilov (1959), Af: Knox (1962), Ag: estimated from Schug (1979), Ah: estimated from Tsee (1980), Aj: qrrk analysis performed, Ak: estimated from Dean (1985), Al: estimated from MacKinzie (1984), Am: estimated from Fahr (1986), An: estimated from Tsang (1986), Ap: estimated from Zabel (1974), Aq: estimated from Nist Data, Ar: estimated from Warnatz (1985), As: estimated from Manion (1988), At: estimated from Tsang (1991), Au: Benson (1982).

Figure A.22: List of reactions used on the mechanism by Borsa [2] (cont.)

The list of the species used for these mechanism is presented below:


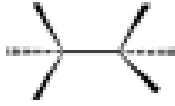





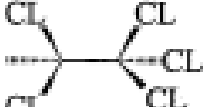
Species character strings	Chemical structures
1. H2 2. CL2 3. HCL 4. CH4 5. CCL4 6. GHCL3 7. GH2CL2 8. CH3CL	- - - - - - -
9. EDC	
10. C2H6	
11. CH2CLCHCL2	
12. CH2CLCH3	
13. CHCL2CHCL2	
14. CH3CHCL2	
15. CH3CCL3	
16. CHCL2CCL3	

Figure A.23: List of species used on the mechanism by Borsa [2]










Species character strings	Chemical structures
17. VCM	
18. C2H4	
19. CH2CCL2	
20. CHCLCHCL_c	
21. CHCLCHCL_t	
22. C2HCL3	
23. C2CL4	
24. C2H2	
25. G2HCL	

Figure A.24: List of species used on the mechanism by Borsa [2] (cont.)









Species character strings	Chemical structures
26. C2CL2	
27. C3H8	
28. C3H6	
29. C3H4CL4_1223	
30. C3H3CL5_112	
31. C3H4CL4_1113	
32. C3H8CL2_13	
33. C3H5CL3_123	

Figure A.25: List of species used on the mechanism by Borsa [2] (cont.)

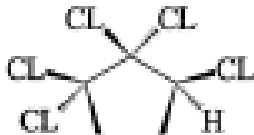







Species character strings	Chemical structures
34. C3H3CL5_113	
35. C3H3CL3_333D	
36. C3H2CL4_12D	
37. C3H2CL4_11D	
38. C3HCL5_1D	
39. C3HCL5_2D	
40. C3H5CL_3D	
41. C3H4CL2_13D	

Figure A.26: List of species used on the mechanism by Borsa [2] (cont.)

Species character strings	Chemical structures
42. C3H2CL4_33D	
43. C3H4CL2_23D	
44. C3H3CL3_113D	
45. C3H3CL3_123D	
46. C3H4CL2_12D	
47. C3H4CL2_11D	
48. C3H5CL_2D	

Figure A.27: List of species used on the mechanism by Borsa [2] (cont.)

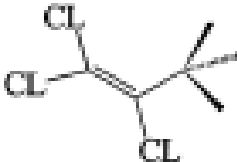



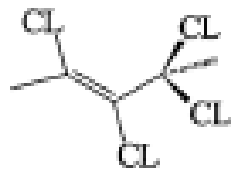


Species character strings	Chemical structures
49. C3H3CL3_112D	
50. C3H5CL_1D	
51. C3H3CL3_133D	
52. C3H4CL2_33D	
53. C3H2CL4_13D	
54. C3H2CL4_23D	
55. C3H3CL3_233D	

Figure A.28: List of species used on the mechanism by Borsa [2] (cont.)

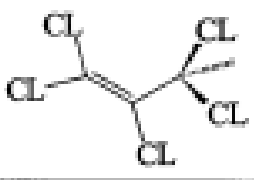
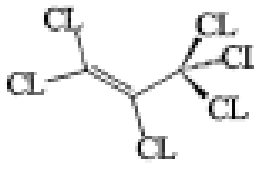
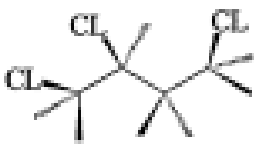
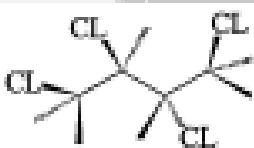

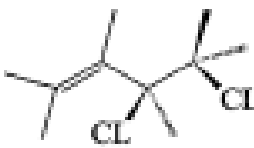

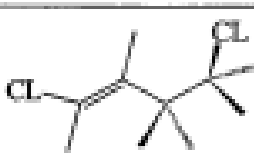
Species character strings	Chemical structures
56. C3HCL5_3D	
57. C3CL6_D	
58. C4H7CL3_124	
59. C4H8CL4_1234	
60. C4H7CL_4D	
61. C4H6CL2_34D	
62. C4H8CL2_24D	
63. C4H8CL2_14D	

Figure A.29: List of species used on the mechanism by Borsa [2] (cont.)


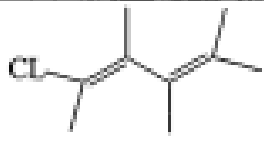
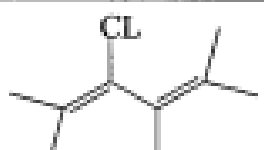
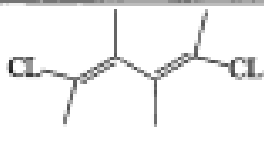
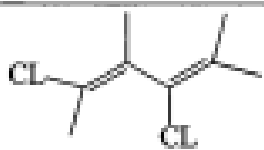


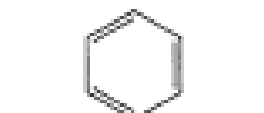
Species character strings	Chemical structures
64. C4H5CL3_134D	
65. C4H5CL_113D	
66. C4H5CL_213D	
67. C4H4CL2_1413D	
68. C4H4CL2_1313D	
69. C4H6_13D	
70. C4H4_DT	
71. benzene	

Figure A.30: List of species used on the mechanism by Borsa [2] (cont.)

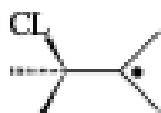






Species character strings	Chemical structures
1. H	-
2. CL	-
3. CH3	-
4. CCL3	-
5. CCL2	-
6. CHCL	-
7. CH2	-
8. CH2CL	-
9. CHCL2	-
10. CH2CLCH2	
11. CH3CHCL	
12. CH3CCL2	
13. CHCL2CH2	
14. CH2CLCHCL	
15. CHCL2CHCL	
16. CCL3CH2	

Figure A.31: List of species used on the mechanism by Borsa [2] (cont.)

Species character strings	Chemical structures
17. CHCL2CCL2	
18. C2H3	
19. C2H5	
20. CHCLCH	
21. CH2CCL	
22. C2CL3	
23. CCL2CH	
24. CHCLOCL	
25. C2H	

Figure A.32: List of species used on the mechanism by Borsa [2] (cont.)

Species character strings	Chemical structures
26. C2CL	
27. GH2CLOCL2CHCL	
28. C3H2CL5_211	
29. C3H3CL4_3112	
30. C3H4CL3_2123	
31. C3H5_3D	
32. C3H2CL3_313D	
33. C3H2CL3_323D	

Figure A.33: List of species used on the mechanism by Borsa [2] (cont.)

Species character strings	Chemical structures
34. C3H3CL2_323D	
35. C3HCL4_33D	
36. C3H3CL2_313D	
37. C3H4CL_33D	
38. C3HCL4_21D	
39. C3H2CL3_211D	
40. C3H3CL2_312D	

Figure A.34: List of species used on the mechanism by Borsa [2] (cont.)




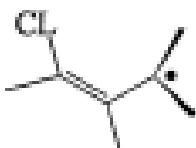




Species character strings	Chemical structures
41. C3H3CL2_311D	
42. C3H4CL_32D	
43. C3H2CL3_333D	
44. C3H4CL_31D	
45. C3H2CL3_312D	
46. C3H3CL2_333D	
47. C3H4CL_14D	
48. C4H8CL_14	

Figure A.35: List of species used on the mechanism by Borsa [2] (cont.)

Species character strings	Chemical structures
49. C4H7CL2_134	
50. C4H6CL3_1134	
51. C4H8CL3_1234	
52. C4H7_4D	
53. C4H8CL_43D	
54. C4H8CL_34D	
55. C4H8CL_42D	
56. C4H5CL2_434D	

Figure A.36: List of species used on the mechanism by Borsa [2] (cont.)

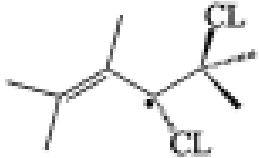
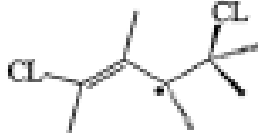






Species character strings	Chemical structures
57. C4H5CL2_334D	
58. C4H5CL2_314D	
59. C4H5CL2_413D	
60. C4H5CL2_423D	
61. C4H4CL3_4134D	
62. C4H4CL3_3134D	
63. C4H5_213D	
64. C4H5_113D	

Figure A.37: List of species used on the mechanism by Borsa [2] (cont.)

Appendix B

Heat Capacity

As mentioned in chapter 4, when using a radical mechanism, the heat capacity is estimated using equation 4.8. The parameters used were estimated using the data present in Borsa [2], and are present in this appendix:

Table B.1: Heat capacities for the molecular species

	a_0	a_1	a_2	b
H2	5.2E-10	-9.0E-07	8.5E-04	6.72
CL2	1.6E-09	-5.2E-06	5.7E-03	6.85
HCL	-1.1E-09	3.3E-06	-1.9E-03	7.28
CH4	-3.4E-09	4.5E-06	1.1E-02	4.74
CCL4	1.0E-08	-3.4E-05	3.7E-02	11.77
CHCL3	8.6E-09	-3.0E-05	3.7E-02	6.98
CH2CL2	5.9E-09	-2.3E-05	3.4E-02	3.94
CH3CL	1.9E-09	-1.2E-05	2.6E-02	3.06
EDC	1.2E-08	-4.5E-05	6.5E-02	1.88
C2H6	1.7E-09	-1.6E-05	4.2E-02	1.23
CH2CLCHCL2	1.3E-08	-4.9E-05	6.7E-02	4.84
CH2CLCH3	8.4E-09	-3.4E-05	5.6E-02	1.02
CHCL2CHCL2	1.6E-08	-5.8E-05	7.4E-02	6.47
CH3CHCL2	8.4E-09	-3.4E-05	5.6E-02	1.02
CH3CCL3	9.2E-09	-3.6E-05	5.4E-02	8.64
CHCL2CCL3	1.6E-08	-5.6E-05	6.7E-02	13.06
VCM	7.8E-09	-3.0E-05	4.4E-02	1.93
C2H4	3.3E-09	-1.8E-05	3.6E-02	1.04
CH2CCL2	9.7E-09	-3.5E-05	4.7E-02	5.00
CHCLCHCL_c	1.0E-08	-3.6E-05	4.8E-02	4.07
CHCLCHCL_t	1.0E-08	-3.6E-05	4.8E-02	4.07
C2HCL3	1.0E-08	-3.7E-05	4.6E-02	8.51
C2CL4	1.1E-08	-3.8E-05	4.4E-02	12.71
C2H2	5.0E-09	-1.7E-05	2.3E-02	5.00
C2HCL	5.4E-09	-1.8E-05	2.3E-02	7.75
C2CL2	2.8E-10	-1.9E-06	4.8E-03	16.16
C3H8	6.6E-09	-3.5E-05	7.1E-02	-0.70
C3H6	5.1E-09	-2.8E-05	5.6E-02	0.93
C3H4CL4_1223	2.6E-08	-8.9E-05	1.1E-01	4.62
C3H3CL5_112	1.8E-08	-6.8E-05	9.0E-02	12.37
C3H4CL4_1113	1.6E-08	-6.1E-05	8.4E-02	10.52
C3H6CL2_13	1.3E-08	-5.2E-05	8.2E-02	2.86

Table B.2: Heat capacities for the molecular species (cont.)

	a_0	a_1	a_2	b
C3H5CL3_123	1.5E-08	-6.1E-05	9.0E-02	4.04
C3H3CL5_113	2.9E-08	-9.7E-05	1.1E-01	7.35
C3H3CL3_333D	1.2E-08	-4.6E-05	6.5E-02	10.06
C3H2CL4_12D	1.5E-08	-5.3E-05	6.9E-02	12.18
C3H2CL4_11D	1.1E-08	-4.3E-05	5.9E-02	15.65
C3HCL5_1D	1.6E-08	-5.5E-05	6.5E-02	18.24
C3HCL5_2D	1.5E-08	-5.3E-05	6.6E-02	16.39
C3H5CL_3D	5.9E-09	-3.4E-05	6.5E-02	1.63
C3H4CL2_13D	1.1E-08	-4.3E-05	6.6E-02	4.80
C3H2CL4_33D	1.1E-08	-4.1E-05	5.6E-02	15.04
C3H4CL2_23D	1.1E-08	-4.1E-05	5.6E-02	15.04
C3H3CL3_113D	1.1E-08	-4.4E-05	6.4E-02	8.86
C3H3CL3_123D	1.1E-08	-4.2E-05	6.1E-02	8.95
C3H4CL2_12D	8.3E-09	-3.4E-05	5.5E-02	8.54
C3H4CL2_11D	8.4E-09	-3.6E-05	5.8E-02	7.24
C3H5CL_2D	5.8E-09	-2.7E-05	5.1E-02	6.40
C3H3CL3_112D	8.8E-09	-3.4E-05	5.1E-02	13.29
C3H5CL_1D	7.8E-09	-3.5E-05	6.0E-02	3.18
C3H3CL3_133D	1.4E-08	-5.2E-05	7.2E-02	6.96
C3H4CL2_33D	1.1E-08	-4.4E-05	6.7E-02	5.15
C3H2CL4_13D	1.2E-08	-4.5E-05	6.3E-02	12.18
C3H2CL4_23D	1.4E-08	-5.3E-05	7.1E-02	10.78
C3H3CL3_233D	1.1E-08	-4.2E-05	5.9E-02	11.28
C3HCL5_3D	1.4E-08	-4.9E-05	6.1E-02	17.19
C3CL6_D	5.8E-09	-2.3E-05	3.4E-02	27.84
C4H7CL3_124	1.8E-08	-7.4E-05	1.1E-01	3.84
C4H6CL4_1234	1.8E-08	-7.4E-05	1.1E-01	3.77
C4H7CL_4D	1.3E-08	-5.6E-05	9.0E-02	0.73
C4H6CL2_34D	1.7E-08	-6.1E-05	8.5E-02	6.54
C4H6CL2_24D	1.4E-08	-5.5E-05	8.5E-02	6.04
C4H6CL2_14D	1.9E-08	-6.7E-05	9.4E-02	3.95
C4H5CL3_134D	7.4E-09	-3.9E-05	7.6E-02	6.92
C4H5CL_113D	1.7E-08	-6.2E-05	8.7E-02	1.20
C4H5CL_213D	1.5E-08	-5.6E-05	7.8E-02	4.17
C4H4CL2_1413D	1.9E-08	-7.0E-05	9.2E-02	2.99
C4H4CL2_1313D	2.6E-08	-8.6E-05	1.0E-01	3.03
C4H6_13D	1.6E-08	-6.1E-05	8.7E-02	-1.81
C4H4_DT	9.9E-09	-3.9E-05	5.9E-02	3.05
Benzene	2.0E-08	-8.2E-05	1.2E-01	-9.87

Table B.3: Heat capacities for the radical species

	a_0	a_1	a_2	b
H	0.00E+00	0.00E+00	0.00E+00	4.97
CL	1.37E-09	-4.12E-06	3.53E-03	4.51
CH3	-5.09E-10	-7.85E-07	8.70E-03	6.66
CCL3	7.30E-09	-2.43E-05	2.68E-02	9.26
CCL2	4.02E-09	-1.25E-05	1.49E-02	7.69
CHCL	2.03E-09	-7.54E-06	1.12E-02	6.05
CH2	-1.66E-09	4.20E-06	2.53E-04	7.65
CH2CL	1.77E-09	-8.48E-06	1.61E-02	6.24
CHCL2	5.16E-09	-1.84E-05	2.35E-02	7.13

Table B.4: Heat capacities for the radical species (cont.)

	a_0	a_1	a_2	b
CH2CLCH2	6.48E-09	-2.63E-05	4.26E-02	4.89
CH3CHCL	8.59E-09	-3.38E-05	5.10E-02	1.69
CH3CCL2	1.06E-08	-4.02E-05	5.56E-02	4.24
CHCL2CH2	1.06E-08	-4.02E-05	5.56E-02	4.24
CH2CLCHCL	8.84E-09	-3.32E-05	4.73E-02	6.44
CHCL2CHCL	1.80E-08	-5.79E-05	6.64E-02	4.87
CCL3CH2	1.15E-08	-4.17E-05	5.33E-02	9.23
CHCL2CCL2	1.80E-08	-5.79E-05	6.64E-02	4.87
C2H3	4.49E-09	-1.89E-05	3.11E-02	2.69
C2H5	2.08E-09	-1.49E-05	3.62E-02	2.49
CHCLCH	7.72E-09	-2.84E-05	3.81E-02	3.94
CH2CCL	6.80E-09	-2.48E-05	3.44E-02	4.64
C2CL3	8.89E-09	-3.06E-05	3.59E-02	10.02
CCL2CH	7.18E-09	-2.61E-05	3.36E-02	8.29
CHCLCCL	9.24E-09	-3.24E-05	3.94E-02	6.79
C2CL	2.53E-09	-9.37E-06	1.26E-02	7.80
C2H	8.76E-11	-9.35E-07	4.60E-03	8.79
CH2CLCCL2CHCL	2.77E-08	-9.25E-05	1.06E-01	4.90
C3H2CL5.211	1.57E-08	-5.87E-05	7.80E-02	13.48
C3H3CL4.3112	1.96E-08	-7.11E-05	9.10E-02	7.22
C3H4CL3.2123	1.17E-08	-4.91E-05	7.53E-02	5.94
C3H5.3D	1.09E-08	-4.52E-05	7.02E-02	-3.14
C3H2CL3.313D	1.28E-08	-4.65E-05	5.98E-02	10.88
C3H2CL3.323D	1.46E-08	-5.38E-05	6.98E-02	6.76
C3H3CL2.323D	9.86E-09	-3.76E-05	5.34E-02	8.81
C3HCL4.33D	9.79E-09	-3.71E-05	5.03E-02	15.45
C3H3CL2.313D	1.28E-08	-4.82E-05	6.60E-02	4.59
C3H4CL.33D	1.06E-08	-4.22E-05	6.27E-02	2.21
C3HCL4.21D	1.84E-08	-6.36E-05	7.54E-02	8.69
C3H2CL3.211D	8.39E-09	-3.37E-05	4.99E-02	11.84
C3H3CL2.312D	8.48E-09	-3.49E-05	5.35E-02	7.55
C3H3CL2.311D	1.07E-08	-4.16E-05	5.95E-02	6.88
C3H4CL.32D	7.74E-09	-3.23E-05	5.13E-02	6.07
C3H2CL3.333D	1.15E-08	-4.23E-05	5.61E-02	11.83
C3H4CL.31D	9.98E-09	-4.04E-05	6.12E-02	2.77
C3H2CL3.312D	1.13E-08	-4.46E-05	6.25E-02	8.78
C3H3CL2.333D	1.31E-08	-5.03E-05	6.92E-02	4.10
C3H4CL.14D	9.59E-09	-3.55E-05	5.36E-02	4.46
C4H8CL.14	1.42E-08	-5.93E-05	9.58E-02	1.46
C4H7CL2.134	1.67E-08	-6.80E-05	1.04E-01	2.60
C4H6CL3.1134	1.89E-08	-7.51E-05	1.10E-01	4.08
C4H6CL3.1234	1.95E-08	-7.72E-05	1.12E-01	4.14
C4H7.4D	1.37E-08	-5.63E-05	8.83E-02	-1.40
C4H6CL.43D	7.20E-09	-3.69E-05	7.07E-02	4.62
C4H6CL.34D	1.54E-08	-6.10E-05	9.09E-02	0.49
C4H6CL.42D	1.23E-08	-4.94E-05	7.63E-02	4.87
C4H5CL2.434D	9.77E-09	-4.39E-05	7.49E-02	6.62
C4H5CL2.334D	9.80E-09	-4.50E-05	7.67E-02	6.62
C4H5CL2.314D	1.76E-08	-6.72E-05	9.45E-02	2.78
C4H5CL2.413D	1.57E-08	-6.04E-05	8.65E-02	7.25
C4H5CL2.423D	8.04E-09	-3.73E-05	6.60E-02	9.86
C4H4CL3.4134D	1.57E-08	-6.04E-05	8.65E-02	7.25
C4H4CL3.3134D	1.42E-08	-5.80E-05	8.67E-02	7.16
C4H5.213D	3.55E-09	-2.18E-05	4.79E-02	7.74
C4H5.113D	2.41E-09	-2.05E-05	4.94E-02	5.60

Appendix C

Emissivity estimation

In this appendix the parameters for the different emissivity correlations are presented.

For correlation 2.10, two parameters are used, b and n , which vary according to the temperature of the flue gas and its $H_2O : CO_2$ ratio. For pL between 0.046 to 1.15 m.atm, the following values are reported by Perry et al. [23]:

Table C.1: Values for the parameter b for correlation 2.10

Temperature (K)	$p_{H_2O}/(p_{CO_2} + p_{H_2O})$					
	0–0.2	0.2–0.4	0.4–0.6	0.6–0.7	0.7–0.8	0.8–1
1000	188	384	416	444	455	416
1500	252	448	495	540	548	548
2000	267	451	509	572	594	632

Table C.2: Values for the parameter n for correlation 2.10

Temperature (K)	$p_{H_2O}/(p_{CO_2} + p_{H_2O})$					
	0–0.2	0.2–0.4	0.4–0.6	0.6–0.7	0.7–0.8	0.8–1
1000	0.21	0.33	0.34	0.34	0.35	0.40
1500	0.26	0.38	0.40	0.42	0.42	0.52
2000	0.32	0.45	0.48	0.51	0.52	0.64

For correlation 2.11, the parameters used, a_0 , a_1 , a_2 , and a_3 also vary according to the temperature of the flue gas and its $H_2O : CO_2$ ratio, and are valid for pL between 0.005 to 10 m.atm [23]:

Table C.3: Values for the parameter a_0 for correlation 2.11

Temperature (K)	$p_{H_2O}/(p_{CO_2} + p_{H_2O})$					
	0–0.2	0.2–0.4	0.4–0.6	0.6–0.7	0.7–0.8	0.8–1
1000	2.2661	2.5754	2.6090	2.6367	2.6432	2.5995
1500	2.3954	2.6451	2.6862	2.7178	2.7257	2.7083
2000	2.4104	2.6504	2.7029	2.7482	2.7592	2.7709

Table C.4: Values for the parameter a_1 for correlation 2.11

Temperature (K)	$p_{H_2O}/(p_{CO_2} + p_{H_2O})$					
	0–0.2	0.2–0.4	0.4–0.6	0.6–0.7	0.7–0.8	0.8–1
1000	0.1742	0.2792	0.2799	0.2723	0.2715	0.3015
1500	0.2203	0.3418	0.3450	0.3386	0.3355	0.3969
2000	0.2602	0.4279	0.4440	0.4464	0.4372	0.5099

Table C.5: Values for the parameter a_2 for correlation 2.11

Temperature (K)	$p_{H_2O}/(p_{CO_2} + p_{H_2O})$					
	0–0.2	0.2–0.4	0.4–0.6	0.6–0.7	0.7–0.8	0.8–1
1000	-0.0390	-0.0648	-0.0745	-0.0804	-0.0816	-0.0961
1500	-0.0433	-0.0685	-0.0816	-0.0990	-0.0981	-0.1309
2000	-0.0651	-0.0674	-0.0859	-0.1086	-0.1122	-0.1646

Table C.6: Values for the parameter a_3 for correlation 2.11

Temperature (K)	$p_{H_2O}/(p_{CO_2} + p_{H_2O})$					
	0–0.2	0.2–0.4	0.4–0.6	0.6–0.7	0.7–0.8	0.8–1
1000	0.0040	0.0017	-0.0006	0.0030	0.0052	0.0119
1500	0.0056	-0.0043	-0.0039	-0.0030	0.0045	0.0012
2000	-0.0016	-0.0120	-0.0135	-0.0139	-0.0065	-0.0165

For a mixture of water vapour and carbon dioxide where $p = 1\text{bar}$ and $0.5 < p_{H_2O}/p_{CO_2} < 2$, VDI-Gesellschaft [28] considers the following parameters for correlation 2.13:

Table C.7: Constants for the degree of emission of the pure gas phase

i	b_{0i}	b_{0i} (1/K)	k (1/(bar m))
1	0.130	0.000265	0.0
2	0.595	-0.000150	0.824
3	0.275	-0.000115	25.907